POLITECNICO
MILANO 1863

SCUOLA DI INGEGNERIA INDUSTRIALE
E DELL'INFORMAZIONE

pH-sensitive tracers for fluorescence-guided glioblastoma surgery

TESI DI LAUREA MAGISTRALE IN
MATERIALS ENGINEERING AND NANOTECHNOLOGY
INGEGNERIA DEI MATERIALI E DELLE NANOTECNOLOGIE

Author: **Nadia Mosca**

Student ID: 968450
Advisor: Prof. Dr. Francesca Baldelli Bombelli
Co-advisor: Dr. Cristina Chirizzi
Academic Year: 2021-22

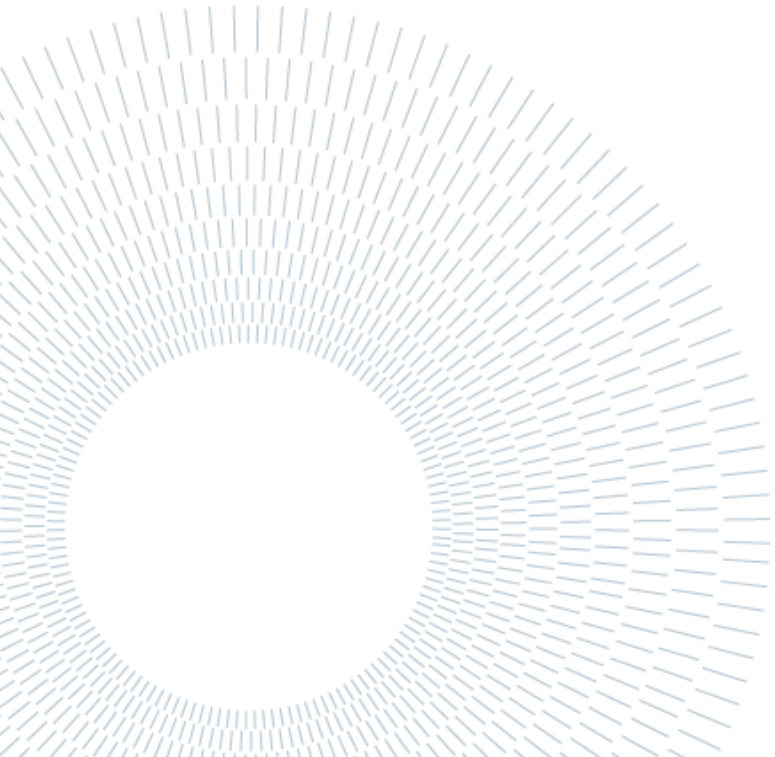

Abstract

Glioblastoma multiforme (GBM) is one of the most common primary brain cancers, corresponding to approximately 17% of all diagnosed tumours. Unfortunately, it is characterized by a high recurrence rate also because the supporting cells of the brain facilitate cancer proliferation. Since ordinary therapies to cure GBM are not available yet, surgical resection represents the first crucial step of the treatment to limit cancer relapse. Considering that during nervous system surgery each volume additionally removed can be associated with serious consequences for the preservation of patients' brain function, several measures are currently used to make the tumour resection as precisely as possible. In this perspective, some of the recent advances involve the fluorescent intraoperative navigation. Among the several investigated fluorophores, Fluorescein has become one of the most ubiquitous probes in biological studies and it is already used in clinical practice thanks to its intense fluorescence, chemical stability, and lack of cytotoxicity at working concentrations. However, its most important limitation is the lack of specificity for cancer cells.

Therefore, this project aims to develop a specific fluorescent tracer able to more selectively label cancer cells during glioblastoma surgical resection. Specifically, we focused on targeting the acidic tumor microenvironment by exploiting the pH-sensitive properties of pH (low) insertion peptides (pHLIPs). Being moderately hydrophobic, pHLIPs have a modest affinity for cellular membranes at physiological pH, but fold and insert across the phospholipid bilayer only at low pH, allowing them to sense pH at the surfaces of cells in diseased tissues, where it is lower. In this study, pHLIPs were directly conjugated to a Fluorescein-maleimide derivative (FL-pHLIP) in order to be employed as fluorescent imaging agents. To evaluate the behavior of this

novel system and verify that the FL-linkage did not affect the pH-dependent membranes insertion, we characterized both Wild Type (WT) and FL- pHLIPs from a chemical-physical perspective. The results on peptide stability and self-assembly are reported together with a study of pHLIP interaction with model systems of the cellular membrane, such as liposomes and supported lipid bilayers (SLBs). Finally, FL-pHLIP labelling efficiency and cytotoxicity were assessed by *in vitro* cellular tests performed on three different lines of patient-derived glioblastoma primary cells in collaboration with Dr. Serena Pellegatta from Carlo Besta Neurological Institute. Results show encouraging and effective specific targeting of proliferative and mesenchymal subtypes of primary glioblastoma cells.

Key-words: glioblastoma multiforme (GMB); fluorescence guided surgery; fluorescein; extracellular acidosis; pH (low) insertion peptides.

Abstract in italiano

Il glioblastoma multiforme (GBM) è uno dei tumori cerebrali primari più comuni, corrispondente a circa il 17% di tutti i tumori diagnosticati. Sfortunatamente, è caratterizzato da un alto tasso di recidiva, anche perché le cellule del cervello facilitano la proliferazione del cancro. Poiché terapie ordinarie per curare il GBM non sono ancora disponibili, la resezione chirurgica rappresenta il primo passo cruciale del trattamento per limitare la recidiva del tumore. Considerando che durante la chirurgia del sistema nervoso ogni volume aggiuntivo rimosso può essere associato a gravi conseguenze per la conservazione della funzione cerebrale dei pazienti, diverse misure vengono attualmente utilizzate per rendere la resezione del tumore il più precisa possibile. In questa prospettiva, alcuni dei recenti progressi riguardano la navigazione intraoperatoria fluorescente. Tra i numerosi fluorofori studiati, la Fluoresceina è diventata una delle sonde più presenti negli studi biologici ed è già utilizzata in clinica grazie alla sua intensa fluorescenza, stabilità chimica e mancanza di citotossicità alle concentrazioni di lavoro. Tuttavia, la sua limitazione più importante è la mancanza di specificità per le cellule tumorali.

Pertanto, questo progetto ha lo scopo di sviluppare un tracciante fluorescente specifico in grado di marcare in modo più selettivo le cellule tumorali durante la resezione chirurgica del glioblastoma. Nello specifico, ci siamo concentrati sull'individuare il microambiente tumorale acido sfruttando le proprietà sensibili al pH di peptidi pHLIP (pH low insertion peptides). Essendo moderatamente idrofobici, i pHLIP hanno una modesta affinità per le membrane cellulari a pH normale, ma si piegano e si inseriscono attraverso il doppio strato fosfolipidico solo in ambiente acido, consentendo loro di percepire il pH sulla superficie delle cellule nei tessuti malati,

dove è più basso. In questo studio, i pHLIP sono stati direttamente coniugati a un derivato della Fluoresceina-maleimide (FL-pHLIP) per essere impiegati come agenti di imaging fluorescenti. Per valutare il comportamento di questo nuovo sistema e verificare che il legame con il fluoroforo non influenzi l'inserimento pH-dipendente nelle membrane, abbiamo caratterizzato sia Wild Type (WT) che FL- pHLIPs da una prospettiva chimico-fisica. I risultati sulla stabilità e il self-assembly dei peptidi sono riportati insieme a uno studio sull'interazione dei pHLIP con sistemi modello di membrana cellulare, come liposomi e doppi strati lipidici supportati (SLB). Infine, l'efficienza di marcatura e la citotossicità dei peptidi FL-pHLIP sono state valutate mediante test cellulari *in vitro* eseguiti su tre diverse linee di cellule primarie di glioblastoma derivate da pazienti in collaborazione con la Dott.ssa Serena Pellegatta dell'Istituto Neurologico Carlo Besta. I risultati mostrano un incoraggiante ed efficace targeting specifico dei sottotipi proliferativi e mesenchimali delle linee cellulari.

Parole chiave: glioblastoma multiforme (GMB); chirurgia guidata dalla fluorescenza; fluoresceina; acidosi extracellulare; peptidi pHLIP.

Contents

1 Introduction

1.1. Glioblastoma multiforme (GBM)

1.1.1. General aspects

Glioblastoma multiforme is the most common primary brain cancer, corresponding to approximately 17% of all diagnosed tumours [1]. In addition to the genetic susceptibility, environmental exposure including vinyl chloride, pesticides, smoking, petroleum by-products, synthetic rubber manufacturing, infection with Simian virus 40, and electromagnetic radiation represent other risk factors for GBM [2]. Usual presenting symptoms include headache, progressive neurological disorder, increased intracranial pressure, and secondary epilepsy [3].

Considering GBM aggressiveness, patients will inevitably experience a high recurrence rate [1] also because the supporting cells of the brain facilitate cancer proliferation and invasiveness [4]. In fact, microglia, which account for 10 –15% of the cells in the brain, are known to promote glioma invasion and growth. Moreover, many of the growth factors and inflammatory cytokines are also expressed by astrocytes, which comprise approximately 50% of the cells in the brain [4]. Astrocytes are an important component of the blood-brain barrier (BBB), which separates circulating blood from extra-cellular fluid by its highly selective permeability, as well as of the tripartite synapse neural network in order to promote bidirectional communication with neurons under physiological conditions [3]. In general, reactive astrocytes help repair injury in the brain by forming a functional barrier, termed as “glial scar”, which serves to restrict and regulate inflammation, isolate the lesion and repair the BBB [3].

However, emerging evidence shows that tumour-associated reactive astrocytes interact with glioma cells and facilitate the progression, aggression, and survival of tumours (Figure 1.1).

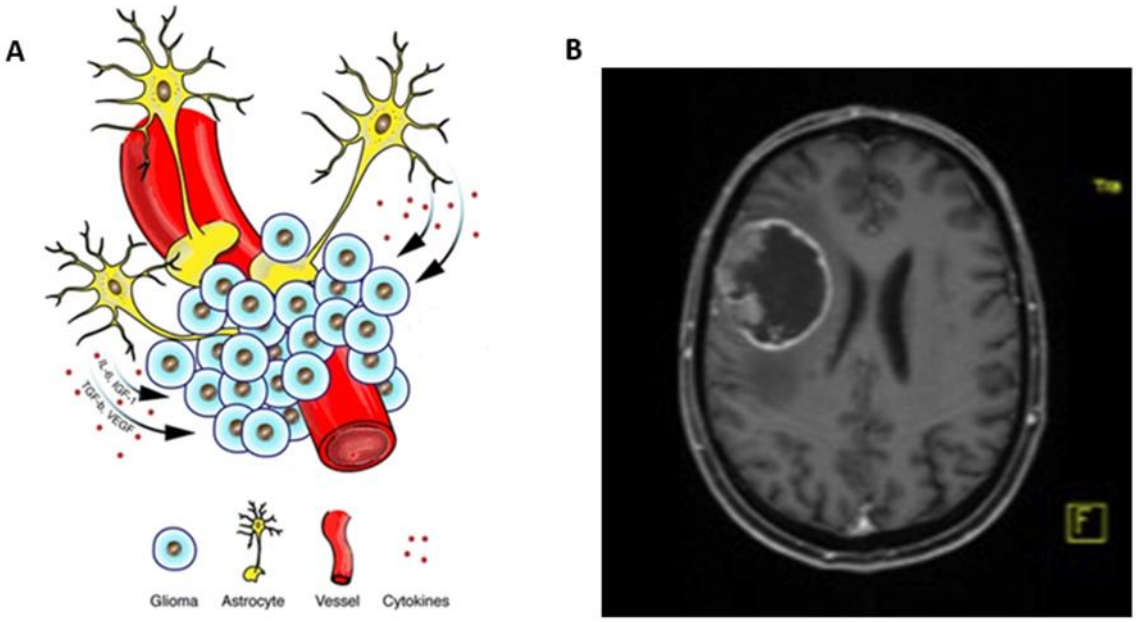

Figure 1.1: A. Schematic illustration of glioma and tumour associated astrocytes. Tumour-associated astrocytes interact in a complex way with glioma cells to promote the proliferation, invasion, and treatment resistance of GBM [3]. B. Preoperative gadolinium-enhanced T1 magnetic resonance imaging showing circular contrast enhancement [1].

1.1.2. Current GBM treatments and surgical resection

Since ordinary therapies to cure glioblastoma are not available yet [5], surgical resection represents the first crucial step of the treatment. However, surgical resection is often not enough on its own and thus requires a multidisciplinary approach including subsequent treatment of radiation and chemotherapy [5]. These procedures nevertheless often fail to prevent tumour recurrence and patients still show significant mortality with a median survival of less than 15 months [6]. To overcome the low effectiveness of available therapies, the use of modern technologies in the context of

medicine, such as immunotherapy, can be promising [2]. Monoclonal antibodies and adoptive cellular therapy have been recently used to modulate the immune response and the results have definitively established that tumours can be treated very effectively without drugging cancer cells [7]. Nanotechnology can substantially improve the utility of adoptive-cell therapy, widening the therapeutic window and enhancing endogenous immune responses [7]. In fact, nanoparticles (NPs) are capable of delivering anticancer drugs or genes into the tumour zone [8]. In this regard, most molecular targeting strategies include specific cancer biomarker proteins such as overexpressed cell surface receptors [9] and different antibodies or other molecules have been already used as targeting ligands for the delivery of imaging or therapeutic agents [8]. However, many cancer biomarker receptors are not uniquely expressed in tumour but also in certain healthy cells, leading to side effects in patients [9]. Moreover, disadvantages including cytotoxicity, neurotoxicity, efficient delivery, short half-life and non-biodegradability have reduced the use of NPs in the clinic [2].

With this in mind, one of the ways to improve the progression-free survival remains, therefore, the optimization of the visualization of tumour margins during GBM surgery. Unfortunately, in the case of nervous system surgery, each volume additionally removed can be associated with serious consequences for the preservation of patients' brain function [5]. For this reason, several measures are used to help the surgeon to perform the procedure as precisely as possible and maximize the extent of resection (EOR) in recurrent GBM. In addition to commonly used white light microscopes, newer devices include neuronavigation, electrophysiological cerebral mapping, and intraoperative magnetic resonance imaging (iMRI) systems [5]. Some of the recent advances involve the fluorescent intraoperative navigation, that is based on the supply of a substance activated by using a proper light wave and resulting in the fluorescence of a given area and the assessment of the tumour margins [5].

1.2. Fluorescence guided surgery

1.2.1. Basic principles

Fluorescence guided surgery (FGS) is an imaging technique that allows the surgeon to visualize different structures and types of tissue during a surgical procedure that may not be as visible under white light conditions [10]. The first use of fluorescence imaging in surgery dates back to 1948 when surgeons used intravenous Fluorescein to enhance intracranial neoplasms [11]. In its simplest form, an FGS system consists of a light source with accompanying filters for excitation of the fluorescence contrast agent, which is often administered prior to surgery [10]. The fluorescence signal emitted by the probe is collected by making the light to pass through appropriate emission filters in order to remove the unwanted radiation [10].

The ideal fluorescent and imaging agent should be characterized by high selectivity for tumour cells, in order to improve contrast between cancer and normal tissues, low toxicity and simple use and delivery [12]. In the context of glioblastoma, fluorophores may target areas of blood-brain barrier (BBB) breakdown, inflammation, or specifically cancer cells. These fluorescent tracers can be administered by different routes, including intravenous injection and oral agents prior to anaesthesia [13].

Importantly, unlike conventional imaging techniques such as computed tomography (CT) and magnetic resonance imaging (MRI), FGS can provide real-time imaging during surgery [14]. Moreover, intraoperative fluorescence imaging offers some benefits as high contrast and sensitivity, low cost, absence of ionizing radiation, easy handling, safety, and high specificity [11].

1.2.2. Imaging agents

Several fluorescent probes have been investigated in preclinical and clinical studies for use in glioma surgery, including 5-Aminolevulinic acid (5-ALA), Fluorescein (FL) and Indocyanine green (ICG) [5]. ICG is the most widely employed near-infrared emitter, first approved in clinical use for angiography and subsequently in ophthalmology and elsewhere for imaging blood vessels [15]. However, the use of ICG in high-grade glioma surgery appears to be the most limited of all the dyes listed above. The reasons reside in its short half-life (about 150–180 s) and in its relatively low luminous intensity [5]. In fact, Hansen *et al*. [16] demonstrated that ICG can highlight glioma cells but only at a very high dose (60 to 120 mg/kg), which significantly exceeds those used in clinics. Also, Britz *et al*. investigated in their study [17] the use of a bradykinin analogue in order to increase the fluorescence resulting from the extravasation of ICG in glioma tissue in animals, but it was not confirmed in the clinical model.

5-ALA is the only approved fluorescent probe for glioma surgery at the moment [18]. Its use is characterized by the greatest effectiveness in visualizing tumours, thanks to the preferential accumulation in cancer cells of protoporphyrin IX, which is synthesized in the mitochondria from 5-ALA after its preoperative oral administration. This behaviour is favoured by the reduced activity of ferrochelatase and/or coproporphyrinogen III oxidase in glioma. Thus, upon excitation with UV or visible blue radiations, 5-ALA allows the identification of the red fluorescent tumour [19]. However, higher costs of the procedure in combination with the need of a special neurosurgical microscope equipment and a special light filter, might be a limiting factor in its use [20].

Instead, FL has become one of the most ubiquitous probes in biological studies and it is already used in clinical practice thanks to its intense fluorescence, chemical stability, and lack of cytotoxicity at working concentrations [21]. FL absorbs blue light with a maximum absorption peak around 490 nm and emits a green light around 515 nm [21].

The development of surgical microscopes fitted with Fluorescein-specific filters (surgical microscope filter YELLOW 560 nm) has facilitated Fluorescein-guided microsurgery and the identification of tumour tissues [1]. Moreover, unlike other dyes, such as ICG, that are dispensed to patients much time before the operation, FL is administered with anaesthesia. FL thus represents an interesting alternative as it is extremely safe, it allows achieving high performance especially in deep surgical field and it has been approved for routine diagnosis [5]. In particular, the results of using this dye in neurosurgery so far show that in GBM gross total resection (GTR) was obtained in 69% of cases [22].

FL mechanism of action is related to the passive staining of the extracellular space due to the enhanced permeation and retention (EPR) effect in areas with a disrupted BBB [1]. In particular, the increased blood vessel formation caused by GBM results in the breakdown of the BBB, and these disruptions enable FL diffusion in the extracellular space. Such extravasation and selective accumulation of the dye in the affected areas facilitate the labelling of the same compromised tissues, making FL a marker of the tumour path into the healthy brain [1]. However, despite the abovementioned advantages, the intraoperative use of Fluorescein also has some limitations [5]. The most important of them results from the mechanism of the dye distribution and the lack of its specificity for cancer cells [23]. In fact, the dependence on the degree of damage to the BBB does not allow an accurate determination of the tumour borders and a reliable resection since even regions with a healthy tissue can be slightly marked as shown in Figure 1.2 [5].

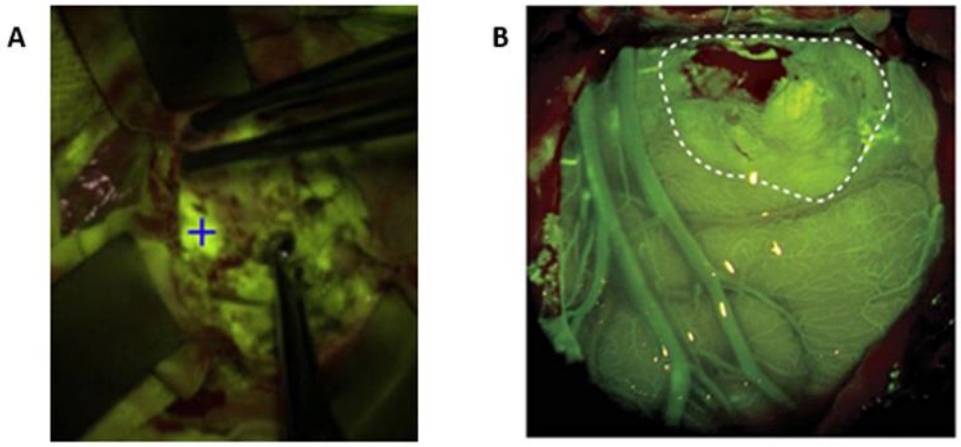

Figure 1.2: A. Bright yellow staining of recurrent tumour tissue (plus sign) [1]. B. Contrast in FL fluorescence between the tumour (area inside the dashed line) and normal surrounding tissue [24].

1.2.3. Acidosis as biomarker for tumour targeting

As explained in the previous section, most of currently available markers as FL, show low specificity for cancer tissues in the areas surrounding the tumour microenvironment upon BBB passage. In this regard, the unspecific staining of healthy and cancer tissues could compromise the success of the surgery [25]. Considering that tumours exhibit clear genetic alterations and malfunctioning metabolism [26], one of the hallmarks associated with metabolic reprogramming, namely the acidosis, could be exploited to specifically target cancer tissues during their surgical removal. With the aim to expand the concept of tumour-related acidosis, it should be stressed that, even in presence of oxygen, cancer cells use the anaerobic pathway more than normal cells do [25]. Specifically, anaerobic metabolism is associated with a high rate of glycolysis and lactic acid fermentation, resulting in the production of protons as a by-product. Additionally, cancer cells overexpress surface carbonic anhydrases, which catalyse the transformation of carbon dioxide and water into carbonic acid [25]. Thus, excessive amounts of acid and protons accumulate in the cytoplasm and tumour cells adapt to this acid-induced toxic environment by stimulating proteins that regulate the

intracellular homeostasis [26]. The cells will pump the additional acidity into the extracellular space in order to keep its intracellular pH at the physiological level, that is around 7.2 – 7.4 [25]. As the blood circulation in diseased tissues is reduced, the pH drops in the poorly perfused tumour regions in the vicinity of the plasma membrane and reaches a value of around 6.7, which is about 0.5 – 0.7 units lower than the bulk extracellular pH [27]. This means that cancer cells have a "crown of acidity" near their cell surfaces that decreases with distance from membrane and then the pH become normal in the vicinity of blood vessels [25]. So, the average pH in tissue is less informative than the pH at cellular surfaces, which might be the main target for the development of pH-sensitive agents [28]. Thus, tumour acidity might be exploited as an important predictive clinical marker of tumour aggressiveness and invasiveness both at very early and advanced stages and could be used in the design of therapeutic agents [29]. Importantly, acidosis is a property of cancer microenvironments that is found in tumours of all sizes, including metastases, and may serve as a general biomarker for targeting methods [9].

1.3. pH Low Insertion Peptide (pHLIP): a sensor of cancer acidosis

1.3.1. Peptide definition and structure

pH (low) insertion peptides (pHLIP® peptides) belong to the class of pH-sensitive membrane peptides, which can target acidic tumours and deliver imaging or therapeutic agents to cancer cells [29]. They are water-soluble peptides composed of 35 amino acids and derived from the bacteriorhodopsin C helix [30]. Being moderately hydrophobic, pHLIPs have a modest affinity for cellular membranes at normal pH, but fold and insert across the phospholipid bilayer only at low pH, allowing them to sense pH at the surfaces of cells in diseased tissues, where it is the lowest [28]. In general, peptides of the pHLIP family contain a mixture of natural and non-natural amino acids that are hydrophobic and protonatable at low pH. While the presence of hydrophobic residues (Leu or Trp) ensures the maintenance of peptide affinity to the membrane, the protonatable residues (Asp or Glu) guarantee solubility at neutral pH when they carry negative charges, or enhance hydrophobicity at low pH when the equilibrium is shifted toward protonation [28]. Specifically, pHLIPs consist of three main domains that are both flanking and transmembrane (TM) sequences (Figure 1.3). The flanking 1 sequence is characterized by an N-terminal region that varies from 3 to 20 residues and mainly consists of polar amino acids that contribute to the overall solubility of the peptide [25]. This region can also be exploited for the conjugation with cargoes destined to the extracellular space. The middle region is the transmembrane sequence that varies from 15 to 25 residues and mainly consists of hydrophobic residues, essential for the interaction with the cellular membrane. It includes also amino acids that are negatively charged at physiological pH, but it becomes neutrally charged at low pH due to protonation. Finally, the membrane-inserting flanking 2 sequence exhibits a C-terminal region that varies from 0 to 10 residues and may

contain a few additional protonatable residues, as well as residues for the conjugation with cargoes that will be delivered across the cellular membrane to the cytoplasm [25]. This region can also contribute to the solubility and affects the rates of peptide insertion/exit from the membrane. Tuning the properties of pHLIPs by sequence variations allows alteration of pharmacokinetics and targeting abilities [28].

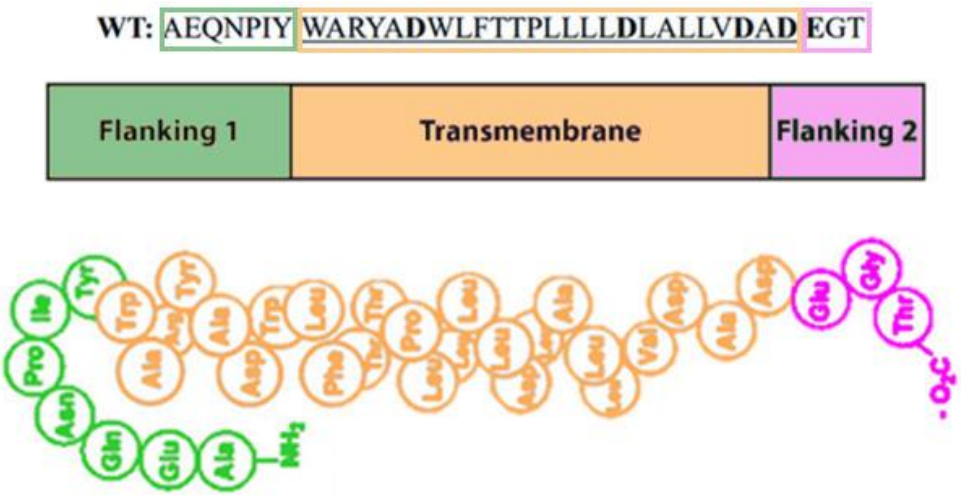

Figure 1.3: Description of pHLIP wild-type (WT) sequence [25] and structure [9].

1.3.2. Mechanism of action and dynamics of α-helix formation

The pHLIP molecular mechanism of action is mainly based on the pH-dependent membrane-associated folding and is highly triggered by the acidic microenvironment [28]. A major attribute of pHLIPs is their ability to exist in various conformations, which are dependent on peptide concentration, pH environment, and presence of lipid bilayers (Figure 1.4). Indeed, in neutral aqueous solution, pHLIP is unstructured and adopts a random coil conformation denoted as State I (Figure 1.4 a) [31]. Previous works have shown that pHLIP exists in the monomeric form up to a concentration of around 7 μM, beyond which it undergoes aggregation. As a result of the interaction with lipid bilayers, the peptide may adopt a conformation with little secondary

structure and can be superficially adsorbed onto membranes in the so-called State II (Figure 1.4 b) [31].

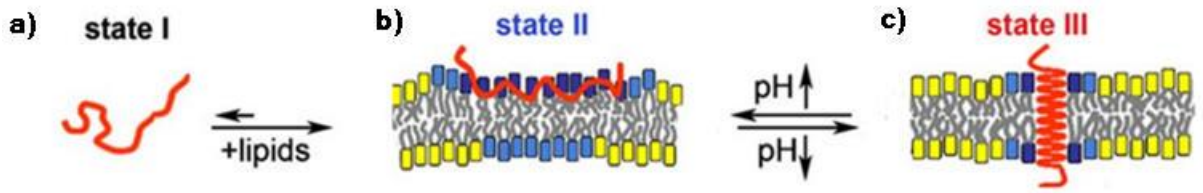

Figure 1.4: Schematic representation of pHLIP in solution and interacting with a lipid bilayer at neutral and low pH values. State I refers to the peptide in solution at normal pH. Upon addition of vesicles, the unstructured peptide is adsorbed on the membrane surface (State II). A drop of pH leads to the formation of a transmembrane α-helix (State III). Lipids directly interacting with the peptide are marked with blue head groups, lipids only influenced by the interaction have cyan head groups, and lipids that are not involved in the interaction have yellow head groups [32].

When the pHLIP encounters a healthy tissue where the extracellular pH is expected to be 7.4, the side chains of Asp and Glu and its C-terminus are deprotonated (4 Asp^-, 2 Glu^- and COO^-), and the side chain of Arg and the N-terminus are protonated (Arg^+ and NH_3^+) [33]. Carrying five net negative charges, the peptide resides at or near to the surface of the cellular membrane [25]. Even if the pHLIP creates some tension on the membrane, it cannot very deeply insert into the lipid bilayer because of the flexibility in this unstructured state [28]. Weakly bound, the pHLIP is washed away from the membrane via normal perfusion and continues circulating across the body [25].

When the pHLIP reaches a tumour tissue characterized by a lower pH, an increased concentration of protons should result in the protonation of the negatively charged residues (Figure 1.5) [28]. The protonation enhances the overall hydrophobicity of the pHLIP, which leads to an increase of the affinity of the peptide to the hydrophobic bilayer of the cellular membrane [34]. This triggers the pHLIP to spontaneously fold

and insert into lipid membranes, resulting in State III with the formation of a transmembrane helix accompanied with the release of energy (Figure 1.4 c) [29].

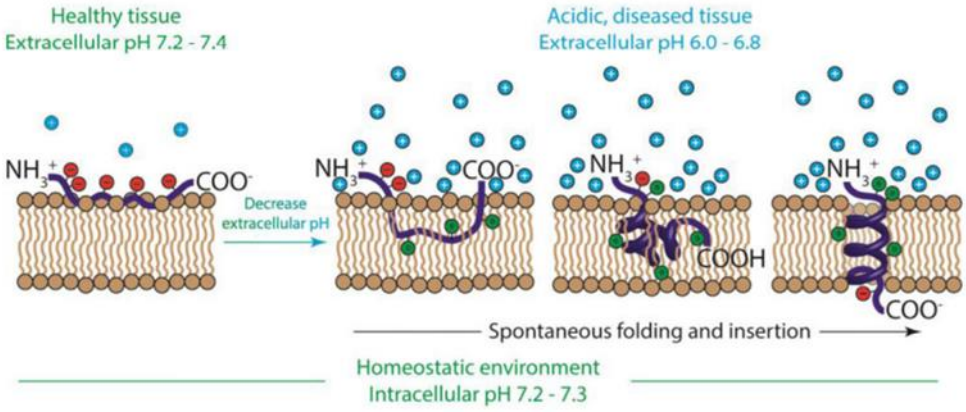

Figure 1.5: Mechanism of pHLIP insertion into the cellular membrane. When the extracellular pH is around pH 7.4, the protonatable residues of the pHLIP (red circles) remain deprotonated and negatively charged. When the pHLIP senses the low extracellular pH at the cancer cell surface, since the concentration of protons (cyan circles) is high, the protonatable residues and negatively charged C-terminal carboxyl group of the pHLIP become neutrally charged (green circles). When the C-terminal protonatable residue and carboxyl group are then exposed to the normal intracellular pH of the cell, they are deprotonated again, becoming negatively charged [25].

The peptide insertion is predominantly unidirectional as the C-terminus tends to propagate across the bilayer and come out in the cytoplasm, while the N-terminus stays in the extracellular region [33]. This is due to the fact that the propagation into the bilayer of the positively charged N-terminal at the flanking-1 end is energetically unfavourable compared to partition of the C-terminal at the flanking-2 end [28]. In fact, the positive charge is difficult to deprotonate and its passage is resisted by the membrane dipole potential [28]. When the terminal protonatable residues are then exposed to the normal intracellular pH of the cell, they are deprotonated again, becoming negatively charged and anchoring the pHLIP in the membrane [25]. A

subsequent increase of pH promotes the reverse reaction that leads to the unfolding of the helix and its exit from the bilayer interior [34].

To a first approximation, the peptide insertion into the membrane can be subdivided into two distinct steps: first the formation of an interfacial helix and then the movement of the helix across the bilayer to adopt a TM orientation [28]. The timescale for the overall process may vary from 0.1 up to 300 s [33]. However, at a more detailed level, different thermodynamic intermediate states were discovered to exist at intermediate pH values and the entire process occurs in four stages: folding, sinking, extending and positioning (Figure 1.6). In the first stage from pH 7.4 to 6.4, pHLIP folds into a bent structure in which the peptide stays laterally embedded in the outer lipid leaflet. Protonation triggers the folding not only of the C-terminal helical segment but also of the entire peptide [35]. In the second stage from pH 6.4 to 6.1, pHLIP is in a compact folded state and sinks deeply into the hydrophobic membrane interior. Thus, at pH 6.1, the whole peptide seems to be buried inside the lipid bilayer [35]. In the critical third stage from pH 6.1 to 5.8, pHLIP extends from the bent configuration and the C-terminal segment crosses the membrane reaching the other side. In this way, a transmembrane helix is formed but it is different from the final State III. In the last stage from pH 5.8 to pH 5.3, data suggest a vertical repositioning of the TM helix down across the bilayer to thread through the membrane [35].

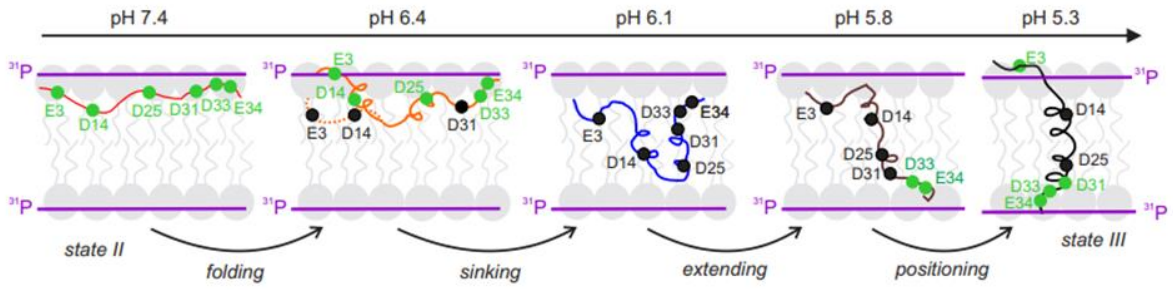

Figure 1.6: Multistage model of pHLIP insertion with distinct thermodynamic intermediates. The green dots denote D or E residues in close proximity to lipid head group phosphates; the black dots represent D or E residues farther away [35].

Considering that the affinity of the peptide for the membrane at low pH is several times higher than at neutral pH, pHLIP could be used to efficiently distinguish and mark acidic diseased tissues [36]. The insertion process is unidirectional, rapid and reversible. Importantly, unlike other membrane active peptides, pHLIP does not cause membrane leakage in any of the membrane associated states and, in addition, it has shown no toxicity to cells in many different studies [9], [37].

1.4. pHLIP as delivery system of therapeutic or imaging agents

1.4.1. pHLIP as a single-molecule transporter

The first pHLIP agent for the *in vitro* and *in vivo* targeting of acidity at the surface of cellular membranes was introduced more than a decade ago [38], [39]. As explained before, the pH-dependent behaviour and inserted conformation of pHLIPs make them useful for delivering cargoes especially to cancer cells [25]. The chemical conjugation of various cargo molecules to pHLIPs is straightforward, thanks to the presence of Lysine or Cysteine residues, as well as other chemical functional moieties, that can be easily included in the synthesis of the peptide in both flanking domains [28]. In particular, S–S disulphide bond or azide-alkyne click reaction are mainly exploited.

In detail, the inserted peptide leaves its N-terminus in the extracellular space, while the C-terminus is translocated across the membrane into the cytoplasm. Therefore, pHLIP peptides possess dual delivery capabilities to tether molecules to the surface of cancer cells or translocate polar cargo molecules across the phospholipid bilayer [29] (Figure 1.7).

In the first case, pHLIPs are employed for diagnostic imaging and fluorescence guided surgery applications [25]. A cargo molecule, such as a fluorescent imaging agent or a metal nanoparticle, is attached to the pHLIP N-terminus in order to remain on the membrane surface after the peptide insertion [30]. When conjugated to a near-IR fluorescent dye, the pHLIP imaging constructs can successfully target acidic tissues *in vivo*, including tumours, kidneys, and sites of inflammation [39]. Andreev *et al*. [15] studied the pHLIP Indocyanine green (ICG) interaction with the cell membrane *in vitro* and *in vivo* (dogs and mice). This system marked blood flow for hours after injection, and effectively delineated tumours on the day after administration. It was able to

target all malignant lesions with a specificity and a sensitivity of 100% (vs. 78.9% of white light) [15]. Also, submillimetre-sized metastatic lesions in lungs were identified by *ex vivo* imaging after intravenous administration of fluorescent pHLIP peptides [29]. Analysis of pHLIP distribution in tumours over time shows that the peptide can stay in tumours for several days, tumour borders can be determined with high accuracy and pHLIP is localized at cancer cell membranes [40]. These properties suggest that fluorescent pHLIP-based agents could be used in image guided resections of tumours during surgery. So far, pHLIP peptides tumour targeting has been demonstrated in human cancerous tissues and in more than 20 different human and murine cancer models including transgenic breast, prostate, pancreatic and skin models [15]. In particular, metastatic tumours, which have been shown to be more acidic, are labelled more effectively by pHLIP than non-metastatic ones [28].

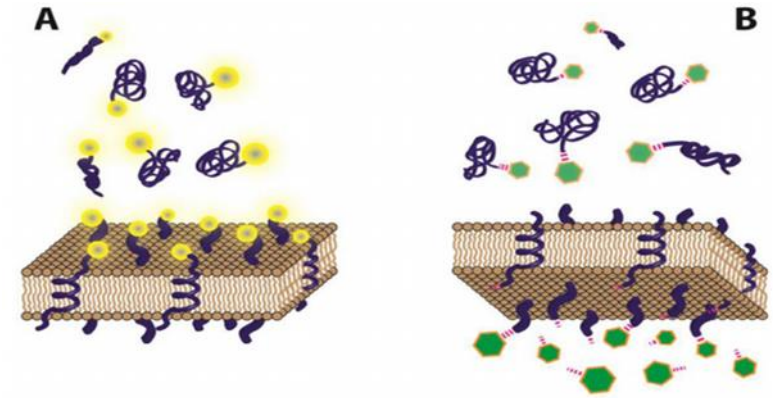

Figure 1.7: pHLIPs delivery capabilities [25]. A. pHLIP (blue) used to target and tether cargo molecules (yellow) to the surfaces of cells in low pH environments. B. pHLIP used for the intracellular delivery of translocating cargoes (green) across the membranes. These payloads are conjugated to the membrane-inserting end of the pHLIP typically via a cleavable link (magenta).

For what concerns polar cargoes translocation, the pHLIP folding across the cellular membrane under acidic conditions is exothermic (by around 2 kcal⁄mol) and the energy released is exploited to deliver otherwise cell-impermeable agents across the lipid bilayer [41]. The cargo is conjugated to the inserting C-terminus by a chemical

bond that is cleaved inside cells, releasing the attached molecule into the cytoplasm [9]. This allows the intracellular delivery of therapeutic molecules to treat primary tumour tissues as well as metastases [25]. Numerous *in vitro* and *in vivo* investigations have demonstrated that pHLIPs can deliver different payloads, such as fluorescent dyes, toxins, drugs, cyclic peptides and peptide nucleic acids [9], [25], [38]. Compared to receptor-targeted delivery of chemotherapeutic agents, this approach has some potential advantages. First of all, it is not sensitive to the heterogeneous expression of receptors or antigens among cancer cells within a tumour and then, larger amounts of therapeutic agents may be delivered per cell with respect to receptor-mediated approaches [9]. Moreover, the possible translocation of fluorescent or therapeutic agents into cancer cells is fast (seconds to minutes), pH- and concentration-dependent and can be modulated by tuning the hydrophobicity of the pHLIP inserting end [28].

Interestingly, pHLIPs do not form oligomers larger than tetramers, even at very high concentrations, a useful property for drugs to be used intravenously, as the local concentration at the injection site is generally much higher than the drug concentration when it reaches the target area, and it is crucial that the drug does not aggregate upon injection [25]. Moreover, the excellent tumour targeting efficiency of peptides conjugated with slightly hydrophobic molecules could be attributed to the stronger interactions of conjugates with plasma membranes of blood cells at neutral pH, which leads to the increase of circulation time in blood and ability to reach cancer cells [29].

Considering that pHLIPs conjugated with cell-impermeable cargoes are single-molecule transporters for direct cytoplasmic delivery into cancer cells, they represent a novel class of delivery agents [28].

1.4.2. pHLIP-mediated delivery of nanoparticles

Targeting cargoes can be conjugated to pHLIPs not only in a one-to-one ratio, but the peptides can also be used to coat nanosystems [25]. Nanoparticles (NPs), for instance, have a wide variety of uses in medical applications, including drug-loaden nanocarriers, particles that enhance another form of therapy, and therapeutic agents themselves [25]. Multiple pHLIPs on the surface of a single NP, which can range in size from a few nanometres to hundreds of nanometres, can promote pH-mediated distortion of cellular membranes, leading to the enhanced delivery of payloads [28]. Decorating NPs with multiple pHLIPs not only results in targeting specificity and greater uptake by cells in acidic diseased environments, but can also provide biocompatibility [25] and stability in solution, as a result of the overall negative charge related to the presence of the peptides onto the surface of the particles [26]. Some pHLIP-coated NPs that have been investigated are lipids (Figure 1.8 B), polymers, and metal-based nanomaterials (schematic representation in Figure 1.8 A).

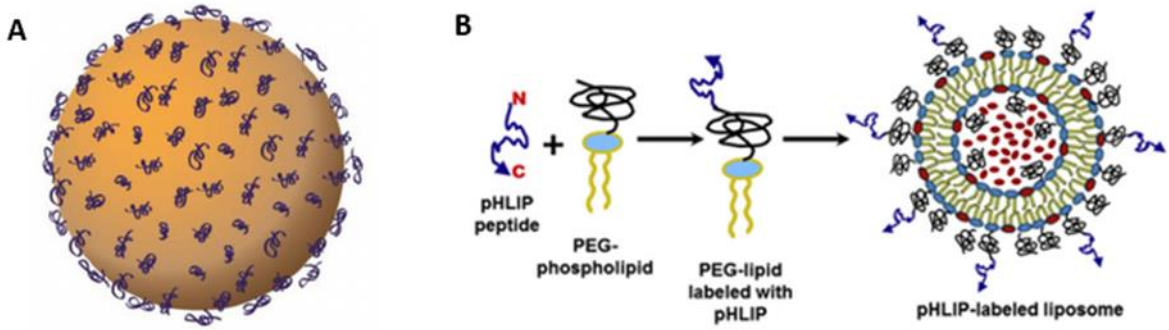

Figure 1.8: A. pHLIPs used to decorate nanoparticles [25]. B. Schematic representation of pHLIP/PEG coated liposomes with encapsulated model payload molecules (red) [42].

Among all available metal NPs, the potential of pHLIP-based gold NPs (AuNPs) in therapeutic and diagnostic cancer applications is becoming increasingly recognized for the important capability of targeting acidic tissues and inserting into cell membranes [30].

Liposomes are also widely used to encapsulate various therapeutics and diagnostic agents. Once internalized by cells, these lipid vesicles must disrupt or fuse with the endosomal membrane in order to release the payload [42]. In pHLIP-coated liposomes, the peptides promote lipid exchange and fusion between the lipid bilayer of the liposome and the cellular membrane in a pH-dependent fashion [25]. Fusion with cellular or endosomal membranes allows the direct release of polar cargos into the cytoplasm, or the transfer of hydrophobic payloads into the membrane lipid bilayer [25]. The energy of membrane-associated folding of pHLIP is utilized to bring liposomal and cellular membranes close to each other to induce lipid mixing [42]. During short incubation period, direct liposomal fusion with plasma membrane predominantly occurs, while during long incubation timing both fusion and cellular internalization through endocytosis could happen. In both cases, the first event is the insertion of pHLIP peptides into target membrane triggered by reduced pH, so pHLIP-coated liposomes represent a novel type of pH-sensitive "fusogenic" liposomes [42]. It is also possible to further optimize NPs by employing new formulations of pH-sensitive PEGylated liposomes by including pHLIP in the liposomal coating. It is useful to mask against opsonization and to increase circulation time in blood. Since extracellular acidity is associated with the development of a wide form of pathological states, pHLIP-coated liposomes could be flexibly translated to deliver and release various diagnostic and therapeutic agents to different diseases [42].

1.5. Aim of the work

In the present project, we propose the development of a specific pH-sensitive fluorescent tracer able to more selectively label cancer cells during glioblastoma surgical resection. Specifically, we aim to target the acidic tumour microenvironment by exploiting the pH-sensitive properties of pHLIP peptides, which can be directly conjugated to a Fluorescein-maleimide derivative (Figure 1.9).

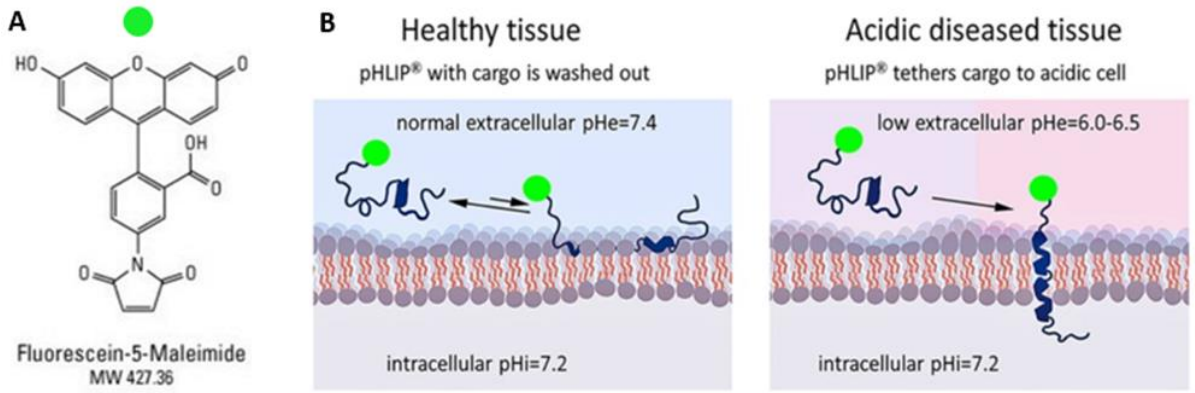

Figure 1.9: A. Structure of Fluorescein-maleimide derivative. B. Targeted pHLIP delivery of FL to acidic cell surfaces. While FL-pHLIP peptide does not accumulate in healthy tissue with physiological cell-surface pH (pH = 7.4) (left), the low pH (6.0–6.5) at the surface of a diseased tissue causes an efficient peptide insertion across the cellular lipid bilayer (right) [43].

The thermodynamics and kinetics of pHLIP-membrane interaction predict preferential accumulation in acidic tissues [28]. Since acidosis is hallmark of tumour development, progression, and aggressiveness, the proposed Fluorescein modified pHLIP should only label cancer tissues avoiding non-specific targeting. In contrast to other pH-sensitive agents, members of pHLIP family perceive pH at cell surfaces, accentuating the pH sensitivity of the peptides [25]. Considering that fluorophore-conjugated pHLIPs have shown utility in accurately identifying head and neck cancer [44], we aim to translate the developed FL-pHLIP based technology for the early identification of tissue damages also in glioblastoma (GBM). Indeed, preclinical studies with pHLIP

Indocyanine green (ICG), including pharmacology and toxicology assessments, motivate the clinical translation of the adduct for real-time blood vessels visualization and identification of cancerous lesions during surgical procedures [15]. Currently, a clinical trial on pHLIP ICG for the fluorescence-guided surgical resection of breast tumours is in progress [45]. Anyway, this system has never been studied for GBM and the choice of using FL as imaging agent may improve the treatment routine as it does not require any pre-administration. So, fluorescence-guided surgery of glioblastoma exploiting FL-pHLIP technology could ease the challenges of tumour resection, such as visualization of all cancerous lesions, including flat lesions, ultimately reducing the number of surgeries and the tumour recurrences.

More in detail, the proposed project can be divided into three phases:

I. Production of the Fluorescein-maleimide derivative chemically conjugated to a Cys residue on the N-terminal end of the pH-sensitive pHLIP peptide. This step is performed in collaboration with Dr. Alessandro Gori from National Research Council (CNR).

II. The chemical-physical characterization of the system in physiological and acidic environment is combined to the investigation of its folding properties in presence of cellular membrane models. In particular, we study a peptide derivative called pHLIP WT (AEQNPIY WARYADWLFTTPLLLLDLALLVDA D EGT) which was used as control and a FL-modified pHLIP (A**C**EQNPIY WA RYADWLFTTPLLLLDLALLVDAD EGT) containing the fluorescent dye at the N-terminus. The following aspects are analysed:

   - evaluation of pHLIP solubility, stability and self-assembly;
   - (FL-)pHLIP interaction with liposomes as a mimic cellular membrane model;
   - quantitative evaluation of inserted FL-pHLIP across the lipid bilayer;

- (FL-)pHLIP interaction with in-flow cellular membrane models.

III. *In vitro* investigation of FL-pHLIP labelling efficacy in glioblastoma through tests on patient-derived glioblastoma cells, in collaboration with Dr. Francesco Acerbi and Dr. Serena Pellegatta from Carlo Besta Neurological Institute. In detail, the cellular tolerance of the proposed system is evaluated in combination to the cancer-targeting efficacy. For this purpose, FL-pHLIP is tested at different concentrations on different glioblastoma cell lines (derived from patients) at both acidic and physiological pH conditions. A scrambled peptide (SC-FL pHLIP) is used as control. SC-FL pHLIP is modified in the transmembrane domain in order to be not pH-sensitive.

2 Materials and Methods

2.1. General overview

All the materials and procedures employed to fully characterize both WT and FL-pHLIPs are described below. First, we proposed a solubilization protocol suitable for both systems and UV-Visible (UV-Vis) spectroscopy was then exploited to verify its efficacy and reproducibility. Then, self-assembly properties and peptides stability over time were studied by Dynamic Light Scattering (DLS) analysis. At this point, liposome-based systems were introduced as a simplified model of eukaryotic cells membrane to thoroughly study peptide-membrane interactions. The efficiency and dynamics of pHLIPs insertion into the membranes were evaluated through Circular Dichroism spectroscopy. In detail, we studied pHLIPs three-dimensional conformation after lipid interactions. Importantly, the insertion efficiency was also confirmed by the intrinsic tryptophan fluorescence analysis. The amount of inserted FL-pHLIP was quantified through UV-Vis analyses on liposomes, which had been previously purified from the excess of unbound peptide by means of a Sephadex (G-25) column. After this first characterization reached thanks to an elementary model, we proposed an in-flow mimic model system to further study the FL-pHLIP sensitivity in a context closer to the cellular environment. For this purpose, we developed supported lipid bilayers (SLBs) as model of cell membrane and a quartz crystal microbalance with dissipation (QCM-D) monitoring was used to study the interaction between pHLIPs and SLBs. Finally, *in vitro* evaluation of FL-pHLIP tolerance and labelling efficacy in patient-derived glioblastoma cells was presented.

2.2. Materials

2.2.1. Solvents

Dulbecco's Phosphate - Buffered Saline 0.1 M pH 7.4 (DPBS, Corning); Phosphate buffered saline 0.1 M pH 6.5 (PBS, prepared with H_2NaO_4P and HNa_2O_4P in deionized water according to Henderson–Hasselbalch Equation (2.1));

$$pH = pK_a + log_{10}\left(\frac{[Salt]}{[Acid]}\right) \quad (2.1)$$

Acetate buffer 0.1 M pH 5.2 (prepared with $C_2H_3NaO_2$ and $C_2H_4O_2$ in deionized water according to Henderson–Hasselbalch equation); TRIS buffer 0,1 M pH 6.5 (prepared from TRIS powder, ≥99.8%, Bio Rad, in deionized water); Acetic acid ($C_2H_4O_2$, ≥99.7%, ACS reagent, Sigma Aldrich); Chloroform ($CHCl_3$, ≥99.5%, Sigma Aldrich); Water ultrapure Type-I Milli-Q Water provided by a Simplicity® water purification system.

2.2.2. Materials and reagents

All pHLIP peptides (WT: AEQNPIY WARYADWLFTTPLLLLDLALLVDAD EGT; FL-derivative: ACEQNPIY WARYADWLFTTPLLLLDLALLVDAD EGT, and SC-FL construct: ACEQNPIY WARYAKWLFTTPLLLLKLALLVDAK EGT) were kindly synthesized by Dr. Alessandro Gori from National Research Council (CNR); Sodium phosphate monobasic (H_2NaO_4P, ≥98%, BioReagent, Sigma Aldrich); Sodium phosphate dibasic (HNa_2O_4P, ≥99%, ACS reagent, Sigma Aldrich); Sodium acetate ($C_2H_3NaO_2$, ≥99%, analytical reagent, Prolabo); Calcium chloride ($CaCl_2$, ≥97%, Sigma Aldrich); 1,2-dioleoyl-sn-glycero-3-phosphocholine (18:1 (Δ9-Cis) PC (DOPC), MW 786.113 g/mol, Avanti Polar Lipids, USA).

2.3. Methods

2.3.1. pHLIP solubilization and UV-Visible analysis

Before performing any analysis, pHLIP WT or FL-pHLIP were firstly dissolved at physiological pH in PBS 0.1 M, which is a buffer commonly used for biological applications. The optimized solubilization procedure turned out suitable for both systems and it consisted in the following experimental steps:

1) Dissolution of the peptides in PBS by vortexing in order to prepare a 100 μM stock solution.
2) The resulting solution was heated at 35 °C for 30 minutes and fully dissolved using an ultrasonic bath (5 minutes at 59 kHz).

The correct solubilization was then verified through UV-Vis spectroscopy. In this technique, a spectrophotometer measures the intensity of light that passes through a sample (I), and compares it to the intensity of light before it crosses the specimen (I_0). The ratio I/I_0 is called the transmittance and based on its percentage value (%T), the absorbance (A) can be calculated from Equation (2.2):

$$A = -\log(\%T/100\%) \tag{2.2}$$

Absorption takes place when a photon has sufficient energy for an electronic transition to occur and since the energy levels are specific to each material, the same is true also for the absorption spectrum. Within a certain range of concentrations and in the presence of monochromatic radiation, the absorbance follows Lambert-Beer Law (2.3):

$$A_\lambda = \varepsilon_\lambda \cdot l \cdot C \tag{2.3}$$

In particular, Lambert-Beer law states that the absorbance of a solution at a specific wavelength (A_λ) is directly proportional to the molar concentration of the absorbing

species (C) and the optical path length (l). Here, ε_λ represents the molar attenuation coefficient and it can be calculated in linear regression by performing UV-Vis analysis at different concentrations in order to obtain a calibration curve. For a properly solubilized sample, the molar attenuation coefficient must be kept constant throughout the concentrations range. Thus, knowing ε_λ and for a fixed optical path, UV-Vis spectroscopy can be used to determine the concentration of the absorber in solution. In this way, each time that a new pHLIP stock solution was prepared it was possible to verify that it contained the expected and calculated amount of peptide.

2.3.1.1. pHLIPs calibration curve

Based on the spectroscopy technique previously described, pHLIPs UV-Vis profile was characterized in detail as follows. WT peptide absorbance (Abs) was studied in the range between 200 and 500 nm with a maximum signal detected at 280 nm. With the aim to obtain a calibration curve, UV-Vis analysis of pHLIP WT was performed on five distinct dilutions ranging from 18.7 to 100 μM. FL-pHLIP Abs was detected in the same spectral range (200 - 800 nm) with a maximum signal detected again at 280 nm. In this case, the calibration curve was obtained analyzing five distinct concentrations ranging from 5 to 15 μM. Each measure was performed in triplicate in order to reach a proper statistical significance. For both WT and FL- peptides, the experimental points collected at a wavelength of 280 nm were imported to Excel and elaborated through a linear fitting, as shown in Figure 2.1.

The same experimental set-up was exploited to quantify the amount of inserted fluorescent peptides into membrane-mimic liposomes, as explained in the following sessions (2.3.6.3.).

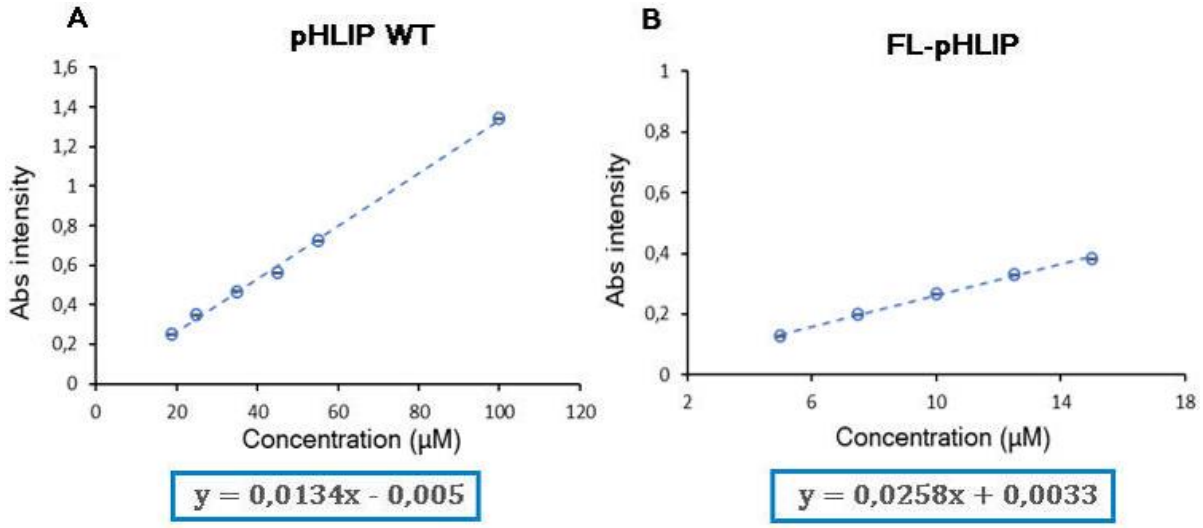

Figure 2.1: pHLIP WT (A) and FL-pHLIP (B) calibration curves at 280 nm and pH 7.4. The obtained fitting linear curves (dashed lines) are characterized by an R^2 value of 0.9978 (A) and 0.9971 (B).

2.3.2. Dynamic Light Scattering

In order to characterize pHLIPs self-assembly and colloidal stability in solution, peptides were analyzed by Dynamic Light Scattering (DLS) technique. This method, also known as Photon Correlation Spectroscopy (PCS), allows to determine the size distribution profile of small particles by measuring their Brownian motion. In a DLS experiment, temporal fluctuations of the light scattered by the sample are analyzed. In particular, a monochromatic and coherent light beam hits the specimen and the particles present in the dispersion scatter the light in all directions depending on their size and shape. The intensity of the scattered light is collected by a detector and the screen will show a speckled pattern consisting of areas of bright light where constructive interference occurs and dark areas where no light is detected due to destructive interference. Since particles in solution move following random trajectories caused by collisions with the molecules of the solvent, the intensity of the scattered light will change over time. Smaller particles move faster and so the

frequency of the fluctuations is higher, while for larger particles the correlation between different displacements disappear at higher times (Figure 2.2).

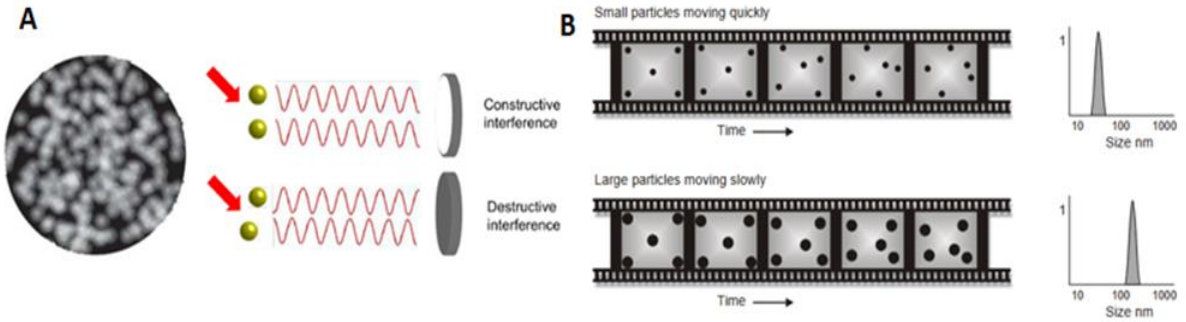

Figure 2.2: A. Speckled pattern with bright areas of constructive interference and dark areas of destructive interference. B. The particles in a liquid move about randomly and their motion speed is used to determine the size of the particle [46].

Therefore, the DLS instrument is used to obtain the diffusion coefficient (D_0) of particles in a solution and from the Stokes-Einstein Equation (2.4), it is possible to determine the hydrodynamic radius (R_H) of a NP if the viscosity of the solvent (η), the temperature and the Boltzmann constant (K_B) are known:

$$D_0 = \frac{K_B T}{6\pi\eta R_H} \tag{2.4}$$

More in detail, DLS measures the normalized time correlation function of the scattered intensity, and the temporal fluctuations of light are elaborated by a digital autocorrelator in order to get the diffusion behavior of nanoparticles in the sample and estimate their size. When we have a monodispersed sample, the correlation function can be expressed as an exponential decaying function. Instead, if the sample is polydispersed, each particle has an own exponential decay correlation function and different algorithms can be used to derive the nanoparticles size.

Specifically in this project, DLS was useful to identify if proteins formed aggregates as the resulting size should have been higher. Data were collected by means of the ALV-

Correlator software and analyzed according to standard procedures that use CONTIN algorithm to apply the Laplace inversion of the time auto-correlation functions through a non-cumulant method. Single angle (90°) DLS was measured with the ALV compact goniometer system, equipped with ALV-5000/EPP Correlator, special optical fiber detector and ALV/GCS-3 Compact goniometer. A He-Ne laser (λ = 633 nm, 22 mW output power) was used as light source and the temperature was controlled through a thermostatic bath set at 25° C.

For both WT and FL- pHLIPs stability assay, 90° DLS measurements were performed on 0,8 mL of 5 μM peptide solution at different pHs (7.4, 6.5 and 5.2) and different time points (T_0, 30 min, 1 h, 2 h and 24 h). In detail, peptide stock solution (100 μM) was diluted 1:20 v/v in 0.1 M Acetate buffer or 0.1 M PBS to perform analyses at pH 5.2 and 6.5 – 7.4, respectively. Each measure was run for 5-10 seconds, with a threshold sensibility of 10% and the apparent hydrodynamic radius was estimated through an intensity unweighted fitting of the auto-correlation function.

2.3.3. Liposomes preparation

As first step to verify pHLIP membrane-insertion properties and to be sure that these features were maintained even after FL-conjugation, we proposed liposomes as suitable model to study peptide-lipid interaction.

Liposomes are small artificial spherical vesicles composed by at least one lipid bilayer. Being constituted by an aqueous solution core that is surrounded by a hydrophobic membrane, liposomes may represent a simplified model of eukaryotic cells phospholipid bilayer. Due to their hydrophobicity and/or hydrophilicity, biocompatibility, particle size and many other properties, liposomes can also be used as drug delivery vehicles for the administration of pharmaceutical drugs and nutrients [47].

For our experiments, liposomes were prepared in the form of large unilamellar vesicles (LUVs) by extrusion. In detail, DOPC (20 mg) was dissolved in 1 mL of chloroform and the solvent was removed by rotary evaporation at 30°C in order to produce an even thin film. The hydration of the dry lipid film was accomplished by adding 1 mL of PBS 0.1 M at pH 7.4 or Acetate buffer 0.1 M at pH 5.2 depending on the application. Freeze-thaw cycles were repeated 5 times by dipping the hydrated film in liquid nitrogen and then heating the solution at 50°C in order to break the multilayer structures and form unilamellar vesicles only. The resulting liposome solution was initially extruded through 200 nm polycarbonate filters, and then 100 nm ones were used (11 times/each filter). To verify the correct formation of liposomes, 90° DLS analysis was performed on samples previously diluted 1:50 v/v in the same hydration buffer. Finally, the liposomes solution obtained was stored at +4°C.

2.3.4. Circular Dichroism spectroscopy

The interaction of WT and FL- pHLIPs with DOPC liposomes was first analyzed by Circular Dichroism (CD), which allowed to estimate the peptides three-dimensional conformation and therefore, to verify their pH-dependent penetration into the lipid bilayer.

CD is a spectroscopic technique that measures the differential absorption between left (L) and right (R) circularly polarized light. Circular polarization of light occurs when the electric field vector rotates counterclockwise (L) or clockwise (R) about its propagation direction, while magnitude remains constant. Only chiral molecules are CD active because left circularly polarized (LCP) and right circularly polarized (RCP) light are themselves not superimposable. During a CD experiment, equal amounts of LCP and RCP light of a selected wavelength are alternately radiated into the sample. When circularly polarized light passes through an absorbing optically active medium, the speeds between R and L polarizations differ as well as the extent to which they are

absorbed. The instrument measures the difference in absorbance (ΔA) between LCP and RCP, and the molar circular dichroism (Δε) can be calculated from Lambert-Beer Law (2.5) by knowing the sample concentration (C) and the optical pathlength (l):

$$\Delta\varepsilon = \varepsilon_L - \varepsilon_R = \frac{\Delta A}{C \cdot l} \tag{2.5}$$

Although ΔA is usually detected, for historical reasons most measurements are reported in degrees of molar ellipticity [θ] (Equation 2.6):

$$[\theta] = 3298.2 \cdot \Delta\varepsilon \tag{2.6}$$

In many practical applications of circular dichroism, the measured CD is not simply an intrinsic property of the molecule, but rather depends on molecular conformation, temperature, concentration, and chemical environment, including solvents. Most notably, CD signals typically in the far UV region (240-180 nm) can be used to investigate the secondary structure of peptides thanks to their characteristic spectral profiles (Figure 2.3 A-B).

CD spectra can be readily used to estimate the fraction of a protein that is in the alpha-helix, in the beta-sheet, in the beta-turn, in the random coil or in some other conformation [48]. This technique gives less specific structural information than X-ray crystallography and protein NMR spectroscopy, as it cannot predict the location of the different conformations within the molecule. However, CD spectroscopy is a valuable and quick method, especially for showing changes in conformation, that does not require large amounts of proteins or extensive data processing.

As explained in the introduction chapter (see Section 1.3.2.), pHLIP is characterized by the formation of distinct thermodynamic intermediates during its insertion through the membrane and each peptide state is associated with a specific secondary structure detectable by CD-analysis [49]. In aqueous solution, pHLIP WT shows a characteristic

CD-spectrum of an unstructured peptide with a single minimum at around 200 nm (StateI, Figure 2.3 C). Instead, a spectrum with a double minimum around 208 and 222 nm is characteristic of α-helix configuration, typical of State III (Figure 2.3 C) [49].

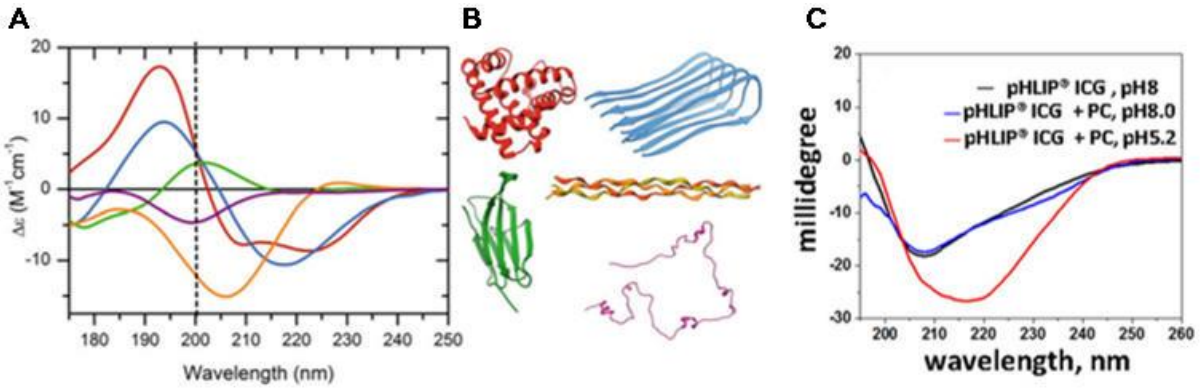

Figure 2.3: A. Characteristic far-UV CD spectra of different protein architectures. B. Proteins of distinct secondary structures such as α-helix (red), parallel β-sheet (blue), antiparallel β-sheet (green), polyproline-helix (orange), and disordered chain (purple) [48]. C. CD spectra of pHLIP ICG measured in phosphate buffer at pH 8 in absence (black) and presence (blue) of POPC liposomes, and at pH 5.2 in the presence of POPC liposomes (red) [15].

In this work, CD measurements were performed by a Jasco® j-815 CD spectrometer. Following the procedure described by T. Crawford *et al*. [15], CD spectra were recorded in a wavelength range between 200 and 260 nm, with steps of 1 nm and a scanning speed of 100 nm/min. Solutions containing 5 μM pHLIP WT and 750 μM DOPC liposomes were measured at different pH values (7.4, 6.5 and 5.2) against a buffer baseline. The analysis at pH 5.2 was repeated at different time points (T_0, 20 min, 40 min, 50 min and 70 min). In particular, peptide stock solution (100 μM) was diluted 1:20 v/v in 0.1 M Acetate buffer or 0.1 M PBS to perform analyses at pH 5.2 and 6.5 – 7.4, respectively. In the same way, solutions containing 5 μM FL-pHLIP and 750 μM DOPC liposomes were measured at different pH values (7.4, 6.5 and 5.2) and different time points (30 min, 2 h and 4h) against a buffer baseline. All measurements were the result of the average of 10 acquisition runs.

2.3.5. pHLIP intrinsic tryptophan fluorescence

To further confirm WT or FL- pHLIP insertion into liposome membranes, we exploited the intrinsic fluorescence of the tryptophan (TPH, W) residues that are present in the peptides transmembrane sequence (See Figure 2.4 A).

Fluorescence is the emission of light by a substance that has absorbed electromagnetic radiation. When a molecule absorbs light, the energy of photons excites electrons, which are raised to a higher energy state. The subsequent return to the ground state results in a re-emission of photons that are characterized by a higher wavelength, and therefore a lower energy, due to the heat dissipated by vibrational relaxation. This causes the light that is emitted to be a different color than the light that is absorbed. The fluorescent signal can be detected by a fluorimeter, an instrument able to measure the intensity and wavelength distribution of the emitted radiation after excitation by a certain spectrum of light.

In the case of pHLIPs, the partitioning of the peptides into the lipid bilayer can be investigated through the shift in the position of the TPH intrinsic fluorescence spectral maximum at lower pH values. In particular, by reducing the pH the pHLIP peptide passes from State I to State II and State III, resulting in an environmental change around the inserting transmembrane region. With the increasing burial of tryptophan residues inside the lipid bilayer, a decrease in the wavelength of maximum emission and a less effective quenching of TPH fluorescence are observed, as the environment become more hydrophobic (See Figure 2.4). The position of the fluorescence spectral maximum (λ_{max}) can be calculated from Henderson–Hasselbalch Equation (2.7):

$$\lambda_{max} = \lambda_{2max} + \frac{\lambda_{1max} - \lambda_{2max}}{1 + 10^{pH - pK_a}} \tag{2.7}$$

where λ_{1max} and λ_{2max} are the fluorescence maximal wavelengths at the beginning and at the end of the transition, respectively, and pK_a is the midpoint of the transition.

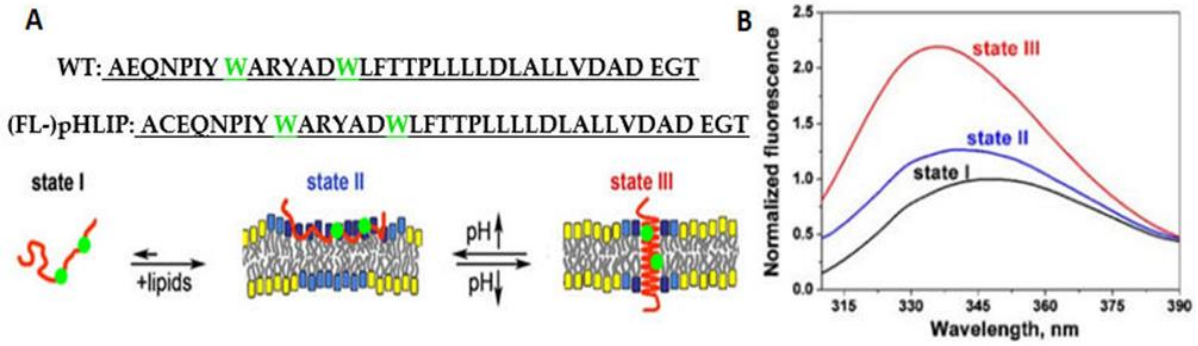

Figure 2.4: A. Schematic representation of the increasing burial of tryptophan residues (green) into the lipid bilayer passing from State I to State II and State III. B. Fluorescence spectra of pHLIP alone at pH 8 (black line), with liposomes at pH 8 (blue line) and with liposomes at pH 4 (red line) [32].

In the present work, WT or FL- pHLIP fluorescence spectra were recorded from 310 to 400 nm using an excitation wavelength of 280 nm. Solutions containing 5 μM pHLIP and 750 μM DOPC liposomes were measured at different pHs (7.4, 6.5 and 5.2). In particular, the peptide stock solution (100 μM) was diluted 1:20 v/v in 0.1 M Acetate buffer or 0.1 M PBS to perform the analyses in an acid environment (pH = 5.2) or at pH 6.5 - 7.4, respectively.

2.3.6. Quantification of inserted FL-pHLIP into purified liposomes

In order to better quantify the amount of inserted FL-pHLIP into liposomes, it was possible to remove the unbound peptide to the membrane and compare the final FL-pHLIP concentration to the starting amount by performing UV-Vis analysis.

2.3.6.1. Purification by Sephadex G-25 column

Liposomes incubated with FL-pHLIP were purified from the non-interacting peptides by following the gravity protocol of a PD-10 Desalting Column containing Sephadex G-25 resin (exclusion limit Mr 50000). This size-exclusion chromatography technique allows the rapid group separation of high molecular weight from low molecular weight compounds, according to their difference in size. Separation occurs because of

porous beads packed in a column. Molecules smaller than the largest pores in the Sephadex matrix will penetrate the cavities to varying extent, increasing their retention time. They have a larger accessible column volume than the large molecules and therefore they will elute last. Conversely, larger analytes are more easily excluded from the matrix and then are eluted first. All columns have a range of molecular weights that can be separated. If a molecule is too large it will not be retained, while if the analyte is too small it may be retained completely. Conforming to this principle, the excess of FL-pHLIP that did not interact with liposomes can be removed since, being smaller in size, it will take more time to exit the column, while the liposomes will exit first (Figure 2.5).

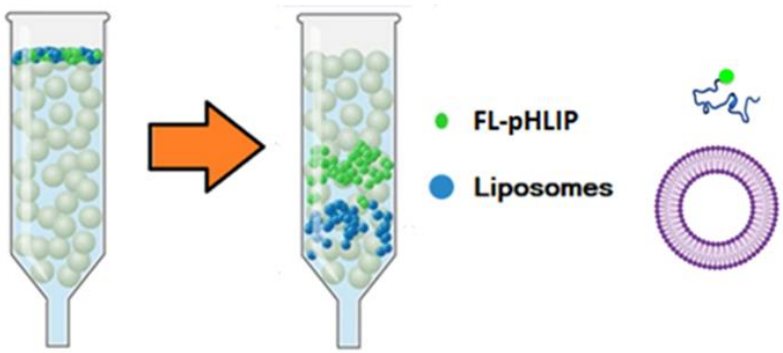

Figure 2.5: Schematic representation of free FL-pHLIP (green) and liposomes (blue) separation by column chromatography.

In detail, DOPC liposomes solution (750 μM) was incubated with FL-pHLIP (5 μM) for different timings (30 min, 2 h and 24 h) and at different pH values (7.4, 6.5 and 5.2). A final volume of 1 mL incubating solution was intended for the analysis. For the purification procedure, about 25 mL of equilibration buffer (0.1 M Acetate buffer or 0.1 M PBS) was added to enter and completely wash the packed bed of the Sephadex G-25 column. Then, the samples were diluted in order to reach a final volume of 2.5 mL (dilution factor = 2.5) that passed through the column by gravity force. Finally, equilibration buffer was added again to completely elute the sample. The eluate was

collected in fractions of 1 mL and analyzed by DLS in order to select only the samples containing liposomes.

2.3.6.2. Concentration procedure

The selected fractions were then pooled and concentrated using Amicon® Ultra centrifugal filters (50 kDa cutoff) in order to reach the original volume of the sample (1 mL). Driven by centrifugal force, solvent and microsolutes were cleared through the ultrafiltration membrane and into a filtrate container positioned below. Separation in centrifuge was performed for 10-15 minutes at 4000 rpm and 25°C. After concentration, colloidal stability of collected samples was ensured by DLS analyses.

2.3.6.3. UV-Vis analysis

The amount of embedded fluorescent peptide was quantified through the UV-Vis detection of Fluorescein before and after liposomes purification by Sephadex G-25 column. Thus, FL-pHLIP concentration was estimated according to Lambert-Beer Law as explained in the previous sections (See Equation 2.3). In detail, the calibration curve was obtained analyzing distinct FL-pHLIP solutions at different range of concentrations depending on the considered pH value (as reported in Table 2.1).

pH	pHLIP [range], μM	Buffer
5.2	10 - 20	Acetate buffer 0.1 M
6.5	1 - 10	PBS 0.1 M

Table 2.1: Parameters considered to obtain FL-pHLIP calibration curve by UV-Vis analysis.

The experimental points collected at a wavelength of 495 nm (for pH 6.5) and 458 nm (for pH 5.2) were imported to Excel and elaborated through a linear fitting, as shown in Figure 2.6.

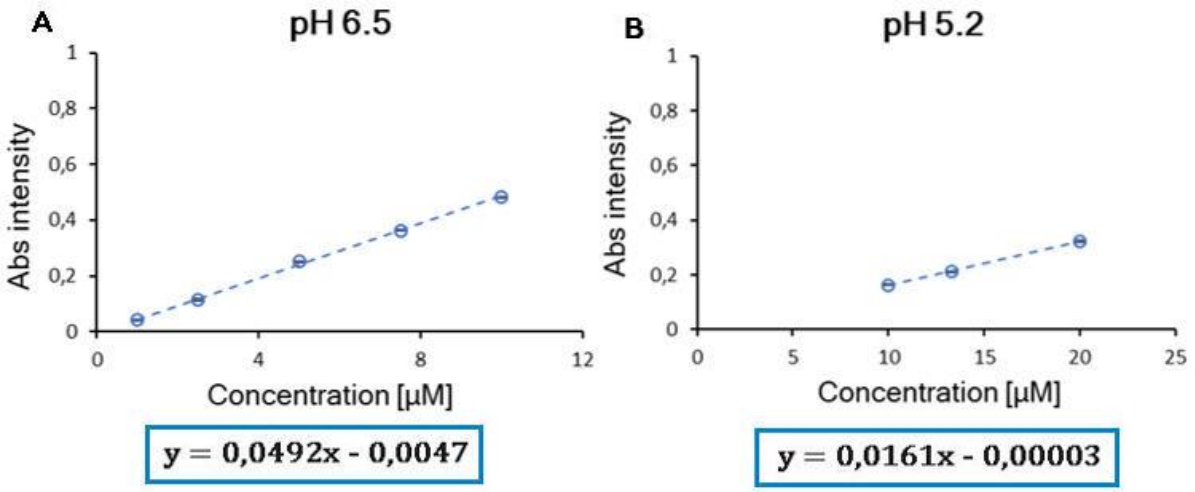

Figure 2.6: FL-pHLIP calibration curve at pH 6.5 (A) and 5.2 (B). The obtained fitting linear curves (dashed lines) are characterized by an R^2 value of 0.999 (A) and 0.9985 (B).

The percentage of inserted peptide was then calculated from Equation (2.8):

$$Inserted\ peptide\ [\%] = \frac{[pHLIP]_{pre}}{[pHLIP]_{post}} \cdot 100 \qquad (2.8)$$

where $[pHLIP]_{pre}$ and $[pHLIP]_{post}$ represent the peptide concentration before and after sample purification, respectively.

2.3.7. Quartz Crystal Microbalance analysis

With the aim to investigate the FL-pHLIP sensitivity in a context closer to the cellular environment, we optimized an 'in-flow' membrane-mimic model by exploiting supported lipid bilayers (SLBs). SLBs are planar structures formed from the rupture of lipid vesicles, and can be deposited on a silicon-coated gold chip in order to perform quartz crystal microbalance with dissipation (QCM-D) analysis. QCM-Ds are based on the transduction mechanism that resides in the piezoelectric properties of a quartz. In particular, alternating current induces vibration of a quartz crystal that changes depending on the mass that is deposited on it. In fact, when molecules are deposited

the mass increases and the frequency of vibration decreases, while the dissipation is enhanced due to the release of a higher amount of energy (Figure 2.7).

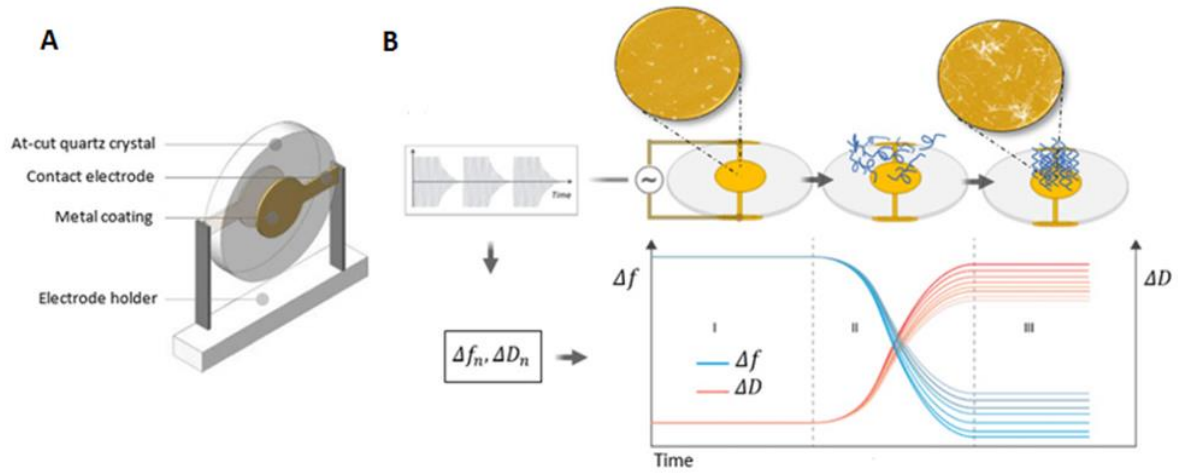

Figure 2.7: A. Basic scheme of QCM-D sensor consisting of a piezoelectric quartz crystal coated with two gold electrodes, one on each side. B. Schematic working principle providing information on variations in frequency (f) and dissipation (D) plotted as molecules become adsorbed on gold sensor surface [50].

When solutions containing the analytes are insufflated, QCM-D is able to measure in real-time both dissipation (ΔD) and frequency changes (Δf), associated to the rigidity of the system and to the deposition of matter (Δm) on the sensor surface, respectively. Thus, it is possible to perform a quantitative analysis according to the Sauerbrey Equation (2.9):

$$\Delta f = -\frac{2f_0^2}{A\sqrt{\rho_q \mu_q}}\Delta m \qquad (2.9)$$

where ϱ_q and μ_q are the density (2.648 g·cm^{-3}) and shear modulus of quartz (2.947 × 10^{11} g·cm^{-1}·s^2), respectively, f_0 is the unloaded crystal frequency, and A is the crystal piezoelectrically active geometrical area, defined by the area of the deposited metallic film on the crystal. Therefore, this technique allows the detection of very small changes (in the order of fractions of a nanogram) at the solution-quartz interface due to

variations in the adhered mass during the flow and its viscoelastic characterization. In our particular case, it was possible to evaluate pHLIP-SLB interaction and thus quantify the amount of peptide that would insert across the bilayer.

In detail, the deposition of the lipid substrate onto the QCM-D chip included the following steps:

1) Insufflation of buffer solution at physiological pH for 5 minutes.
2) Vesicles break was induced by adding 3 mL of calcium chloride to an equal volume of DOPC liposome solution (750 μM). The resulting mixture was then insufflated for 8 minutes in order to form the solid lipid bilayer.
3) PBS 0.1 M was introduced again for 5 minutes.
4) To remove the excess of lipid and stabilize the bilayer, a 5-minutes flow of MilliQ water was followed by 15 minutes in PBS 0.1 M.

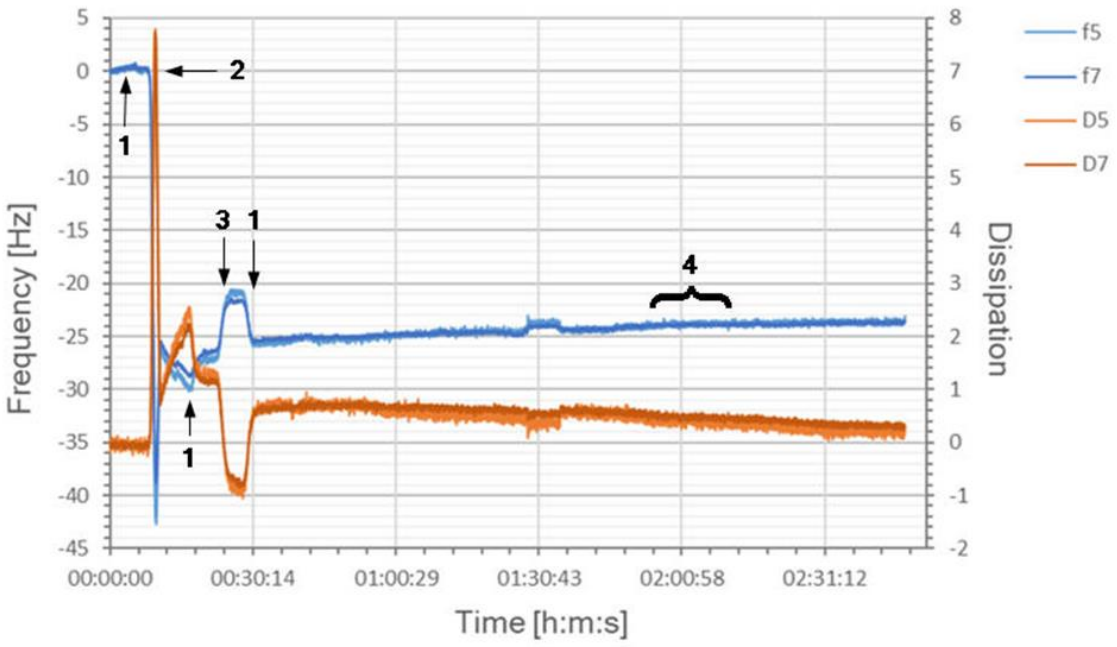

Figure 2.8: Representative QCM-D measurement for the formation of a SLB formed by DOPC liposomes at pH 7.4: dissipation (red line) and frequency (blue line). The numbers indicate the flow of the following solutions: 1 = PBS 0.1 M pH 7.4, 2 = Liposomes solution + $CaCl_2$, 3 = MilliQ water, 4 = Static mode (no flow).

A unilamellar SLB is properly formed if the frequency reaches a value of around -25 Hz with an associated dissipation below 1 and tending to 0 for a more rigid system [51] (See Figure 2.8 above). The superimposition of the different harmonics also confirms the rigidity of the system. After the SLB formation, for optimizing the environment for the study of the pHLIP interaction, another 5-minutes flow of MilliQ water was followed by 15 minutes with the buffer used for QCM-D study. In particular, 0.1 M Acetate, 0.1 M TRIS buffer and 0.1 M PBS were used for analyses at pH 5.2, 6.5, and 7.4, respectively.

Lastly, the peptide solution was injected and insufflated for a specific timing. After that, the pump was switched off to leave the system in static incubation. In the end, a final wash in the proper buffer was performed. The procedure details are reported below.

pHLIP WT – Experimental conditions				
Concentration	**pH**	**Peptide flow**	**Static incubation**	**Final buffer wash**
• 5 μM • 0.5 μM	• 7.4 • 6.5 • 5.2	• 15 min • 30 min	• 15 min • 30 min	• 15 min • 30 min

Table 2.2: Experimental conditions used for QCM-D measurements of DOPC SLBs treated with solutions of pHLIP WT.

FL-pHLIP – Experimental conditions				
Concentration	**pH**	**Peptide flow**	**Static incubation**	**Final buffer wash**
• 0.5 μM	• 7.4 • 6.5 • 5.2	• 15 min	• 15 min	• 15 min

Table 2.3: Experimental conditions used for QCM-D measurements of DOPC SLBs treated with solutions of FL-pHLIP.

2.3.8. *In vitro* cellular tests

FL-pHLIP tolerance and labelling efficacy were finally evaluated *in vitro* on patient-derived glioblastoma cells in collaboration with Dr. Francesco Acerbi and Dr. Serena Pellegatta from Carlo Besta Neurological Institute. Specifically, three distinct glioblastoma primary cell lines with different metabolic alterations were kindly provided by Dr. Pellegatta (See Table 2.4).

Cell lines	Subtype description
BT 592	Proliferative
BT 1007	Mesenchymal
GBMR16-NS	Cells derived from cancer recurrence; proneural/mesenchymal

Table 2.4: Description of tested cell lines.

For cell maintenance culture medium Dulbecco's Modified Eagle Medium (DMEM, Lonza Bioscience, Italy) was supplemented with 10% fetal bovine serum (FBS, Lonza Bioscience, Italy), 100 mg/ml of streptomycin, 100 U/ml of penicillin and 2 mM of L-glutamine (Gibco-Invitrogen). To prepare the acidic environment, the selected cells were grown in a glucose-enriched medium for several days. Thus, their metabolic activity was enhanced and it caused a reduction of the extracellular pH. The acid culture medium, thus obtained, was then collected, stored at -20°C and used at the time of the cellular experiment.

In particular for FL-pHLIP cellular staining, cells were seeded at a density of 100k cells/well in a 12-well plate and incubated with the peptide for 2 hours at different concentrations (0.5 μM, 5 μM, and 10 μM). Both acid (pH 6.4 – 6.7) and physiological conditions (pH 7.2 – 7.4) were investigated. Labelled cells were then collected and washed in abundant culture medium (3 × 1000 rpm for 5 min) in order to remove the excess of unbound peptide. After labelling, cell viability, and thus pHLIP tolerance,

was evaluated through 7-Aminoactinomycin D (7-AAD) staining by Flow cytometry assay (FACS). The amount of inserted fluorescent peptide was evaluated by quantifying the mean fluorescence index of cells positive to pHLIP through FACS analysis.

As a control, a scrambled peptide (SC-FL pHLIP) that was not pH-sensitive was kindly produced by Dr. Alessandro Gori from National Research Council (CNR). In detail, Aspartic acid residues (D) present in the transmembrane sequence were replaced by Lysine residues (K) in the SC-FL pHLIP (ACEQNPIY WARYAKWLFTTPLLLLKLALL VDAK EGT).

3 Results and discussion

3.1. pHLIP WT characterization

3.1.1. pHLIP solubility and chemical-physical properties

In the perspective of being clinically translatable, the proposed pH-sensitive tool was studied in biological buffers. For this purpose, Phosphate Buffered Saline solution (0.1 M PBS) was selected as the most suitable medium to dissolve pHLIP WT. Peptide solubility was thoroughly investigated together with its chemical-physical properties. Indeed, small amounts of buffer were added to 1 mg of peptide at physiological pH in order to detect the solubility limit of the system. Experimental evidences showed that the highest dissolution was achieved only after sample heating combined with vortex agitation and bath sonication (Figure 3.1) as reported in Table 3.1. Importantly, the maximum concentration of the peptide that could properly be dissolved within the physiological medium was set at 0.65 mM corresponding to 2.5 mg/mL.

[pHLIP], mM	Treatment steps			Solution quality	pHLIP solubility
	Vortex	Sonication	Heating		
2.5	✓	X	X	Totally insoluble	Absent
1.25	✓	X	X	Presence of lumps	Poor
0.83	✓	✓	X	Homogeneous, opaque	Medium
0.62	✓	✓	✓	Homogeneous, transparent	Good

Table 3.1: Experimental conditions for pHLIP WT solubility tests.

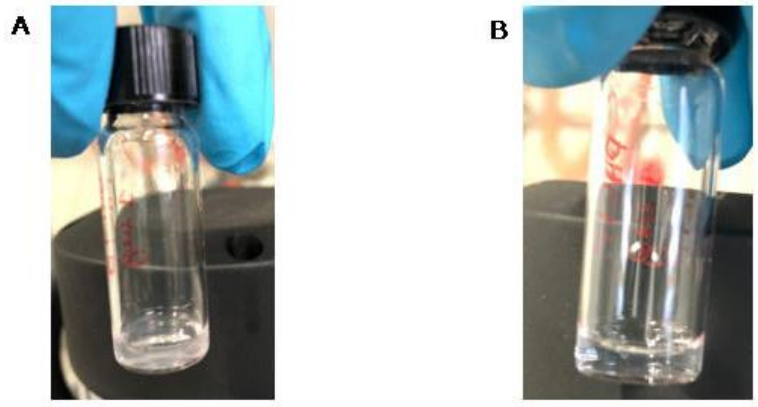

Figure 3.1: Pictures of pHLIP WT solutions in 0.1 M PBS at physiological pH: 0.83 mM (opaque, A) and 0.62 mM (transparent, B).

An optimized solubilization protocol was therefore developed and a good reproducibility in terms of preparation of peptide stock solutions was ensured by working at concentrations far from the solubility limit. Details are reported as follows:

- Dissolution of 100 μM pHLIP WT (0.4 mg/mL) in PBS at pH 7.4;
- Vortex agitation for 1 minute;
- Heating at 35°C for 30 minutes;
- Bath sonication at 59 kHz for 5 minutes.

pHLIP WT dissolution efficiency was qualitatively assessed by monitoring lack of macroscopic aggregates and transparency of the solution. The correct solubilization was then checked by UV-Vis analysis. In detail, different peptide concentrations were acquired (Figure 3.2) and the molar attenuation coefficient ε_λ at the maximum absorbance peak (λ = 280 nm) was calculated from Lambert-Beer Law as explained in the method section and reported below (Equation 2.3):

$$A_\lambda = \varepsilon_\lambda \cdot l \cdot C \tag{2.3}$$

The efficacy of the solubilization protocol was confirmed by the ε_λ value that, as expected, was kept constant throughout all different concentrations:

$\varepsilon_\lambda = 13286 \pm 457\ M^{-1}cm^{-1}$ at 280 nm

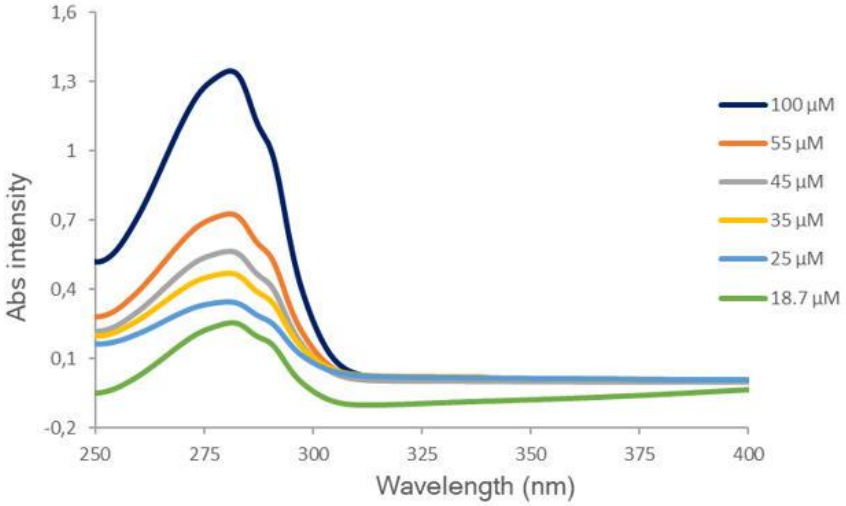

Figure 3.2: UV-Vis absorption spectra of pHLIP WT at different concentrations.

Importantly, once the molar attenuation coefficient was known, the effective amount of peptide dissolved in the stock solution could be checked through Equation 2.3. Thus, the solubilized peptide was verified for all newly prepared stocks.

After that, the pHLIP WT colloidal stability in solution was evaluated over time through DLS analyses at 90°. Once in aqueous solution, in fact, the peptide adopts a specific self-assembly that can be studied through light scattering measurements. Specifically, different time points ranging from T_0 to 24 h were investigated. Results in Figure 3.3 clearly showed as the peptide was stable in aqueous environment within 24 hours at physiological pH and did not aggregate. Indeed, despite the high signal to noise ratio due to the low count rate (i.e., the intensity of scattered light in DLS) (Figure 3.3 A), the correlation functions and the size distributions overlapped (Figure 3.3 B).

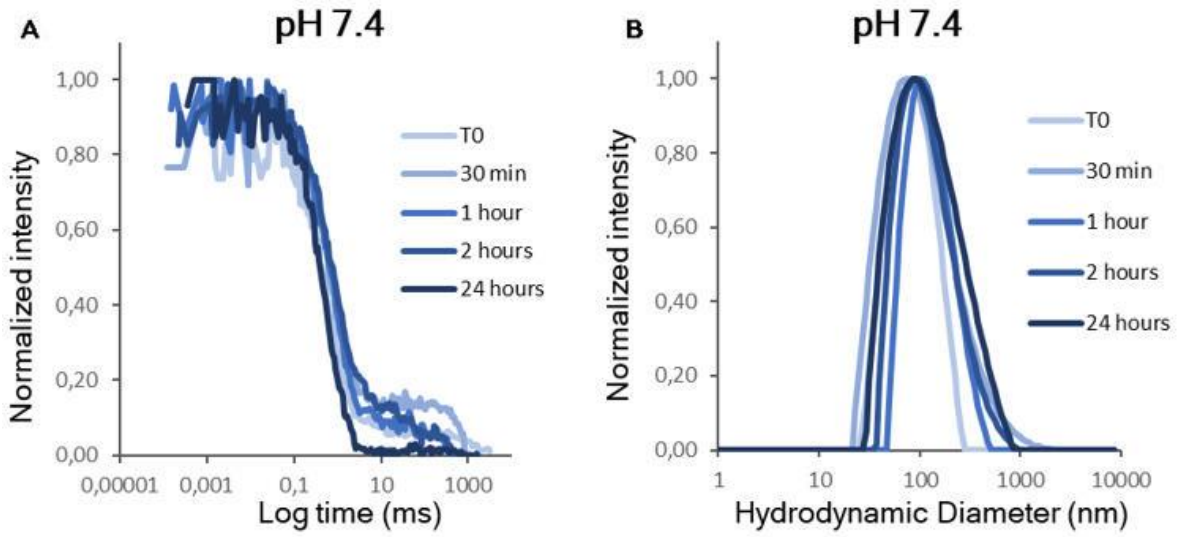

Figure 3.3: DLS experiments performed at 90°: autocorrelation functions (A) and unweighted size distributions (B) of pHLIP WT measured at five different time points and pH 7.4.

3.1.2. Self-assembly properties in physiological and acidic environment

Once the pHLIP WT stability in solution was ensured at physiological pH, self-assembly properties were investigated in acidic environment (pH 6.5 and 5.2). As shown by DLS results in Figure 3.4, more the pH was reduced, more the peptide tended to form aggregates. As explained in the Introduction (Chapter 1), pHLIP WT becomes more hydrophobic in acidic environment as the net charge is minimized, and the reduced electrostatic repulsion between peptide molecules enhances their aggregation. As a proof of that, the decay of the autocorrelation functions shifted towards higher times and DLS profile moved to larger sizes by decreasing the pH (Figure 3.4).

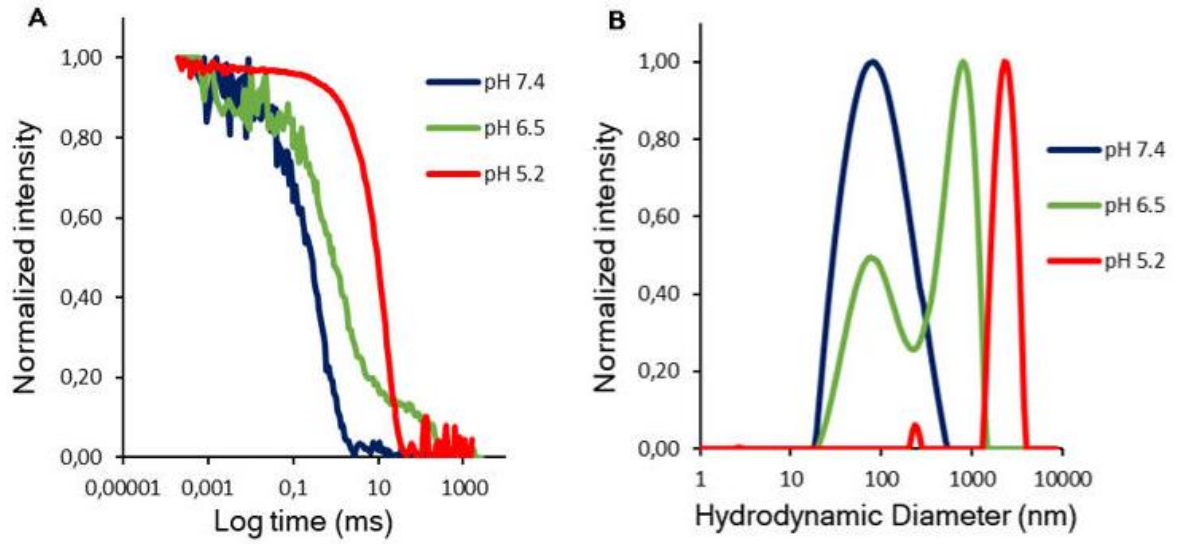

Figure 3.4: DLS experiments performed at 90°: autocorrelation functions (A) and unweighted size distributions (B) of pHLIP WT measured at pH 7.4 (blue), 6.5 (green) and 5.2 (red).

The next step was studying peptide colloidal stability in acidic environment over time, in order to evaluate its dynamic of aggregation. DLS results in Figure 3.5, demonstrated that the formation of aggregates was faster and clearer at highly acidic pH (pH 5.2) (Figure 3.5 A-B) compared to slightly acidic conditions (pH 6.5) (Figure 3.5 C-D). However, in both cases pHLIP WT aggregated within 24 hours and thus fresh solutions of peptide were always required.

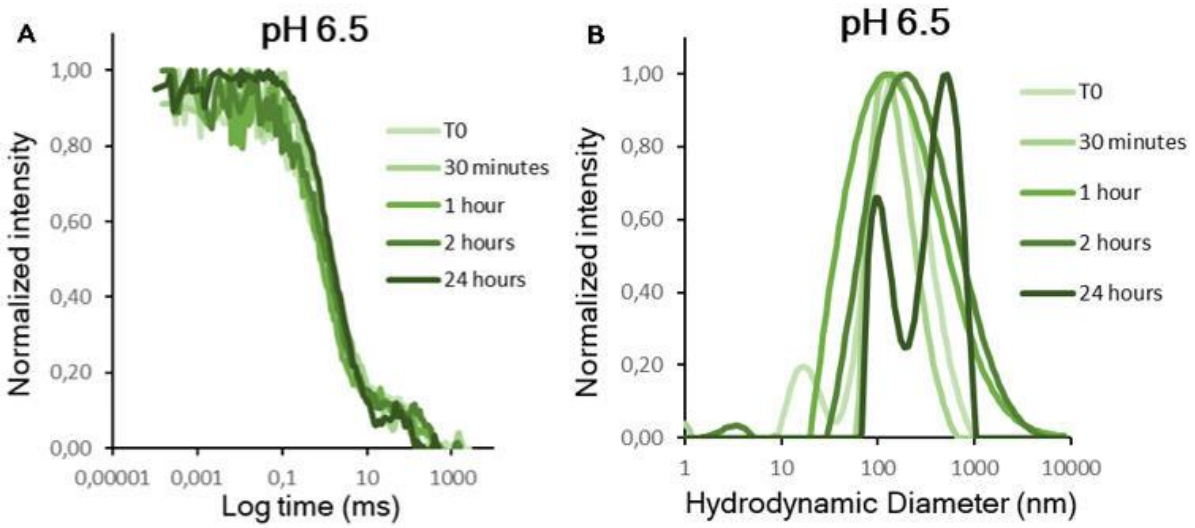

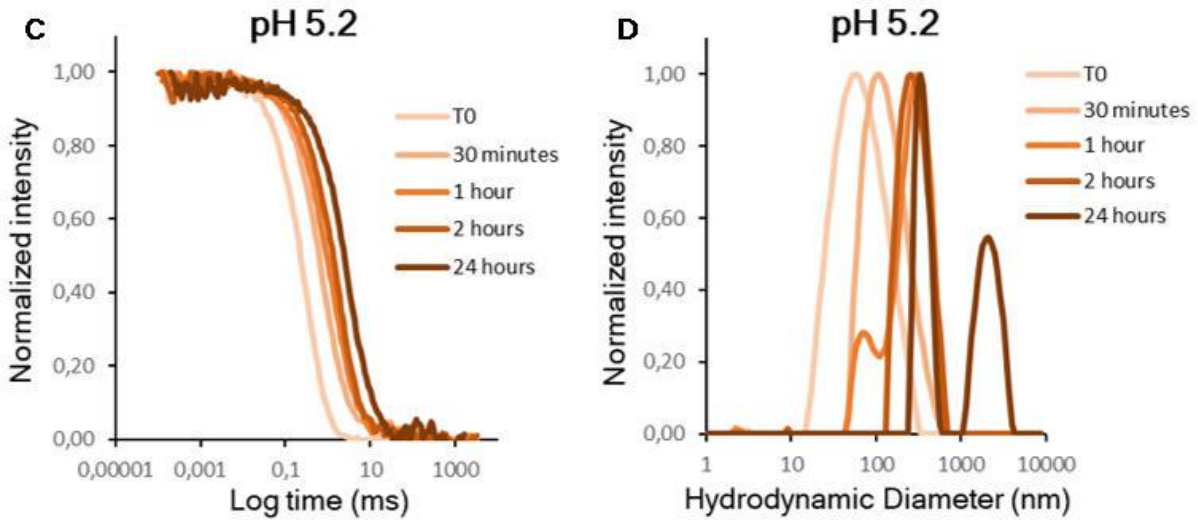

Figure 3.5: DLS experiments performed at 90°: autocorrelation functions at pH 6.5 (A) and 5.2 (C) and unweighted size distributions at pH 6.5 (B) and 5.2 (D) of pHLIP WT measured at five different time points.

3.1.3. Peptide structuring and membrane insertion properties

Once the enhanced hydrophobicity of pHLIP WT in acidic environment was demonstrated, we developed a characterization procedure able to verify peptide membrane insertion properties. For this purpose, DOPC liposome-based systems were introduced since they represent a simplified model of eukaryotic cells. Specifically, after 15 minutes of peptide-lipids incubation (see details in Method section, Chapter 2.3.5), the intrinsic fluorescence intensity (IFI) of the tryptophan (Trp) residues belonging to the pHLIP WT transmembrane sequence was quantified. Indeed, Trp IFI signals of pHLIP was exploited to follow membrane surface adsorption and insertion of the peptide [52] (and its FL-variant) across the bilayer. WT pHLIP in solution at low concentrations is expected to be unfolded and monomeric. For this reason, Trp residues are exposed to the polar environment, resulting in an emission spectrum with a maximum at 351 nm (Figure 3.6 A-B, light blue label). Because of incubation with DOPC vesicles, Trp fluorescence of WT pHLIP was blue shifted and the intensity was increased (Figure 3.6 A-B dark blue line). When the pH was decreased to first pH 6.5

and then 5.2, the fluorescence shifted further since tryptophan residues were moved into the hydrophobic core of the bilayer. Consequently, the IFI increased more.

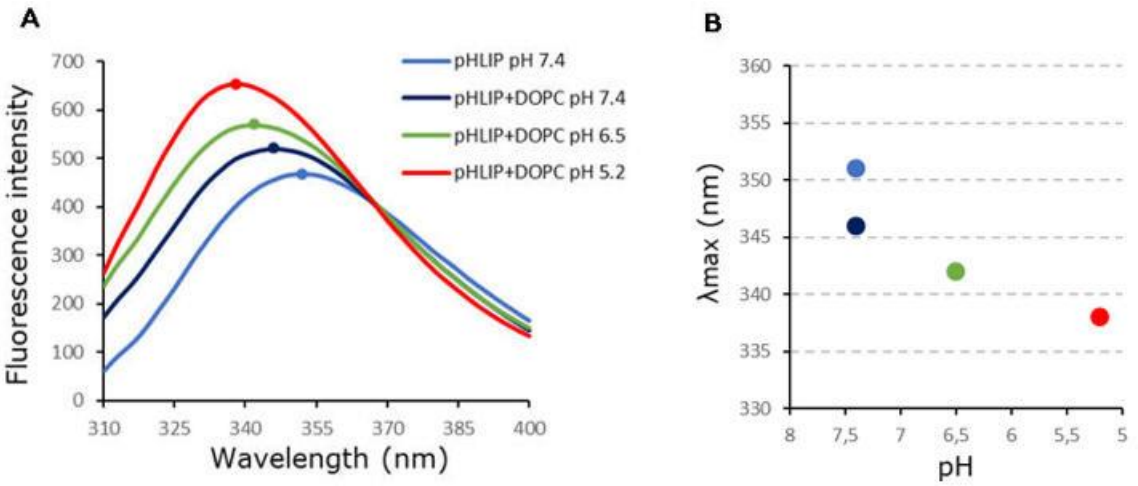

Figure 3.6: A. Fluorescence spectra of pHLIP WT at pH 7.4 (light blue) and in presence of DOPC liposomes at pH 7.4 (blue), 6.5 (green) and 5.2 (red) measured by fluorimeter analysis. B. Blueshift of maximum emission as a function of the pH.

To further prove the insertion of pHLIP WT into liposome-membranes and the formation of the α-helix, the peptide three-dimensional conformation was characterized through CD analysis. Results in Figure 3.7 A showed as in absence of liposomes the spectral profile of the peptide changed from a random coil to a β-sheet conformation by reducing the pH, as a consequence of peptide aggregation in acidic environment. These results are in line with DLS analyses previously described (section 3.1.2).

With the introduction of DOPC liposomes into the peptide solution, it was still possible to recognize a random coil secondary structure at physiological pH, meaning that the pHLIP WT conformation was not much affected by the presence of the lipid vesicles since the interaction was minimal (Figure 3.7 B, dark blue line). On the other hand, the CD pattern started to change at slightly acidic pH reaching a clear α-helix profile at pH 5.2, which is characterized by a double minimum at 208 and 222 nm. This spectral profile evolution well described pHLIP WT insertion stages through the lipid bilayer.

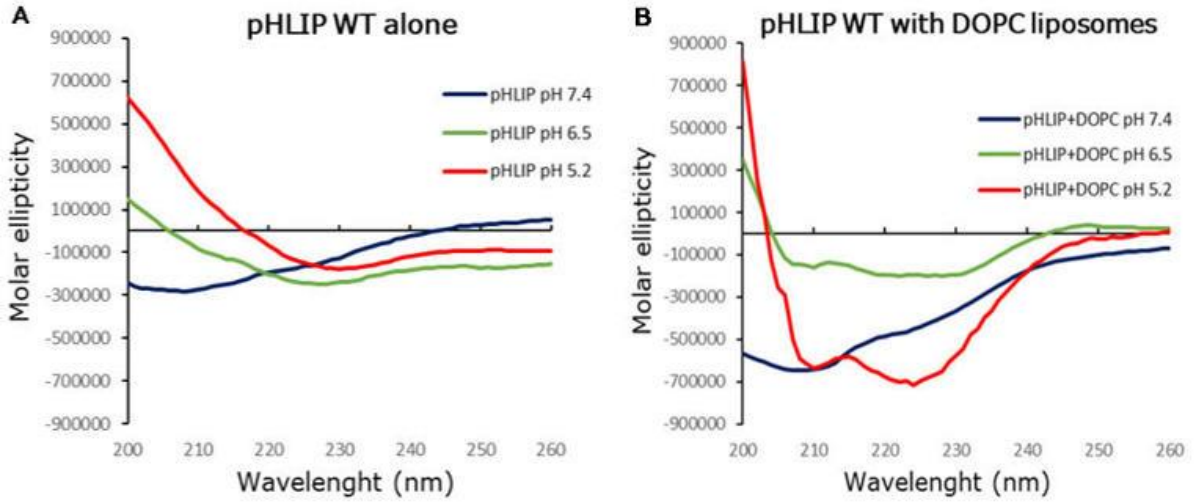

Figure 3.7: CD profiles and absorption spectra of pHLIP WT alone (A) or in presence of DOPC liposomes (B) at different pH values.

3.1.4. Dynamics of membrane insertion at highly acid pH values

The kinetics of pHLIP WT membrane insertion was mainly investigated at very low pHs (5.2) through CD analyses. In detail, experiments were performed at different timings up to 70 minutes (T_0, 20, 40, 50 and 70 minutes). Results showed as peptide folding occurred immediately, as the α-helix configuration could be recognized from the spectrum profile already at T_0 (Figure 3.8). Moreover, once the pHLIP WT was inserted in the lipid bilayer, its three-dimensional conformation was stable over time suggesting that the peptide was steadily anchored to the membrane. Thus, the membrane insertion process at acid pH values was very fast and stable.

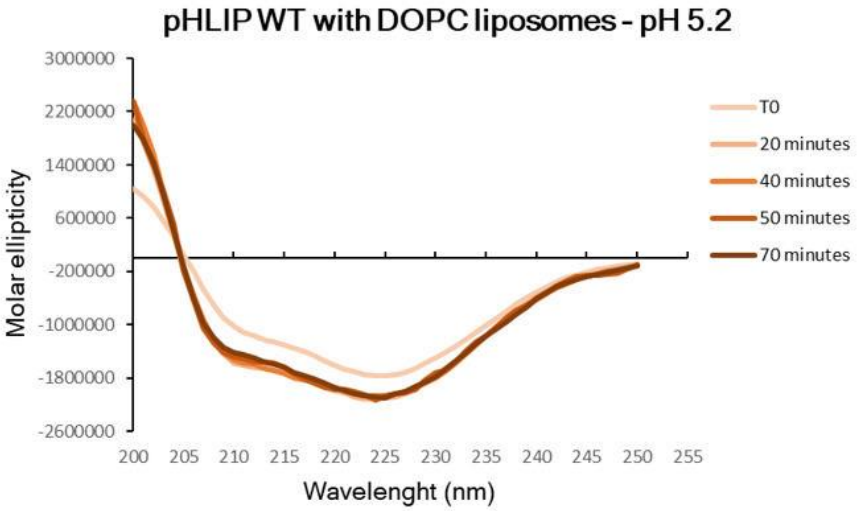

Figure 3.8: CD spectra of pHLIP WT in presence of DOPC liposomes at pH 5.2 measured at five different time points.

3.1.5. Peptide-membrane interaction: in-flow model of eukaryotic cells membrane

After a first characterization, which was widely described in the previous sections, we proposed an in-flow mimic model system to further evaluate pHLIP sensitivity in a context closer to the cellular environment. In particular, we exploited the supported lipid bilayers (SLBs) as model of cell membrane and pHLIP-SLB interaction was observed by a quartz crystal microbalance with dissipation monitoring (QCM-D).

In a first and preliminary experiment, a pHLIP WT solution, corresponding to 5 μM as concentration of incubation, was insufflated at physiological pH onto the SLB for 30 minutes. After the introduction of the peptide (arrow 4 in Figure 3.9), it was possible to observe just a slight increase in the dissipation indicating a mild interaction between the pHLIP WT and the lipid bilayer. The enhanced dissipation was kept constant during the 30-minutes static incubation, while it started decreasing as soon as a final 30-minutes washing was performed with PBS buffer. This meant that the peptide adsorbed onto the SLB was simply removed during the final washing steps.

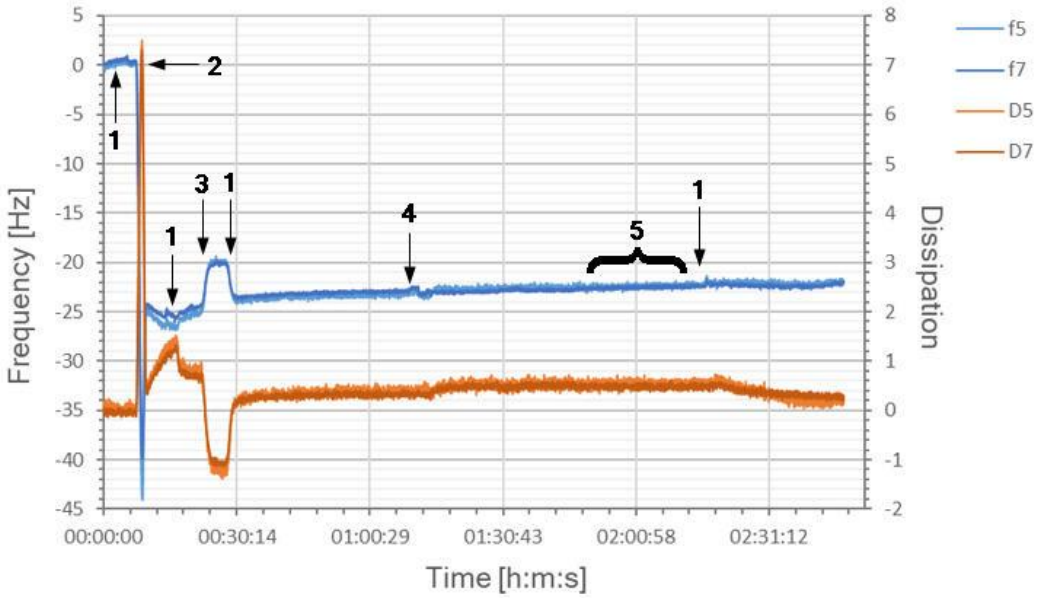

Figure 3.9: Representative QCM-D measurement for the SLB-pHLIP WT interaction at pH 7.4: dissipation (red line) and frequency (blue line). The numbers indicate the flow of the following solutions: 1 = PBS 0.1 M pH 7.4, 2 = Liposomes solution + $CaCl_2$, 3 = MilliQ water, 4 = pHLIP WT solution (5 μM), 5 = Static incubation.

This result was further confirmed by the mass deposition quantification. Indeed, while the mass profile of a SLB alone at physiological pH was kept constant over time (Figure 3.10), a clear increment in mass was assessed when pHLIP WT was added to the system (Figure 3.11). However, during the last washing the mass came back to its original value suggesting the peptide removal.

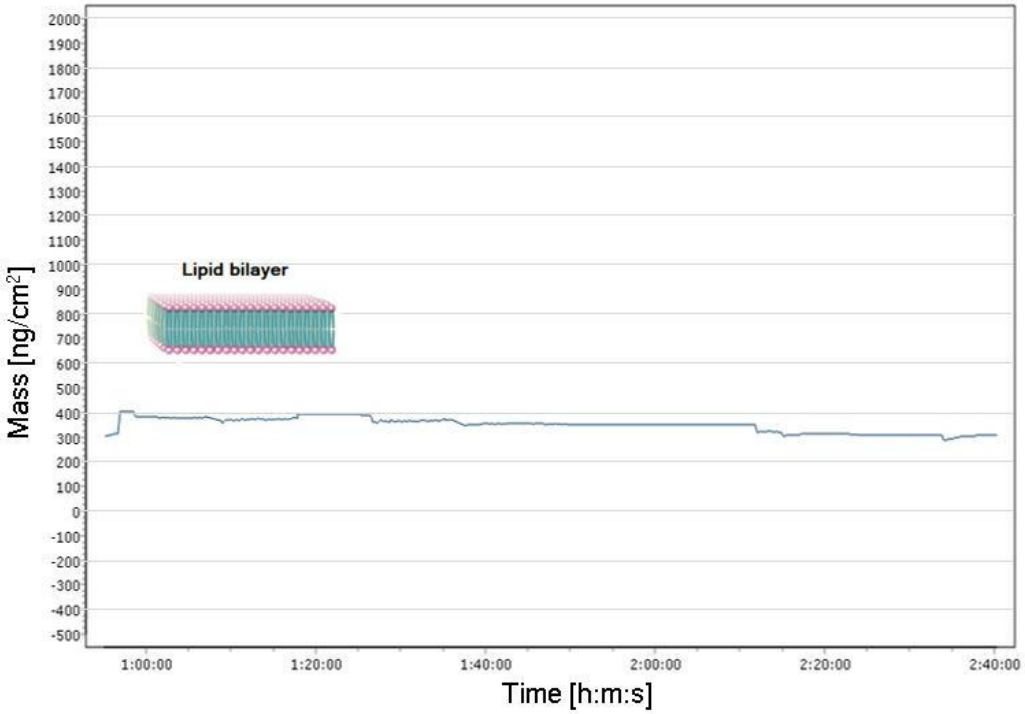

Figure 3.10: Mass profile of a SLB at pH 7.4 measured by QCM-D analysis.

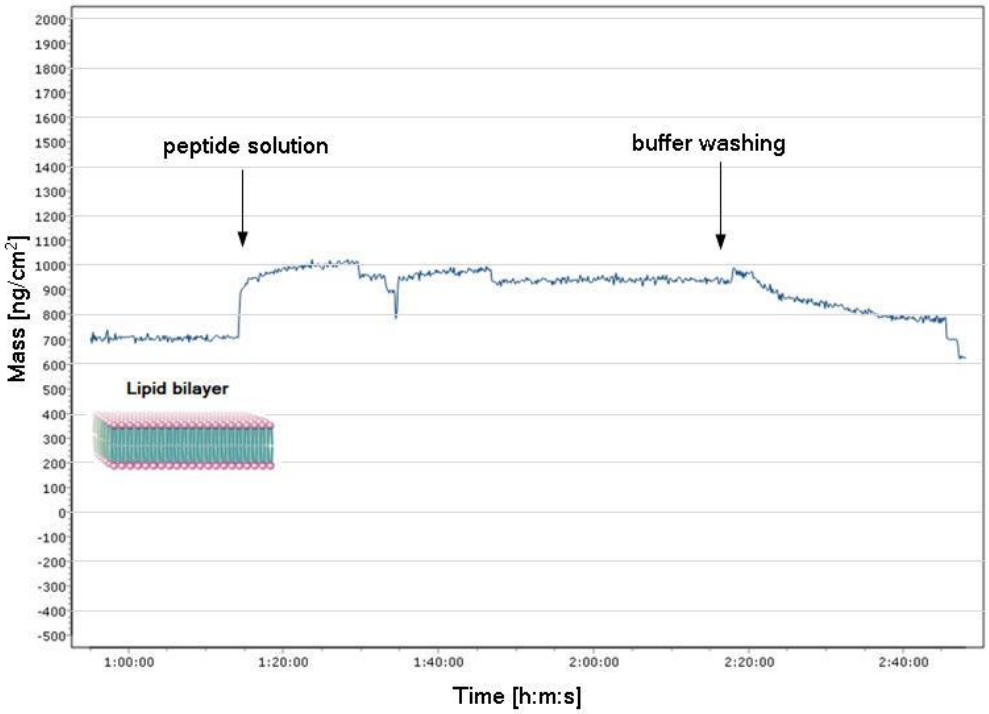

Figure 3.11: Mass profile of a SLB and pHLIP WT at pH 7.4 measured by QCM-D analysis.

The same investigation was then repeated performing faster dynamics of incubation with a lower amount of pHLIP WT equal to 0.5 μM peptide solution. For this purpose, we not only reduced the peptide insufflation, but also the static incubation and the final washing-step timings (15 minutes for each experimental phase). Importantly, similar results were obtained with an even more modest peptide-SLB interaction (Figure 3.12).

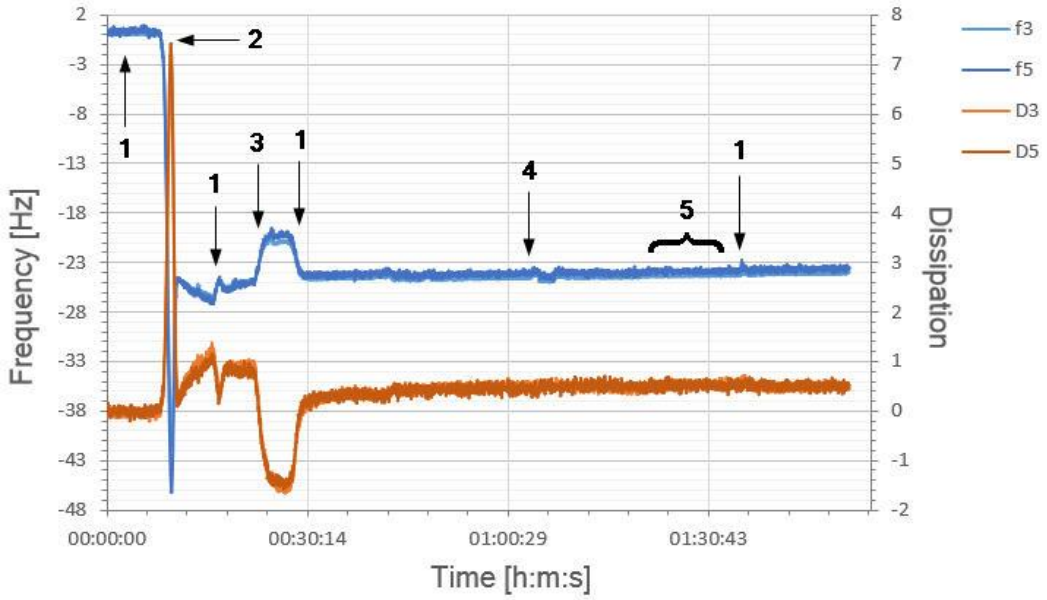

Figure 3.12: Representative QCM-D measurement for the SLB-pHLIP WT interaction at pH 7.4: dissipation (red line) and frequency (blue line). The numbers indicate the flow of the following solutions: 1 = PBS 0.1 M pH 7.4, 2 = Liposomes solution + $CaCl_2$, 3 = MilliQ water, 4 = pHLIP WT solution (0.5 μM), 5 = Static incubation.

These findings suggested that previously we were probably working with an excess of peptide. Thus, 10-times lower pHLIP amounts were sufficient to get the same performance avoiding a peptide-lipids non-specific interaction.

Analogous experiments were accomplished also at very low pH (5.2). The idea was to monitor how the proposed system was sensitive to the peptide folding change depending on the decrease in pH. We expected to observe pHLIP WT insertion into

the lipid bilayer. For this purpose, we evaluated 5 μM peptide concentration at both slow (30 minutes) and fast (15 minutes, Figure 3.13) dynamics.

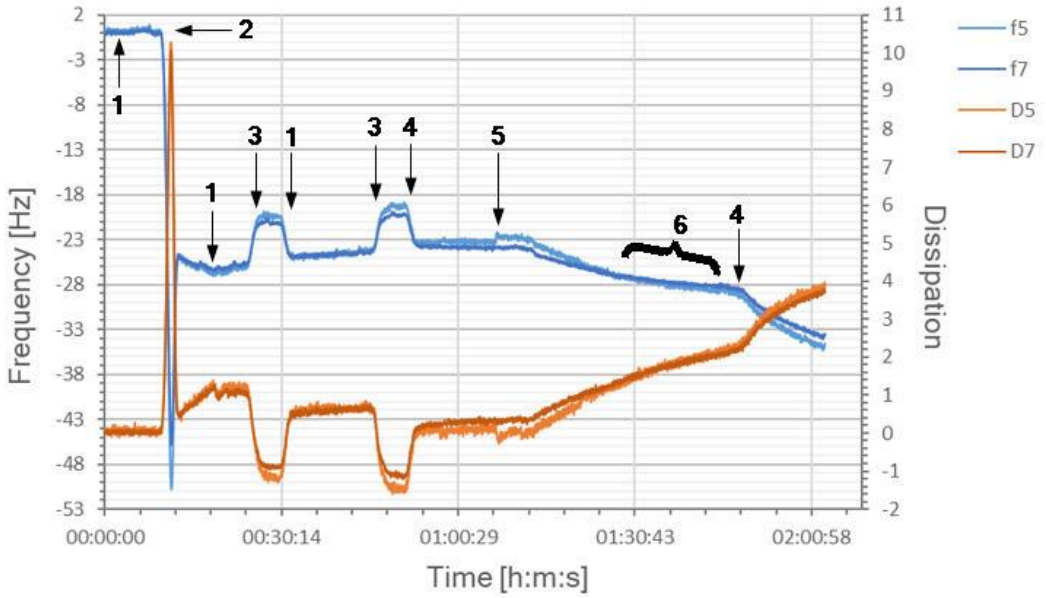

Figure 3.13: Representative QCM-D measurement for the SLB-pHLIP WT interaction at pH 5.2: dissipation (red line) and frequency (blue line). The numbers indicate the flow of the following solutions: 1 = PBS 0.1 M pH 7.4, 2 = Liposomes solution + $CaCl_2$, 3 = MilliQ water, 4 = Acetate buffer 0.1 M pH 5.2, 5 = pHLIP WT solution (5 μM), 6 = Static incubation.

As shown in Figure 3.13, we found a significant increase in dissipation and decrease in frequency upon peptide insufflation, indicating a very strong interaction with the SLB. Of note, frequency values related to the different harmonics were superimposed suggesting that the system steadily remained rigid even after the peptide interaction. Importantly, the peptide was not removed after the washing steps with buffer since pHLIP insertion into the lipid bilayer seemed to be very stable. As a proof of these findings, while the mass profile of a SLB alone at the same pH was kept constant over time (Figure 3.14), a clear increase in mass was observed when pHLIP WT was added to the system (Figure 3.15). In detail, an average deposited mass of 2458 ng/cm^2 was detected.

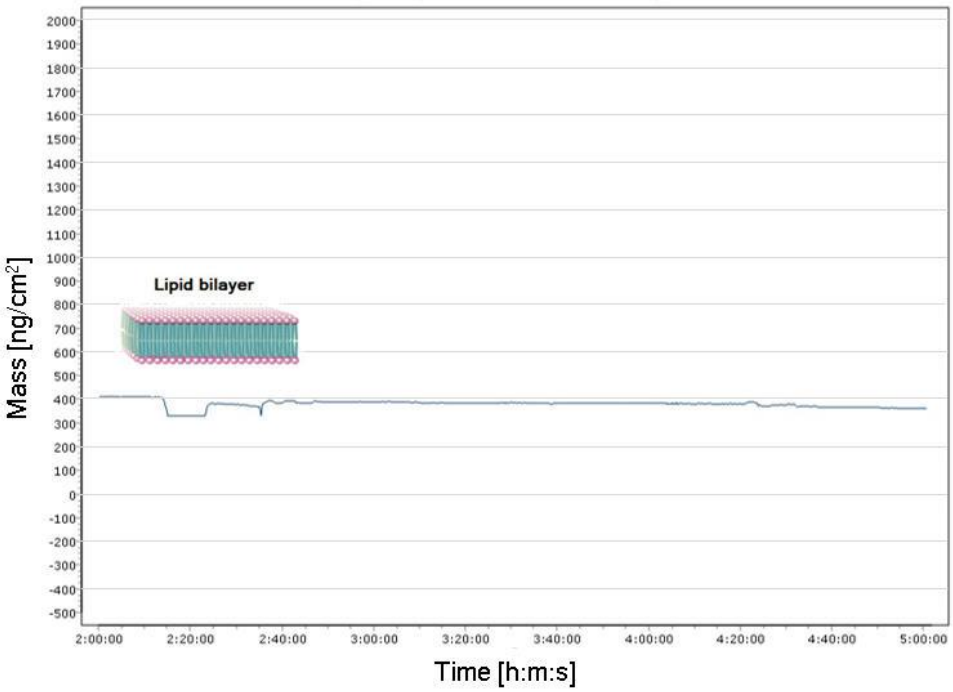

Figure 3.14: Mass profile of a SLB at pH 5.2 measured by QCM-D analysis.

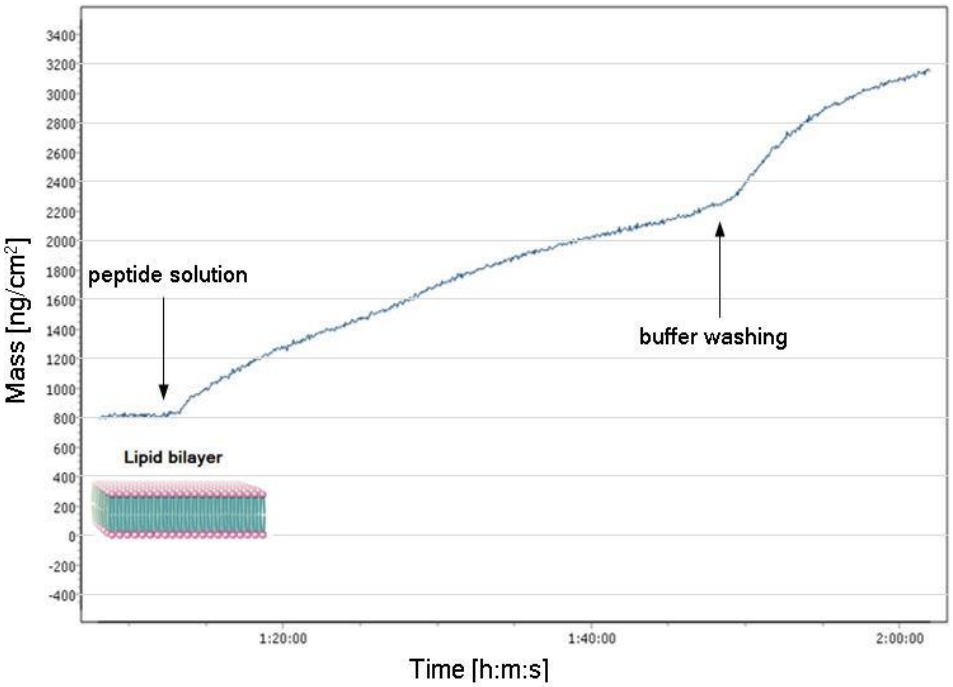

Figure 3.15: Mass profile of a SLB and pHLIP WT at pH 5.2 measured by QCM-D analysis.

Interestingly, if the final washing was performed using a buffer at physiological pH, the deposited peptide was completely lost (Figure 3.16) and the mass related to the

lipid bilayer alone was restored (Figure 3.17), suggesting a reversibility of the insertion process.

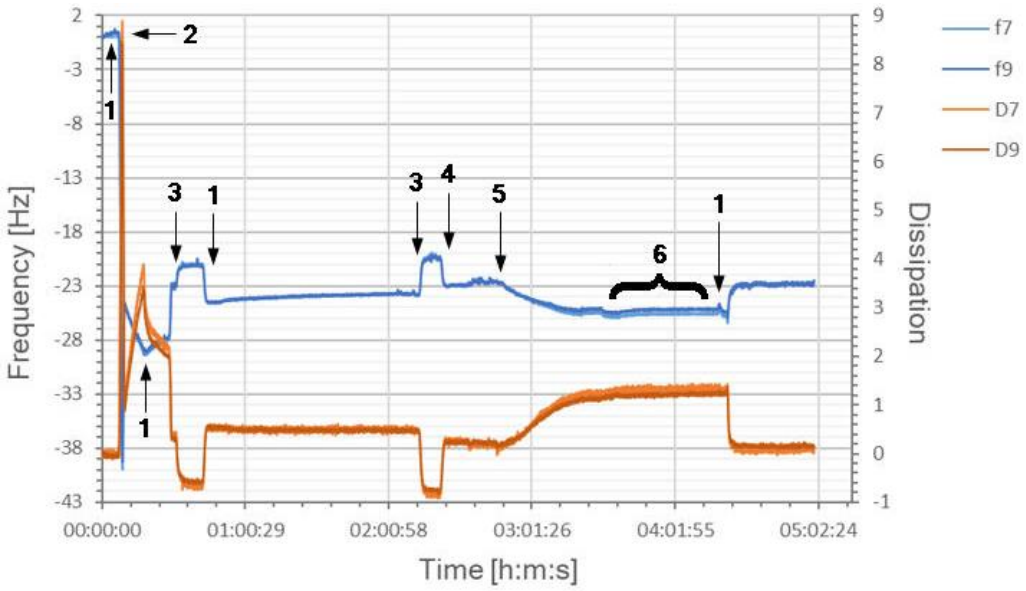

Figure 3.16: Representative QCM-D measurement for the SLB-pHLIP WT interaction at pH 5.2: dissipation (red line) and frequency (blue line). The numbers indicate the flow of the following solutions: 1 = PBS 0.1 M pH 7.4, 2 = Liposomes solution + $CaCl_2$, 3 = MilliQ water, 4 = Acetate buffer 0.1 M pH 5.2, 5 = pHLIP WT solution (5 μM), 6 = Static incubation.

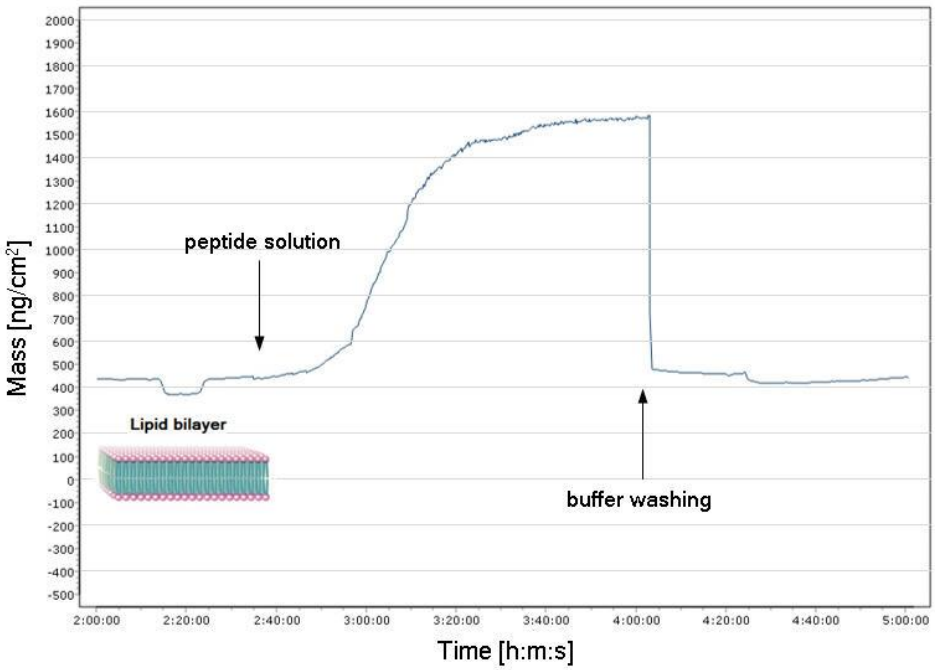

Figure 3.17: Mass profile of a SLB and pHLIP WT measured by QCM-D analysis.

In addition to the high pHLIP WT concentration (5 μM), we also considered 0.5 μM peptide dose using fast dynamics (Figure 3.18).

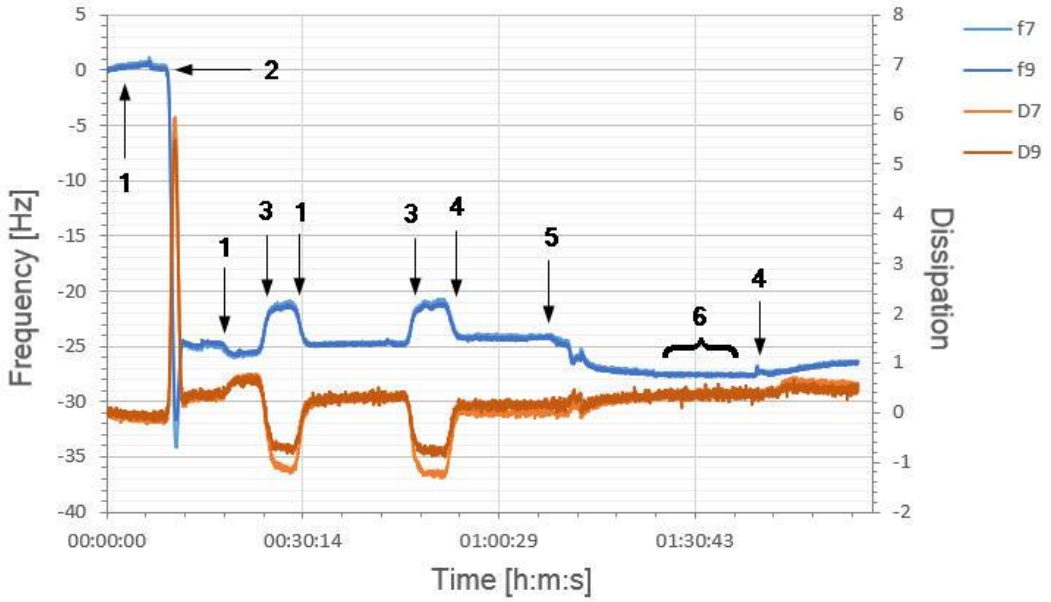

Figure 3.18: Representative QCM-D measurement for the SLB-pHLIP WT interaction at pH 5.2: dissipation (red line) and frequency (blue line). The numbers indicate the flow of the following solutions: 1 = PBS 0.1 M pH 7.4, 2 = Liposomes solution + $CaCl_2$, 3 = MilliQ water, 4 = Acetate buffer 0.1 M pH 5.2, 5 = pHLIP WT solution (0.5 μM), 6 = Static incubation.

Even if the amount of deposited mass (about 513 ng/cm^2) was lower compared to the previous conditions, the reduced pHLIP concentration (0.5 μM) was again sufficient to detect the peptide-lipids interaction. Importantly, working at non-excessive pHLIP doses helped to prevent peptide aggregation especially at acidic pH values.

To better mimic the extracellular pH value expected in GBM tumor cells, we also investigated a slightly less acidic environment. Therefore, similar experiments were performed at pH 6.5. In this case, working with a high pHLIP WT dose (5 μM) and slow dynamics (30 minutes of incubation) gave the same effects achieved at low peptide concentrations (0.5 μM) and faster dynamics. Specifically, the peptide

insufflation caused both an increase in dissipation and a decrease in frequency, implying a strong pHLIP WT-SLB interaction (Figure 3.19, arrow 5). Importantly, also in this case the described behavior was not reversed during the last washing step meaning that the interacting peptides were permanently inserted into the lipid bilayers. These encouraging results confirmed that the proposed system worked well in pH conditions consistent with glioblastoma tumor extracellular environment.

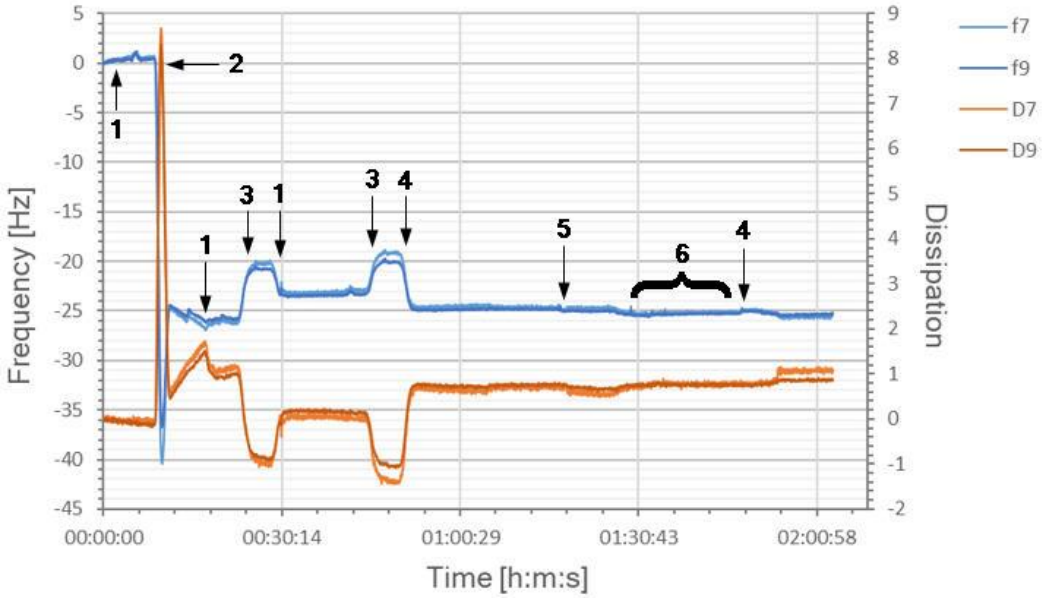

Figure 3.19: Representative QCM-D measurement for the SLB-pHLIP WT interaction at pH 6.5: dissipation (red line) and frequency (blue line). The numbers indicate the flow of the following solutions: 1 = PBS 0.1 M pH 7.4, 2 = Liposomes solution + $CaCl_2$, 3 = MilliQ water, 4 = TRIS 0.1 M pH 6.5, 5 = pHLIP WT solution (0.5 μM), 6 = Static incubation.

Finally, the quantification of the deposed mass on the solid lipid bilayer allowed appreciating an important deposition of 750 ng/cm^2 (Figure 3.20).

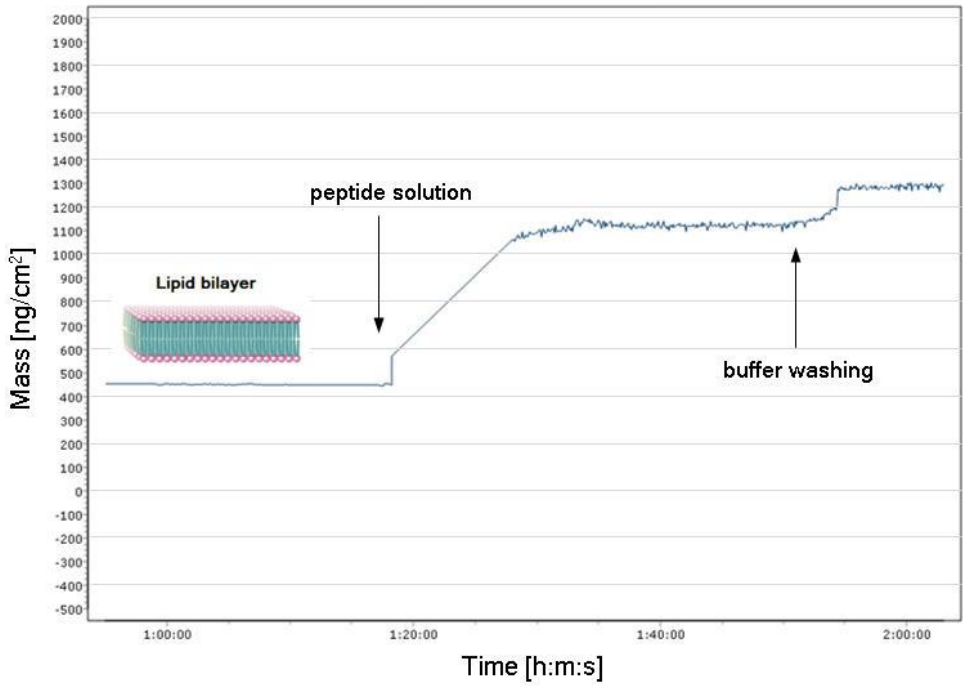

Figure 3.20: Mass profile of a SLB and pHLIP WT at pH 6.5 measured by QCM-D analysis.

The quantification of pHLIP WT mass deposition on the SLB during the different QCM-D experiments are summarized below (Table 3.2 and Figure 3.21).

Concentration (μM)	pH	Incubation time (min)	Deposited mass (ng/cm²)
5	6.5	30	717 ± 379
0.5		15	750 ± 141
5	5.2	30	3332 ± 1886
5		15	2458 ± 293
0.5		15	513 ± 18

Table 3.2: Experimental conditions for pHLIP WT QCM-D analyses and related deposited mass.

Results in Figure 3.21 show that at highly acidic pH (5.2) the experimental conditions (i.e., time of incubation and peptide concentration) havean important influence on the amount of deposited peptide. In particular, by keeping fixed the concentration (5 μM)

and reducing the incubation time, a less deposited mass was detected. Similarly, keeping constant the time of incubation (15 minutes) but decreasing the peptide concentration (0.5 μM) led to a considerable decrease of the pHLIP WT deposited. Of note, a larger standard deviation observed at pH 5.2, especially for high pHLIP concentrations and slower dynamics, could be associated to aggregation phenomena, as explained in the first part of this section. Instead, the results obtained from QCM-D analyses at slightly acid pH (6.5) at different experimental conditions were all in the same range. Importantly, the amount of deposited peptide at low concentration and fast dynamics was comparable both at pH 6.5 and 5.2. Therefore, working at non-excessive pHLIP doses and shorter incubation timings helped to avoid peptide-lipids non-specific interactions and aggregation.

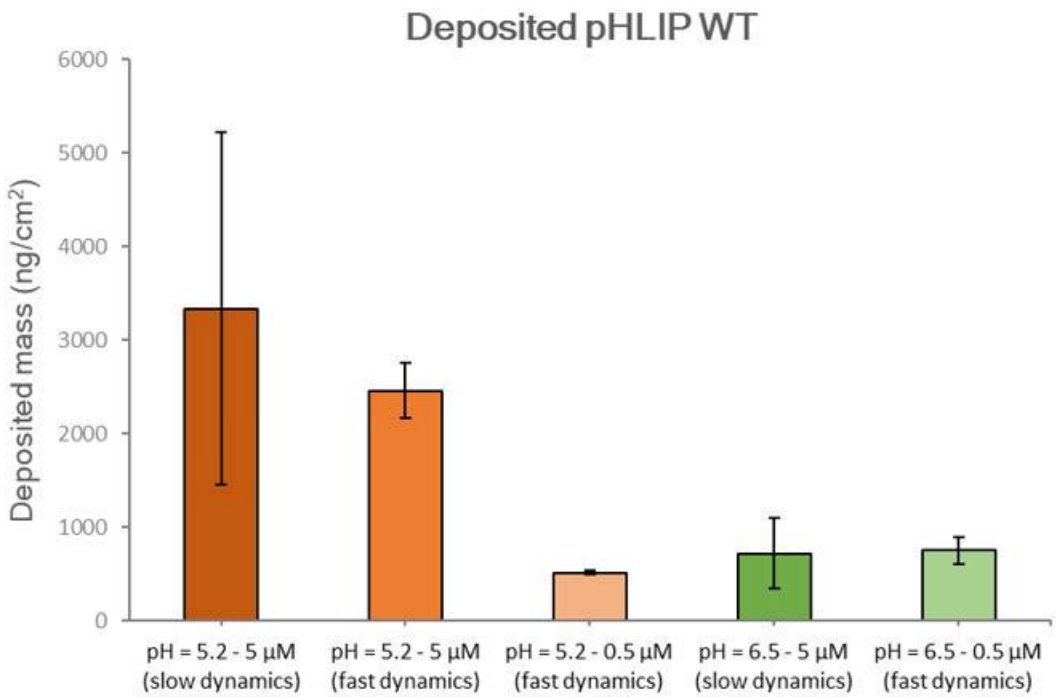

Figure 3.21: Quantification of deposited pHLIP WT during QCM-D analysis at pH 5.2 (orange) and 6.5 (green) at different experimental conditions.

3.2. FL-pHLIP characterization

3.2.1. pHLIP solubility and chemical-physical properties

The optimized characterization procedure, which was previously developed and described for the WT pHLIP derivative, was then fully extended to the FL enriched peptide. Indeed, the chemical-physical properties were evaluated starting from 100 µM (0.46 mg/mL) stock solution in PBS 0.1 M using the same solubilization method optimized for pHLIP WT (section 3.1.1).

The efficacy of peptide solubilization, also this time, was ensured calculating the molar attenuation coefficient ε_λ of FL-pHLIP at the peptide absorbance peak (λ = 280 nm) (Equation 2.3) on different concentrations (Figure 3.22).

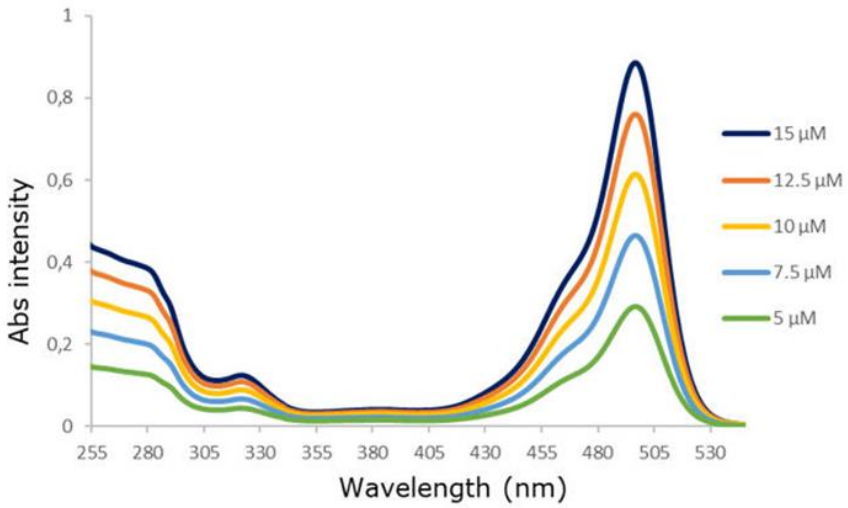

Figure 3.22: UV-Vis absorption spectra of FL-pHLIP at different concentrations.

If FL-pHLIP was correctly solubilized, the value of ε_λ should have been kept constant throughout the entire range of investigated concentrations, as reported below:

$$\varepsilon_\lambda = 26119 \pm 620\ M^{-1}cm^{-1} \text{ at } 280\ nm$$

Importantly, the effective amount of peptide dissolved in the stock solution could be easily verified through Equation 2.3 each time that a new stock was prepared.

Subsequent studies able to evaluate FL-pHLIP colloidal stability over time after solubilization showed that the peptide was stable in aqueous environment at physiological pH within 24 hours. As proof of that, both the correlation functions and the size distributions, related to DLS data collected on 5 μM peptide solution at different time points (T_0, 30 minutes, 1, 2, and 24 hours), clearly were overlapped (Figure 3.23). Compared to WT peptide, FL-pHLIP self-assembly at physiological pH was definitely different, as the correlation curve in the presence of Fluorescein was shifted towards higher values suggesting the formation of larger structures.

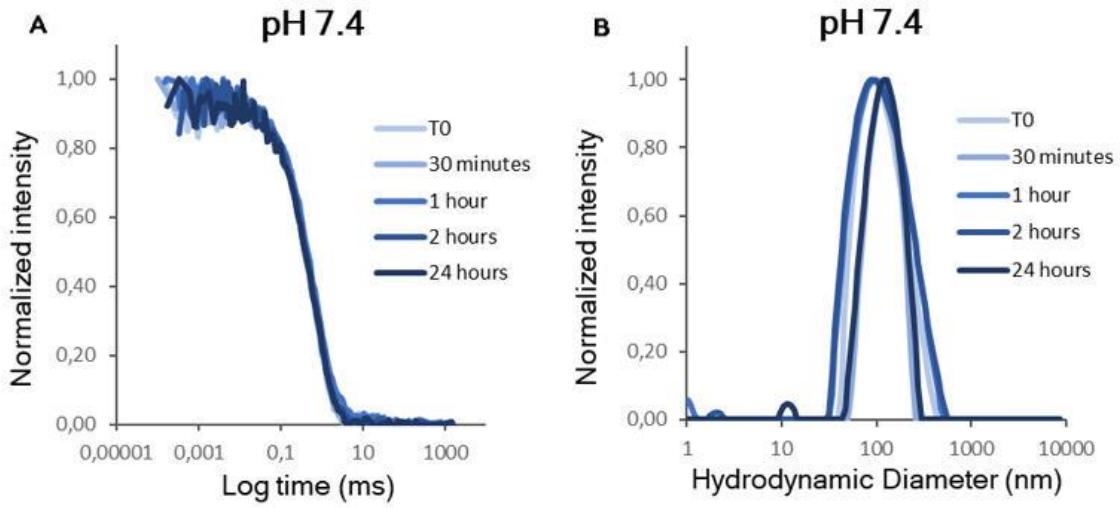

Figure 3.23: DLS experiments performed at 90°: autocorrelation functions (A) and unweighted size distributions (B) of FL-pHLIP measured at five different time points and pH 7.4.

So, in summary, both FL- and WT pHLIP were dispersible in physiological buffers and were colloidal stable within 24 hours. Thus, the conjugation with FL did not significantly affect peptide dispersibility.

Furthermore, FL-pHLIP UV analyses were clearly characterized by a second intense peak at 497 nm related to the presence of the dye. Interestingly, the peak at 280 nm increased in intensity when the peptide was conjugated to Fluorescein as the dye itself absorbs in the same range of wavelengths.

3.2.2. Self-assembly properties in physiological and acidic environment

Once the FL-pHLIP stability in solution had been assessed at physiological pH, self-assembly properties were also investigated in acidic environment (pH 6.5 and 5.2). In this perspective, DLS data pointed out the same behavior observed for pHLIP WT. Specifically, the peptide tended to form larger assemblies and less stable over time at more acidic pHs (Figure 3.24).

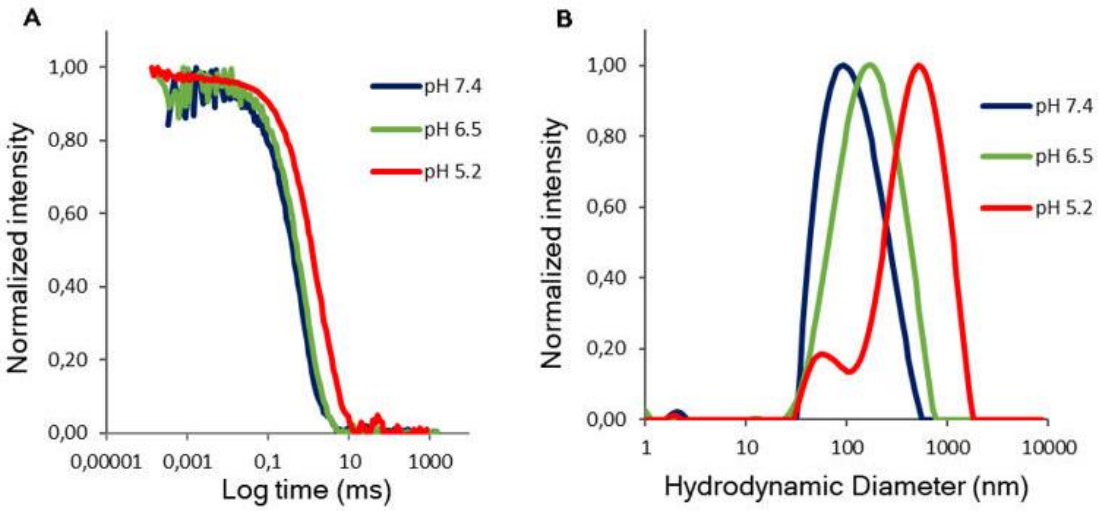

Figure 3.24: DLS experiments performed at 90°: autocorrelation functions (A) and unweighted size distributions (B) of FL-pHLIP measured at pH 7.4 (blue), 6.5 (green) and 5.2 (red).

Indeed, FL-pHLIP became more hydrophobic in acidic environment as the net charge was minimized, and the reduced electrostatic repulsion between peptide molecules enhanced their aggregation. As a result, the decay time of the autocorrelation function shifted towards higher values and the DLS profile moved to larger sizes.

Importantly, FL-pHLIP seemed to aggregate less in a slightly acidic environment (pH 6.5) compared to the control pHLIP WT. In fact, the first remained quite stable in solution at that pH value. Thus, the steric effects related to the presence of the dye could probably reduce the aggregation of the peptide and increase its stability in solution.

If we study in detail the dynamics of peptide aggregation in acidic environment, we observed more aggregated assembled structures at highly acidic pHs (pH 5.2), compared to slightly acidic conditions (pH 6.5) (Figure 3.25). Specifically, FL-peptides tend to aggregate reaching micrometer sizes within 24h at very acidic conditions (Figure 3.25 C and D). For this reason, fresh solutions were required in order to perform further analyses.

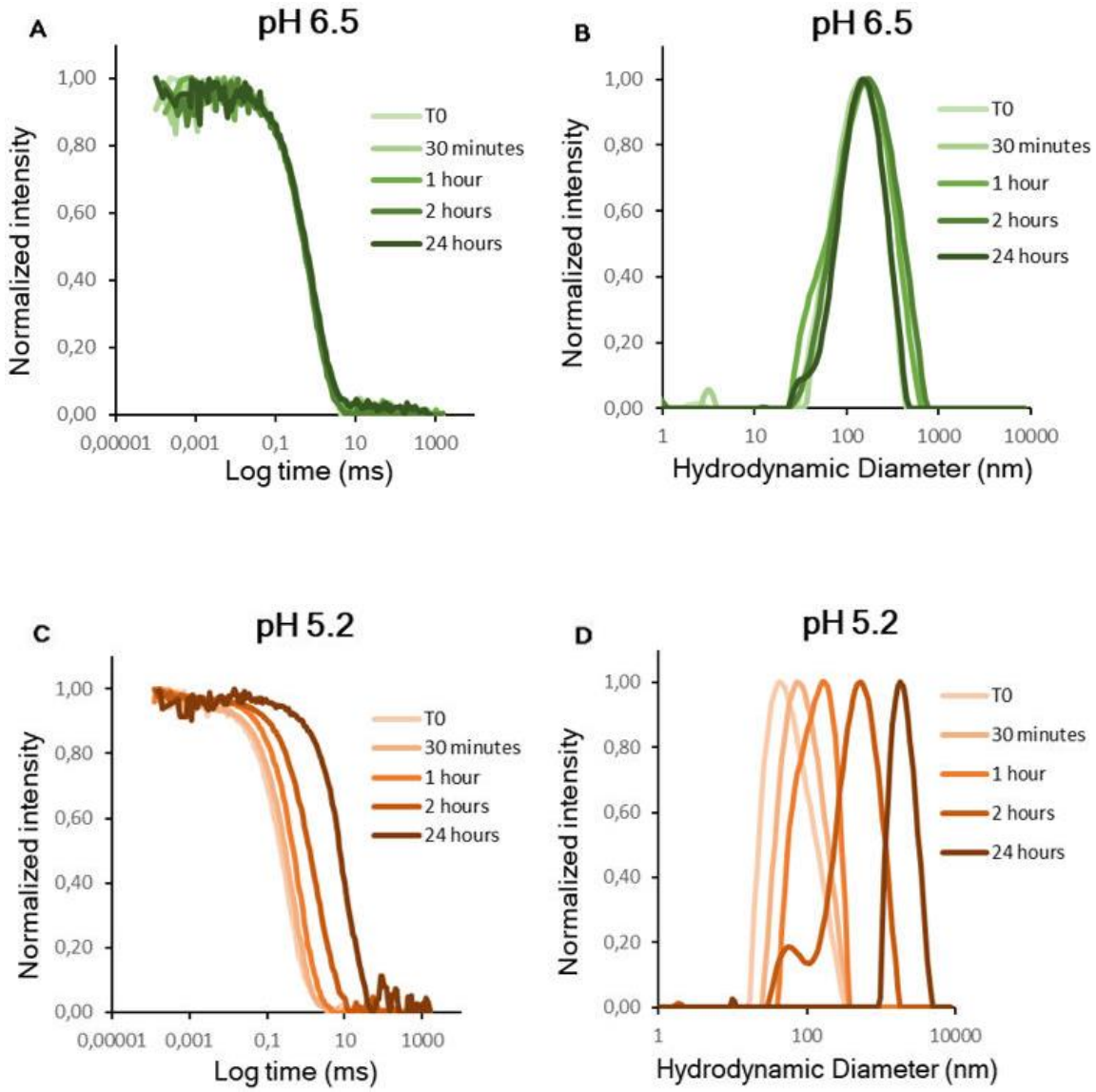

Figure 3.25: DLS experiments performed at 90°: autocorrelation functions at pH 6.5 (A) and 5.2 (C) and unweighted size distributions at pH 6.5 (B) and 5.2 (D) of FL-pHLIP measured at five different time points.

3.2.3. Peptide structuring and membrane insertion properties

As explained in section 3.1.3. for pHLIP WT, also for the FL-derivative we evaluated the membrane insertion properties starting from a very simple model of eukaryotic cell membrane, namely DOPC liposomes. In particular, the intrinsic tryptophan (Trp) fluorescence intensity was again estimated as an indication of the peptide-lipids interaction after a 15-minutes incubation. As for WT peptides, a blueshift of the emission spectrum maximum from 351 nm (Figure 3.26 A-B, light blue label) to 346 nm (figure 3.26 A-B, dark blue label) was also observed in case of FL-pHLIP with the lipid vesicles because the Trp residues were exposed to a less polar environment. The wavelength of maximum emission moved to even lower values by reducing the pH, confirming the peptide transmembrane folding across the hydrophobic lipid bilayer in acidic environment (pH 6.5 and 5.2). While for pHLIP WT this behavior was also demonstrated by the less effective quenching of Trp fluorescence, we observed an opposite trend for the FL-derivative. This difference is related to the dye itself, which in this range of wavelengths contributes to the overall fluorescence. In fact, Fluorescein has a pKa of 6.4 and its ionization equilibrium leads to a lowering of the fluorescence intensity at acid pH [53].

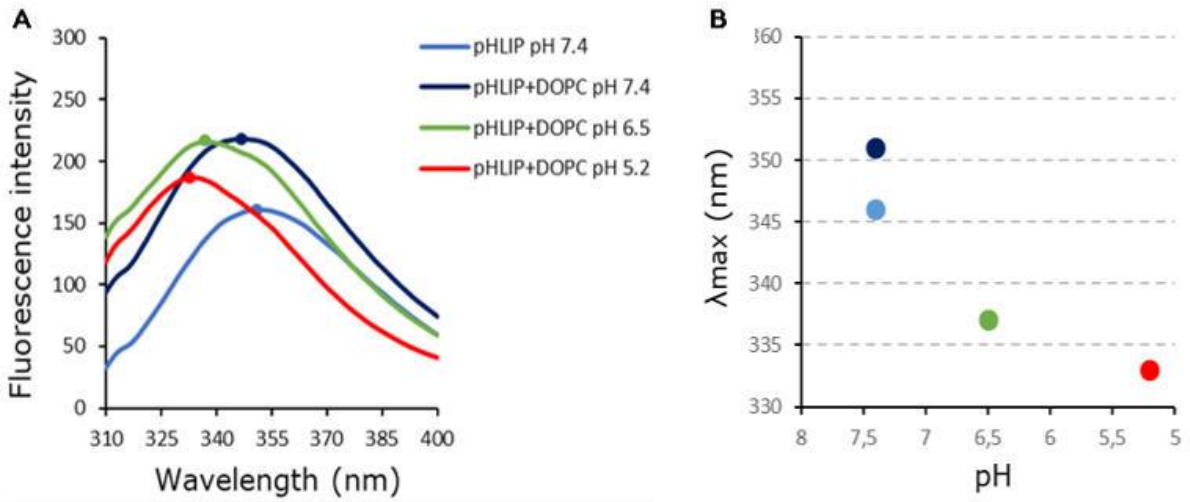

Figure 3.26: A. Fluorescence spectra of FL-pHLIP at pH 7.4 (light blue) and in presence of DOPC liposomes at pH 7.4 (blue), 6.5 (green) and 5.2 (red) measured by fluorimeter analysis. B. Blueshift of maximum emission as a function of the pH.

To deeply investigate FL-pHLIP three-dimensional conformation, we performed CD analyses. Conforming to the results previously obtained by DLS analyses (section 3.2.2), data reported in Figure 3.27 A show a similar spectral profile of the peptide both at physiological and slightly acidic pH (6.5) in absence of liposomes, while at pH 5.2 the configuration changed upon FL-pHLIP aggregation.

Importantly, CD measurements performed in presence of DOPC vesicles represented another proof showing that FL-conjugation did not influence the membrane insertion properties of the peptide. Indeed, FL-pHLIP was characterized by a random coil secondary structure at physiological pH that progressively changed into an α-helix conformation by reducing the pH (Figure 3.27 B). Exactly the same behavior was observed in case of WT pHLIP (section 3.1.3).

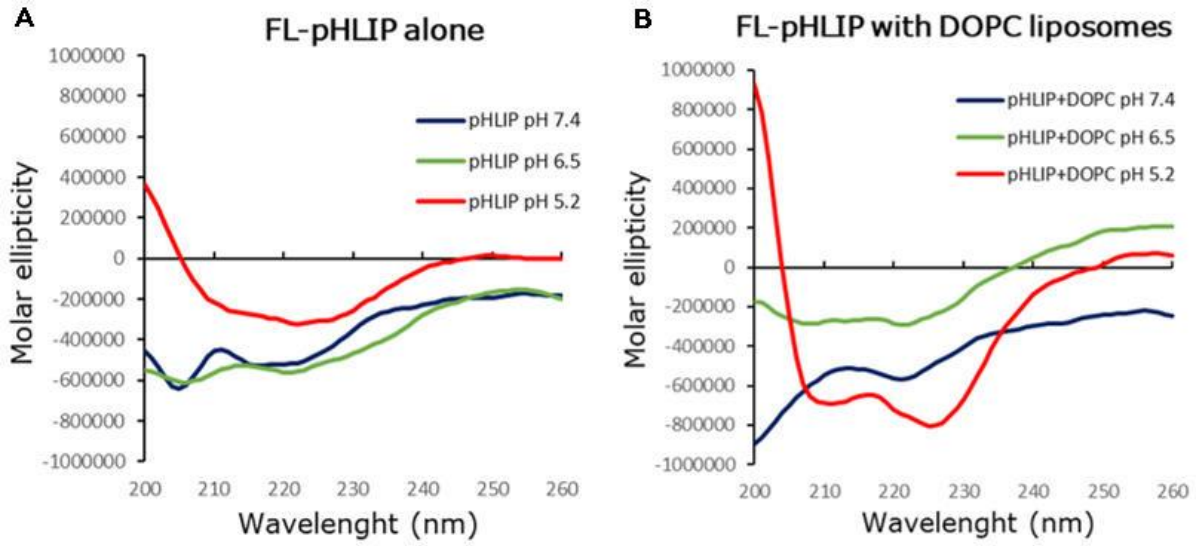

Figure 3.27: CD profiles of FL-pHLIP alone (A) or in presence of DOPC liposomes (B) at different pH values.

3.2.4. Dynamics of membrane insertion at acid pH values

With the aim to study the dynamics of FL-pHLIP membrane insertion, CD analyses were performed in acid environment (pH 6.5 and pH 5.2) at different timings (30 min, 2 h and 4 h). As shown in Figure 3.28, once the peptide interacted with the lipid bilayer, the three-dimensional conformation was maintained the same over time meaning that FL-pHLIP did not tend to return back in solution. Therefore, the membrane insertion process at acid pH values was very rapid and stable.

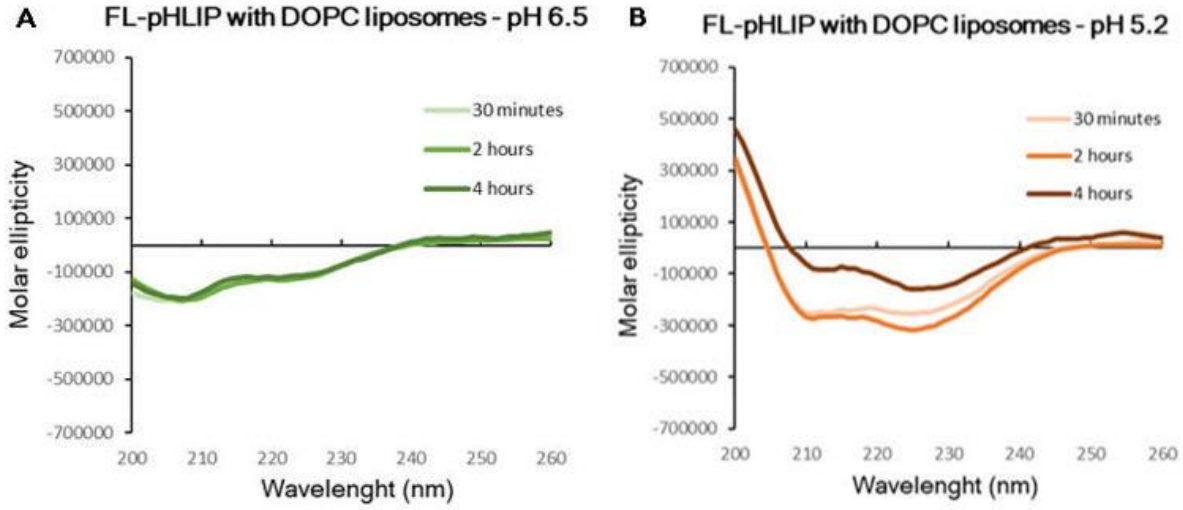

Figure 3.28: CD profiles of FL-pHLIP in presence of DOPC liposomes at pH 6.5 (A) and 5.2 (B) measured at three different time points.

3.2.5. Quantification of inserted peptide into the lipid bilayer

With the purpose of further quantifying the amount of inserted FL-pHLIP, DOPC liposomes were incubated with the peptide at different pH values (7.4, 6.5, and 5.2) and for different timings (30 minutes, 2 and 24 hours). After a first UV-Vis analysis of the samples able to quantify the starting FL-pHLIP amount, the liposomes were purified from the excess of unbound peptide by gel permeation by Sephadex G-25 columns. DLS analyses on purified samples showed a slight increase of the liposomes

size by reducing the pH without change in PDI, likely indicating that the increase in the hydrodynamic size is due to the insertion of FL-pHLIPs in the outer leaflet of the lipid membrane, which modify the surface properties of the liposome and its hydration sphere (Figure 3.29).

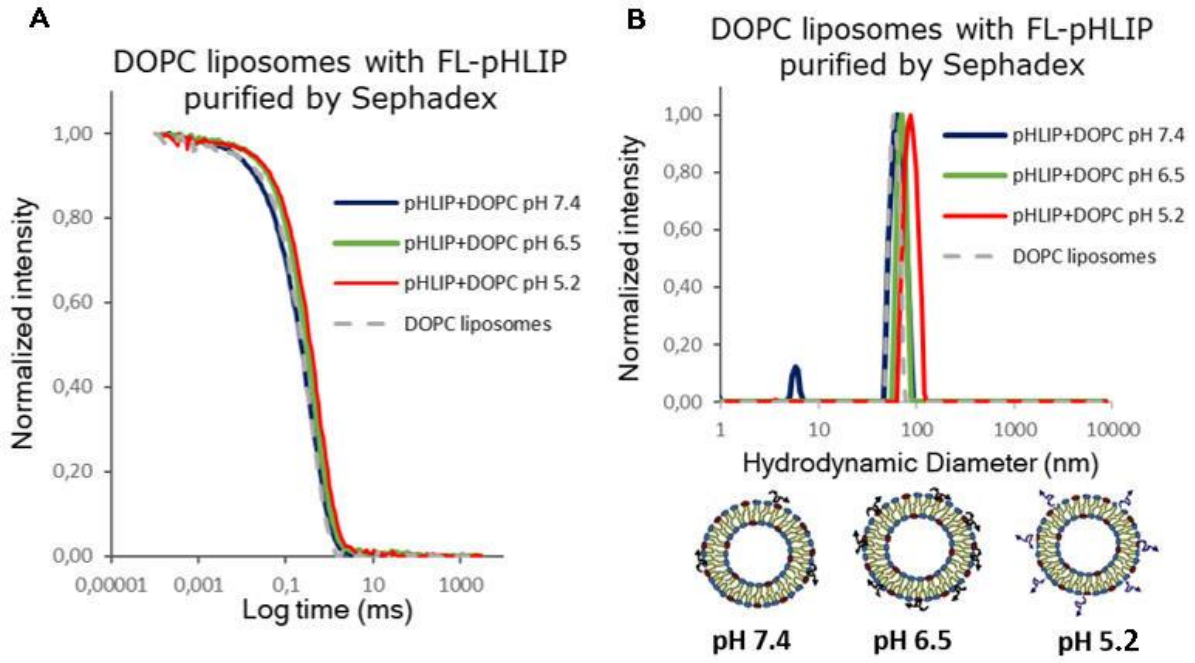

Figure 3.29: 90° DLS analysis: autocorrelation functions (A) and unweighted size distributions with a schematic representation (B) of purified liposomes incubated with FL-pHLIP (24 hours) at pH 7.4 (blue), 6.5 (green) and 5.2 (red). The grey dashed line indicates the untreated DOPC liposomes.

UV-Vis analyses were also performed after sample purification in order to evaluate the decrease in the λmax of the peak related to the dye (in the range between 450 and 500 nm). Although Fluorescein is a pH sensor and its absorbance decreases in acidic environment (Figure 3.30 A), after purification it was possible to observe a higher intensity for more acidic pHs compared to physiological conditions where no peak was detected (Figure 3.30 B). This meant that the FL-pHLIP observed before the purification at pH 7.4 (Figure 3.30 A) was related to a weakly membrane-interaction or at least to the unbound fraction. Indeed, it was absent in the purified samples where

the amount of peptide was greater at acid pH, indicating a clear insertion into liposomes.

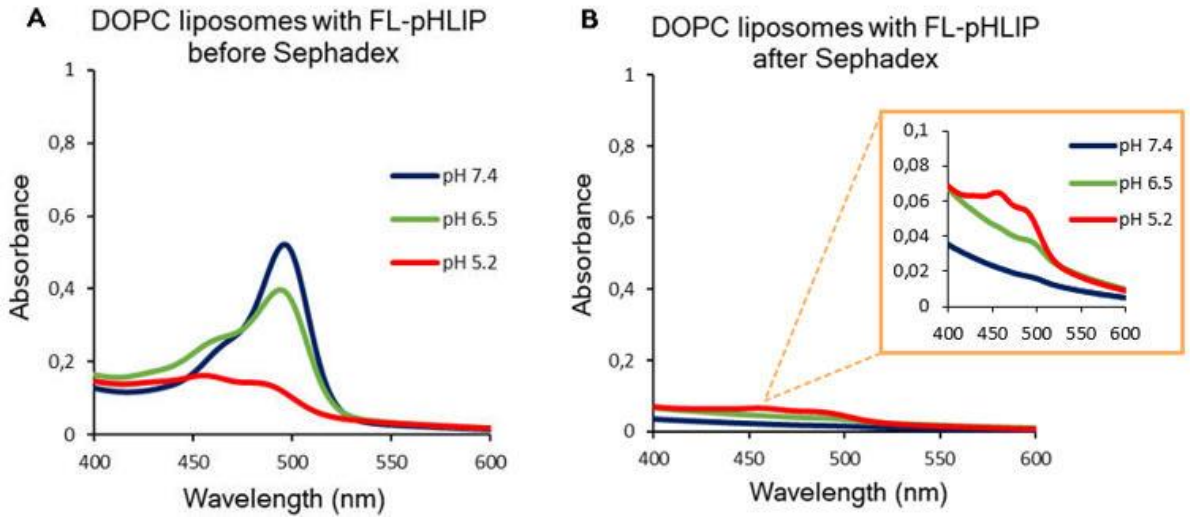

Figure 3.30: UV-Vis absorption spectra of DOPC liposomes incubated with FL-pHLIP before (A) and after purification (B) measured at different pH values.

Importantly, the inserted peptide into liposome could be quantified from the comparison of FL-pHLIP concentrations before and after Sephadex purification. Results are summarized below in Figure 3.31.

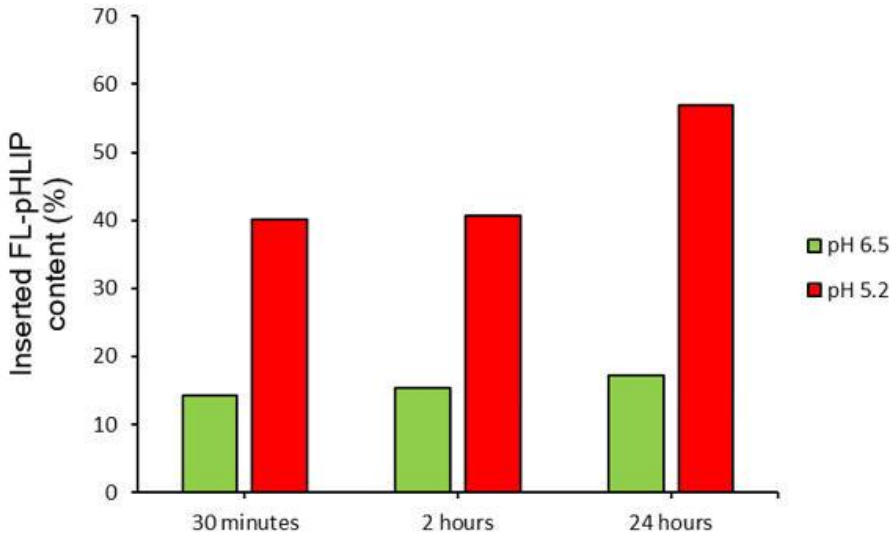

Figure 3.31: Quantification of inserted FL-pHLIP into DOPC liposomes after purification at pH 6.5 (green) and 5.2 (red) at different incubation times.

As previously observed, the percentage of inserted FL-pHLIP raised by decreasing the pH. In particular, at pH 6.5 the amount of peptide progressively increased from 14.3% to 17.2% by performing a longer incubation time. Instead, in highly acidic environment (5.2) a considerable content of FL-pHLIP (40%) entered the membrane immediately after 30 minutes and the value remained constant for hours until reaching a maximum of 57% after one day.

3.2.6. Peptide-membrane interaction: in-flow model of eukaryotic cells membrane

As final step, we considered an in-flow model of eukaryotic cells membrane to study its interaction with the peptide in a context closer to the cellular environment. Again, we exploited the supported lipid bilayers (SLBs) as model of cell membrane and pHLIP-SLB interaction was observed by a quartz crystal microbalance with dissipation monitoring (QCM-D). Specifically, the QCM-D procedure previously optimized for the WT derivative in terms of both peptide concentration and incubation timings (section 3.1.5) was extended to the FL-containing peptide.

Indeed, in a first experiment, a 0.5 μM FL-pHLIP solution was insufflated at physiological pH onto the SLB for 15 minutes. As observed for the WT, also in this case the introduction of the peptide (arrow 4 in Figure 3.32), was followed by a slight decrease in the frequency suggesting a mild FL-pHLIP-lipid bilayer interaction. However, during the 15-minutes static incubation and with the final 15-minutes washing in PBS, the frequency decreased and reached again its original value. This confirmed that the low peptide amount adsorbed onto the SLB easily returned back in solution.

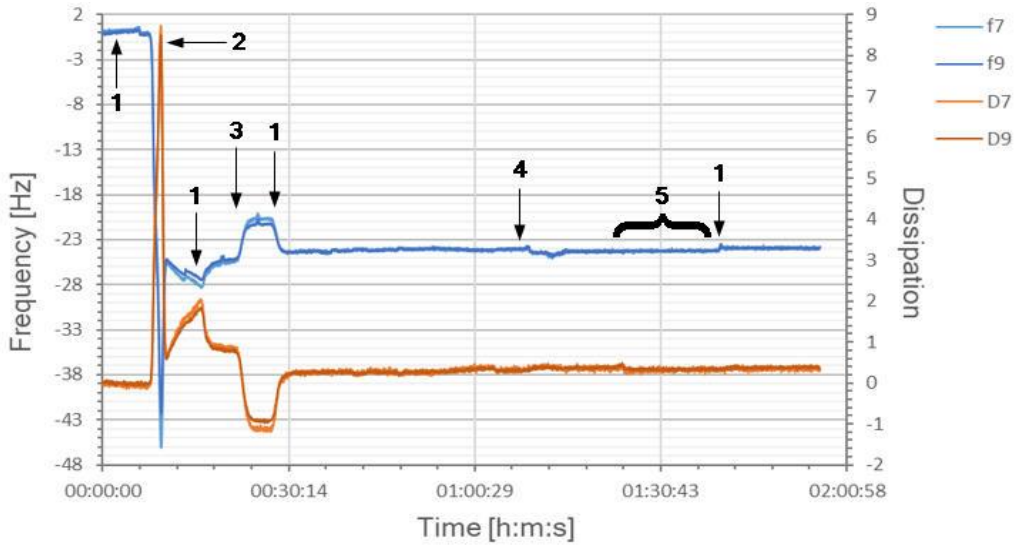

Figure 3.32: Representative QCM-D measurement for the SLB-FL-pHLIP interaction at pH 7.4: dissipation (red line) and frequency (blue line). The numbers indicate the flow of the following solutions: 1 = PBS 0.1 M pH 7.4, 2 = Liposomes solution + $CaCl_2$, 3 = MilliQ water, 4 = FL-pHLIP solution (0.5 μM), 5 = Static incubation.

If we observe the mass deposition (Figure 3.33), a very small increase is appreciated when FL-pHLIP was added to the system. Importantly, during the static incubation the amount of deposited peptide tended to zero since the mass comes back to the SLB starting value.

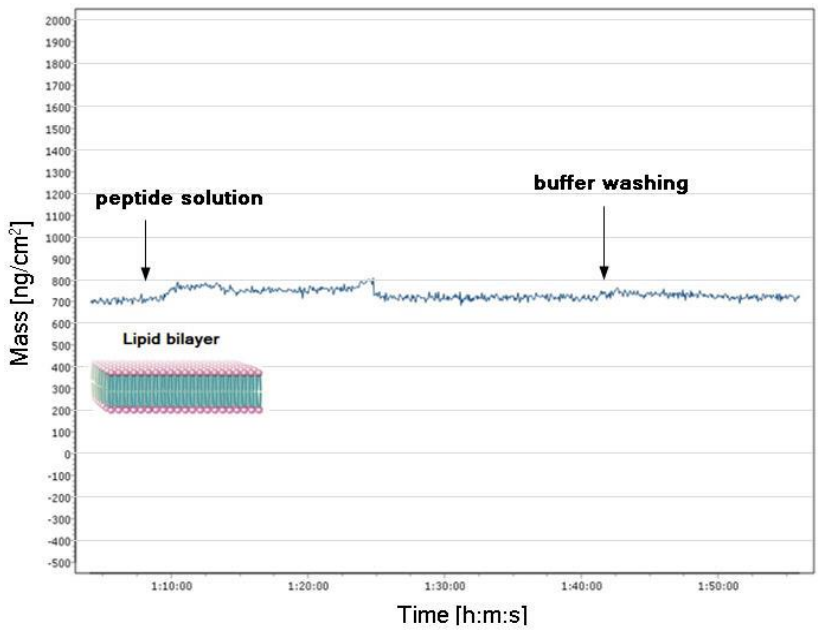

Figure 3.33: Mass profile of a SLB and FL-pHLIP at pH 7.4 measured by QCM-D analysis.

The same analysis was accomplished also at slightly acidic conditions (pH 6.5). However, in this case both an increase in dissipation and a decrease in frequency were observed immediately after the peptide flux (arrow 5 in Figure 3.34). Thus, a strong FL-pHLIP- SLB interaction occurred. Importantly, these trends were not reversed during the final buffer washing meaning that the interacting peptides were not removed from the lipid bilayer.

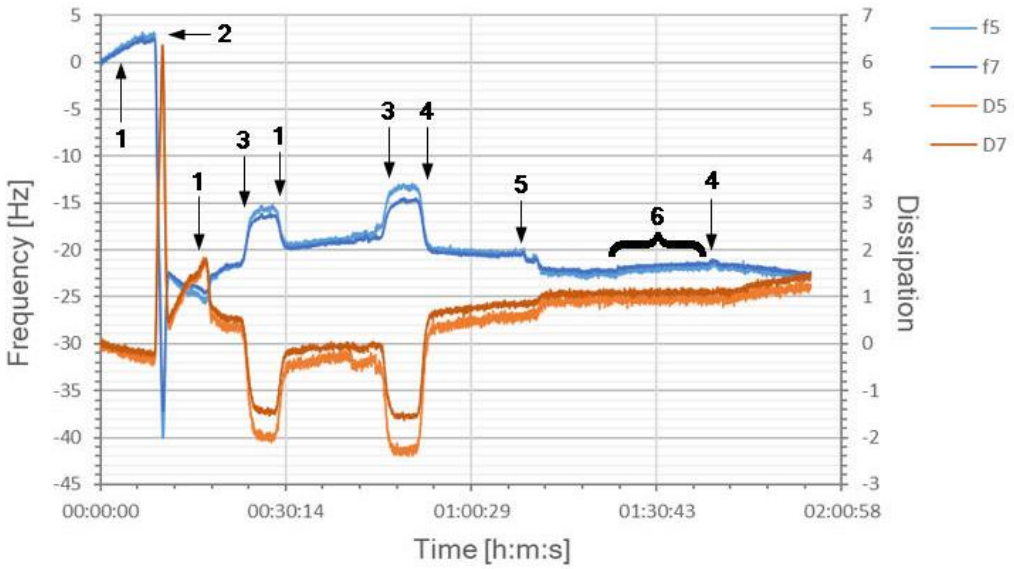

Figure 3.34: Representative QCM-D measurement for the SLB-FL-pHLIP interaction at pH 6.5: dissipation (red line) and frequency (blue line). The numbers indicate the flow of the following solutions: 1 = PBS 0.1 M pH 7.4, 2 = Liposomes solution + $CaCl_2$, 3 = MilliQ water, 4 = TRIS 0.1 M pH 6.5, 5 = FL-pHLIP solution (0.5 μM), 6 = Static incubation.

As shown in Figure 3.35, a great increase in mass was evaluated and quantified after the FL-pHLIP incubation. Specifically, a value of 663 ng/cm^2 of deposited peptide was detected.

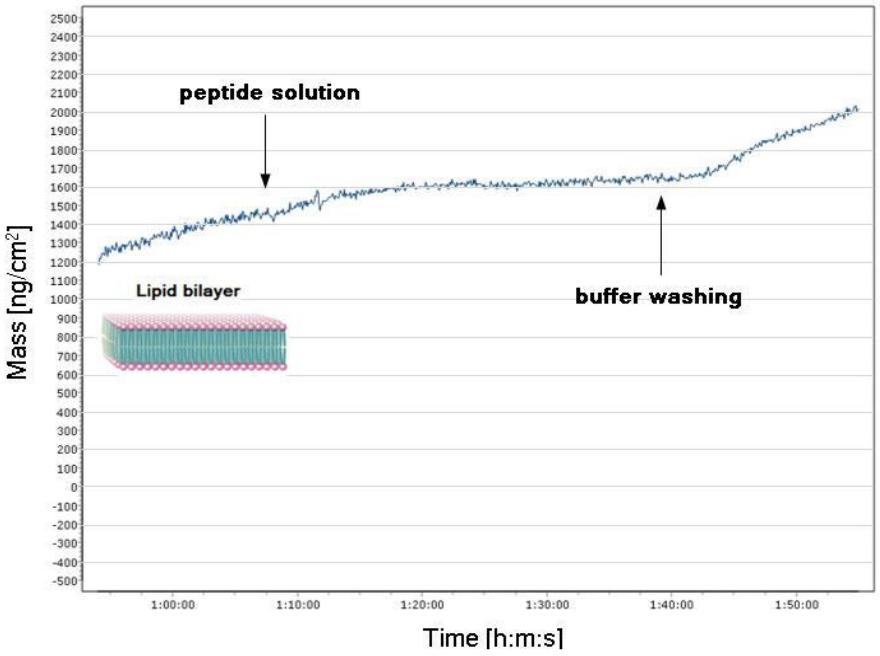

Figure 3.35: Mass profile of a SLB and FL-pHLIP at pH 6.5 measured by QCM-D analysis.

Finally, QCM-D measurements were repeated in highly acidic environment (pH 5.2). Here, the increase in dissipation and the decrease in frequency after the peptide insufflation were significant, indicating an even stronger interaction with the SLB compared to pH 6.5 condition (Figure 3.36). Also in this case, the peptide was not washed away when only the buffer was flowing, suggesting a stable insertion into the lipid bilayer. The important peptide-SLB interaction was confirmed by the considerable increase in mass when FL-pHLIP was added to the system (Figure 3.37). In particular, 2258 ng/cm^2 of deposited peptide were estimated.

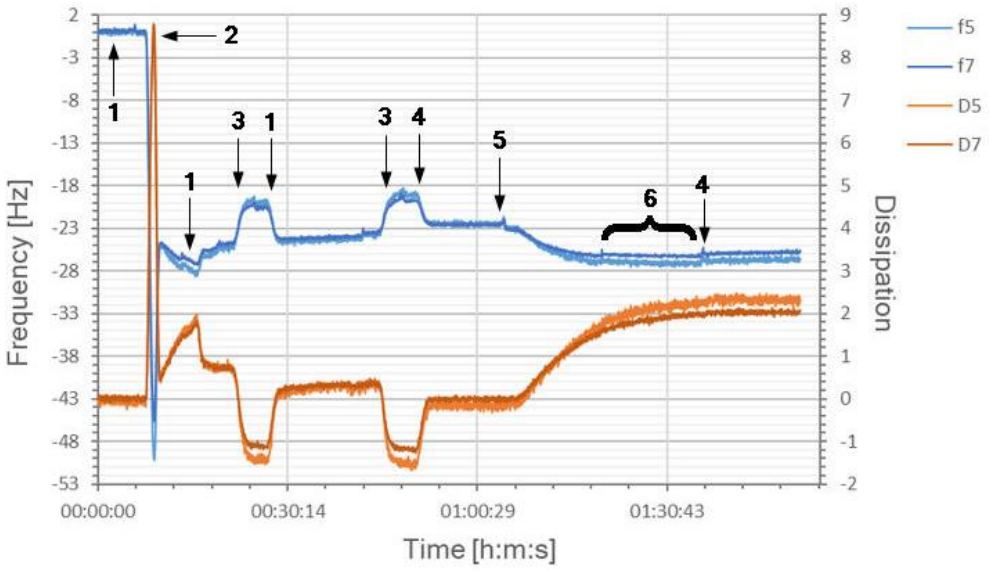

Figure 3.36: Representative QCM-D measurement for the SLB-FL-pHLIP interaction at pH 5.2: dissipation (red line) and frequency (blue line). The numbers indicate the flow of the following solutions: 1 = PBS 0.1 M pH 7.4, 2 = Liposomes solution + $CaCl_2$, 3 = MilliQ water, 4 = Acetate buffer 0.1 M pH 5.2, 5 = FL-pHLIP solution (0.5 μM), 6 = Static incubation.

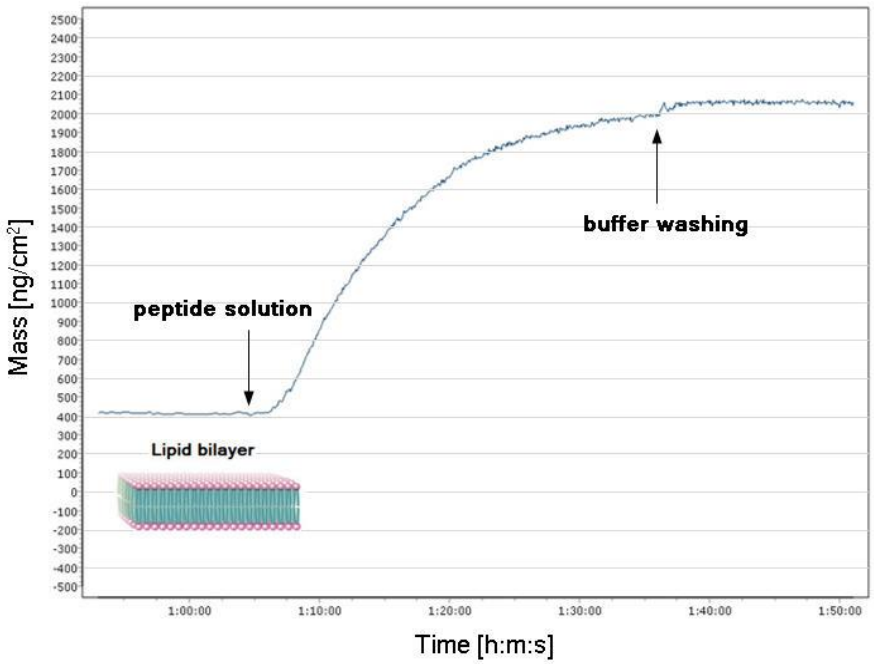

Figure 3.37: Mass profile of a SLB and FL.pHLIP at pH 5.2 measured by QCM-D analysis.

The quantification of inserted FL-pHLIP reached in the different QCM-D experiments are summarized below in Figure 3.38.

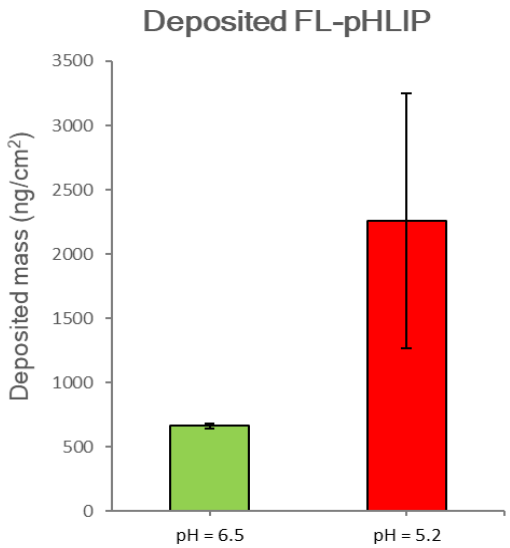

Figure 3.38: Quantification of deposited FL-pHLIP during QCM-D analysis at pH 6.5 (green) and 5.2 (red).

The results reported in Figure 3.38 show that at the same peptide concentration (0.5 μM) and incubation time (15 minutes), the amount of deposited mass at pH 5.2 was much higher compared to slightly acidic conditions (pH 6.5). However, aggregation phenomena might have occurred in highly acid environment since an increase in the standard deviation was also observed.

In conclusion, QCM-D analyses demonstrated that while at physiological pH just a mild and temporary interaction with the lipid bilayer was observed for both FL- and WT pHLIPs, the acidic environment clearly promoted a greater deposition of both peptides on the SLB. These results confirmed that the FL-conjugation did not affect either the affinity of the peptide for the lipid bilayer at pH 7.4 or its insertion properties in acid environment even when a dynamic model was considered. Moreover, for both FL- and WT pHLIPs, a concentration equal to 0.5 μM was sufficient to detect an interaction with the SLB.

3.3. *In vitro* tests on patient-derived glioblastoma cells

In the last part of this thesis work, cellular tests were performed according to the procedure described in section 2.3.8 thanks to the collaboration with the group of Dr. Serena Pellegatta at Carlo Besta Neurological Institute (Milan). The aim was to verify FL-pHLIP labelling efficiency and cytotoxicity on three different patient-derived glioblastoma primary cells (BT 592, BT 1007, and GBMR16-NS). Briefly, cells were incubated for 2 hours with the FL-peptide at different concentrations at both physiological and acidic pHs. A scrambled peptide (SC-FL pHLIP) that was not pH-sensitive was used as a control.

Results related to peptides cellular tolerance (Figure 3.39) show an almost negligible cytotoxicity as the cellular viability after incubation remained in an acceptable range comparable to the untreated cells (dotted line), especially for the mesenchymal (BT 1007) and proneural (GBMR16-NS) subtypes.

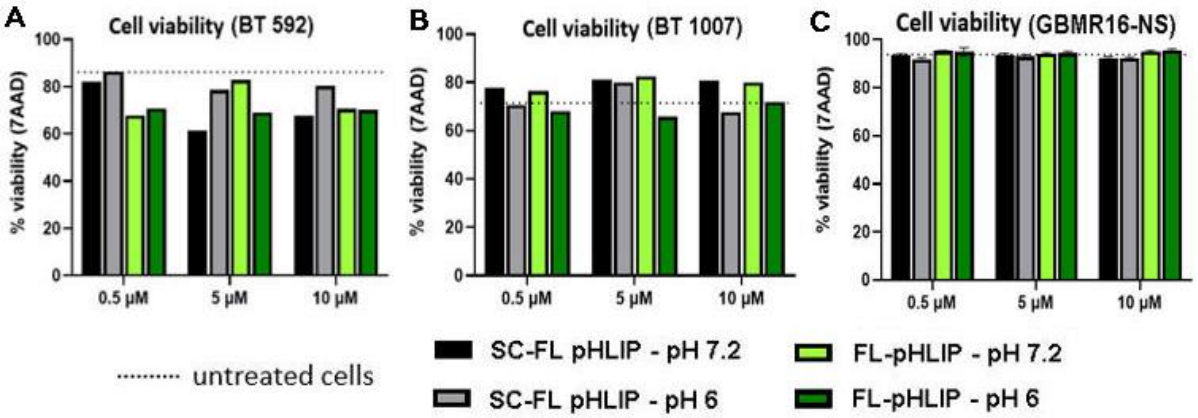

Figure 3.39: Viability of proliferative (A), mesenchymal (B) and proneural (C) subtypes of glioblastoma cells incubated for 2 hours with FL- and SC-FL pHLIPs measured at different pHs by FACS.

FACS analyses regarding the cellular positivity to Fluorescein show that both FL- and SC-FL pHLIPs have a good affinity for the cellular membrane even at physiological pH for both BT 592 and BT 1007 cell lines (Figure 3.40 and Figure 3.41). This result was

expected considering the hydrophobic residues that are present in both peptides. However, SC-FL pHLIP exhibited the same behavior in physiological or acid environment (Figure 3.40 A) or even opposite tendencies depending on the concentration (Figure 3.41 A), confirming that the peptide was not pH-sensitive. On the other hand, FL-pHLIP presented an interesting trend as the cellular positivity to the FL increased in acidic conditions, especially in the range of concentrations from 0.5 to 5 μM (Figure 3.40 B). These data suggest that FL-pHLIP can be effectively used as fluorescent tracer for proliferative and mesenchymal subtypes of primary glioblastoma cells. In particular, the most relevant result was obtained for BT 1007 cells using a peptide concentration of 0.5 μM (Figure 3.41 B). Here, the cell labelling at physiological pH was minimal, and thus useful to avoid unspecific targeting. On the contrary, FL-positivity at pH 6 reached a very high value meaning that the contrast between marked and unmarked cells was really evident. For this reason, further in-depth analyses will be performed on these cells in order to evaluate all the benefits that FL-pHLIP can offer as an imaging agent. Specifically, confocal microscopy studies will be performed to better understand the cellular morphology upon membrane interaction.

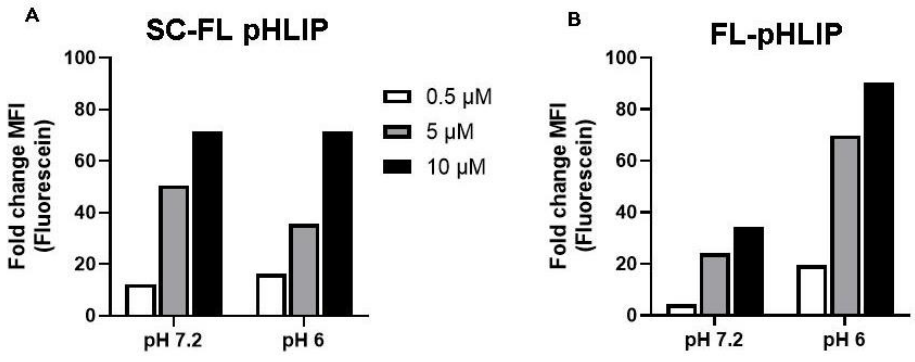

Figure 3.40: FL-positivity of proliferative subtype of primary glioblastoma cells (BT 592) incubated for 2 hours with SC-FL pHLIP (A) and FL-pHLIP (B) measured at different pH values by FACS.

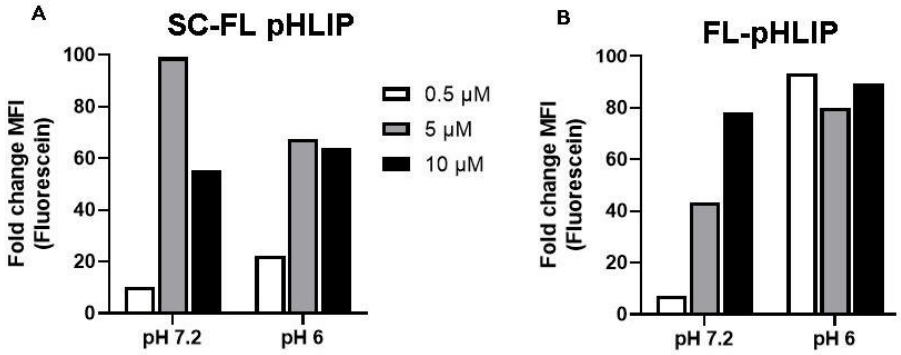

Figure 3.41: FL-positivity of mesenchymal subtype of primary glioblastoma cells (BT 1007) incubated for 2 hours with SC-FL pHLIP (A) and FL-pHLIP (B) measured at different pH values by FACS.

Finally, to conclude the analyses related to the *in vitro* studies, we also evaluated pHLIP performance on proneural subtype cells derived from a recurrent glioblastoma (GBMR16-NS). Also in this case, the measurements of cellular positivity to Fluorescein confirmed the not pH-dependent behavior of SC-FL pHLIP (Figure 3.42 A). Importantly, FL fluorescence intensity increased at acidic pH only when cells were incubated with FL-pHLIP (Figure 3.42 B). However, this trend was much less evident in GBMR16-NS cells compared to the other investigated cell lines. Furthermore, FL-pHLIP positivity of cells incubated at physiological conditions was not negligible, which meant a high unspecific targeting. The ambiguous behavior of GBMR16-NS may be attributed to the high response variability of the recurrent cell lines.

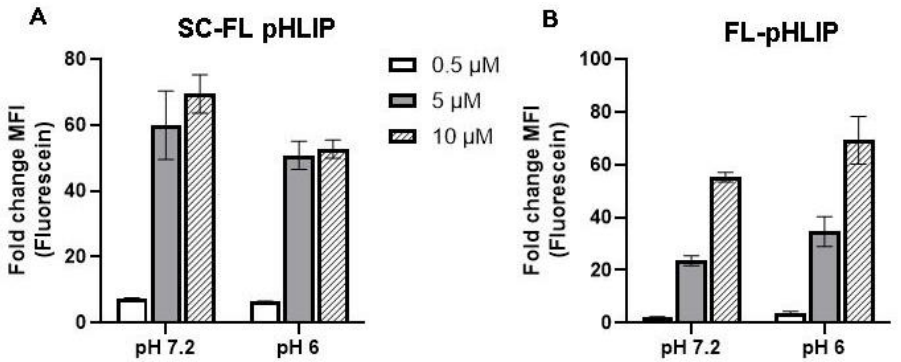

Figure 3.42: FL-positivity of proneural subtype of recurrent glioblastoma cells (GBMR16-NS) incubated for 2 hours with SC-FL pHLIP (A) and FL-pHLIP (B) measured at different pH values by FACS.

4 Conclusions and future developments

The purpose of this project was the characterization of a pH-sensitive peptide conjugated to a Fluorescein derivative (FL-pHLIP) able to target the acidic tumour microenvironment. In detail, this novel fluorescent tracer was developed to more selectively label glioblastoma cancer cells during surgical resection. The behavior of the proposed system was analyzed from a chemical-physical perspective and compared to the Wild Type peptide (pHLIP WT) in order to verify that the linkage with the fluorescent dye did not affect the pH-dependent insertion into cellular membranes.

First, we developed a solubilization protocol that could be applied for the dissolution of both WT and FL- pHLIPs and we checked the efficiency of the procedure by performing UV-Vis and DLS analyses. The peptides were stable in solution at physiological pH within 24 hours, while a more acidic environment favored their aggregation. Therefore, pHLIP solubility and its enhanced hydrophobicity due to protonation were not significantly influenced by the presence of FL. However, in less acidic conditions the WT derivative aggregated more than FL-pHLIP, indicating a moderately higher stability of the peptide in solution probably related to a steric effect of the dye.

Then, DOPC liposomes were used as a simplified model of eukaryotic cells membranes to evaluate pHLIP insertion properties. From tryptophan intrinsic fluorescence analysis of both WT and FL- pHLIPs, we observed a blueshift of the maximum emission reducing the pH, confirming the increasing insertion of the residues inside the lipid bilayer in acidic environment. We also evaluated the peptide secondary conformation by CD analysis and obtained similar spectra for WT and FL-

pHLIPs. In particular, we could recognize a random coil secondary structure at physiological pHs that progressively changed into an α-helix configuration by reducing the pH. The transmembrane α-helix formation was proved to be rapid and stable over time.

Once we had verified that the functionalization with FL did not interfere with the peptide insertion properties, we quantified the amount of inserted FL-pHLIP. Performing DLS analysis on liposomes incubated with the peptide and purified by a Sephadex G-25 column, we noticed a more marked increase in size reducing the pH, revealing a more consistent peptide functionalization of the vesicle surface. As a further proof, the percentage of inserted FL-pHLIP, that we were able to estimate by UV-Vis analysis of the purified samples, increased for more acidic conditions from a value of 14% - 17,5% at pH 6.5 to 40% - 57% at pH 5.2.

Motivated by these encouraging results, we transferred the system to an in-flow lipid membrane model in order to better mimic a real cellular environment before starting the *in vitro* tests. Therefore, the interaction between the pHLIP and a supported lipid bilayer (SLB) was evaluated through a quartz crystal microbalance with dissipation monitoring (QCM-D). We observed just a mild and temporary interaction of both WT and FL- pHLIPs with the lipid bilayer at physiological pH, while in acidic conditions a quantifiable mass of peptides was deposited onto the SLB. Interestingly, the peptide deposited in acidic environment was washed away when a physiological pH was restored, demonstrating the reversibility of the insertion process. To complete these studies, we plan to perform similar QCM-D experiments incubating the SLB with culture media at different pHs, which have been also in contact with GB primary cells. These studies will allow the evaluation of possible interactions of the FL-pHLIPs with biomolecules present in the biological environments, which can have an effect on its interaction with the SLB. Moreover, fluorescence microscopy experiments on the SLBs upon incubation with FL-pHLIP and FL-SC peptides are planned in order to better understand the membrane behavior upon peptide insertion.

Finally, FL-pHLIP labelling efficiency and cytotoxicity were assessed on three different lines of patient-derived glioblastoma primary cells in collaboration with Dr. Serena Pellegatta from Carlo Besta Neurological Institute. Specifically, we tested a proliferative (BT 592), a mesenchymal (BT 1007) and a proneural derived from recurrent glioblastoma (GBMR16-NS) cells subtypes. The compatibility of the peptide was proved for all the cell lines. Importantly, cellular positivity to FL evaluated through FACS showed an interesting trend for FL-pHLIP as the fluorescence intensity increased in acidic environment with respect to physiological conditions, especially in the range of peptide concentrations between 0.5 and 5 μM. In particular, the most important result was obtained by the high labelling efficacy on BT 1007 at a peptide concentration of 0.5 μM. For this reason, further in-depth analyses will be performed on this cell line in order to evaluate all the benefits that FL-pHLIP can offer as an imaging agent. Specifically, confocal microscopy studies will be performed to better understand the peptide folding.

Bibliography

[1] J. Höhne, K. M. Schebesch, C. de Laurentis, M. O. Akçakaya, C. Bonde Pedersen, A. Brawanski, F. R. Poulsen, T. Kiris, C. Cavallo, M. Broggi, P. Ferroli, and F. Acerbi, "Fluorescein Sodium in the Surgical Treatment of Recurrent Glioblastoma Multiforme", *World Neurosurgery*, vol. 125, p. 158–164, 2019.

[2] V. Rezaei, A. Rabiee, and F. Khademi, "Glioblastoma multiforme: a glance at advanced therapies based on nanotechnology", J*ournal of Chemotherapy*, vol. 32, p. 107–117, 2020.

[3] X. Guan, M. N. Hasan, S. Maniar, W. Jia, and D. Sun, "Reactive Astrocytes in Glioblastoma Multiforme", *Molecular Neurobiology*, vol. 55, p. 6927–6938, 2018.

[4] A. L. Placone, A. Quiñones-Hinojosa, and P. C. Searson, "The role of astrocytes in the progression of brain cancer: complicating the picture of the tumor microenvironment", *Tumor Biology*, vol. 37, p. 61–69, 2015.

[5] M. Mazurek, B. Kulesza, F. Stoma, J. Osuchowski, S. Mańdziuk, and R. Rola, "Characteristics of Fluorescent Intraoperative Dyes Helpful in Gross Total Resection of High-Grade Gliomas—A Systematic Review", *Diagnostics*, 2020.

[6] F. Szulzewsky, S. Arora, L. de Witte, T. Ulas, D. Markovic, J. L. Schultze, E. C. Holland, M. Synowitz, S. A. Wolf, and H. Kettenmann, "Human Glioblastoma-associated Microglia/Monocytes Express a Distinct RNA Profile Compared to Human Control and Murine Samples", *GLIA*, vol. 64, p. 1416–1436, 2016.

[7] M. S. Goldberg, "Improving cancer immunotherapy through nanotechnology", *Nature Reviews Cancer*, vol. 19, p. 587–602, 2019.

[8] B. Caffery, J. S. Lee, and A. A. Alexander-Bryant, "Vectors for Glioblastoma Gene Therapy: Viral & Non-Viral Delivery Strategies", *Nanomaterials*, vol. 9, 2019.

[9] M. An, D. Wijesinghe, O. A. Andreev, Y. K. Reshetnyak, and D. M. Engelman, "pH-(low)-insertion-peptide (pHLIP) translocation of membrane impermeable phalloidin toxin inhibits cancer cell proliferation", *Proceedings of the National Academy of Sciences of the United States of America*, vol. 107, 2010.

[10] H. L. Stewart, and D. J. S. Birch, "Fluorescence Guided Surgery", *Methods and Applications in Fluorescence*, vol. 9, 2021.

[11] T. Nagaya, Y. A. Nakamura, P. L. Choyke, and H. Kobayashi, "Fluorescence-Guided Surgery", *Frontiers in Oncology*, 2017.

[12] R. Sun, H. Cuthbert, and C. Watts, "Fluorescence-Guided Surgery in the Surgical Treatment of Gliomas: Past, Present and Future", *Cancers*, vol. 13, 2021.

[13] A. J. Schupper, M. Rao, N. Mohammadi, R. Baron, J. Y. K. Lee, F. Acerbi, and C. G. Hadjipanayis, "Fluorescence-Guided Surgery: A Review on Timing and Use in Brain Tumor Surgery", *Frontiers in Neurology*, 2021.

[14] Y. Zheng, H. Yang, H. Wang, K. Kang, W. Zhang, G. Ma, and S. Du, "Fluorescence-guided surgery in cancer treatment: current status and future perspectives", *Annals of Translational Medicine*, vol. 7, 2019.

[15] T. Crawford, A. Moshnikova, S. Roles, D. Weerakkody, M. DuPont, L. M. Carter, J. Shen, D. M. Engelman, J. S. Lewis, O. A. Andreev and Y. K. Reshetnyak, "pHLIP ICG for delineation of tumors and blood flow during fluorescence-guided surgery", *Scientific Reports*, vol. 10, 2020.

[16] D. A. Hansen, A. M. Spence, T. Carski, and M. S. Berger, "Indocyanine green (ICG) staining and demarcation of tumor margins in a rat glioma model", *Surgical Neurology*, vol. 40, p. 451–456, 1993.

[17] G. W. Britz, S. Ghatan, A. M. Spence, and M. S. Berger, "Intracarotid RMP-7 enhanced indocyanine green staining of tumors in a rat glioma model", *Journal of Neuro-Oncology*, vol. 56, p. 227–232, 2002.

[18] H. Yano, N. Nakayama, N. Ohe, K. Miwa, J. Shinoda, and T. Iwama, "Pathological analysis of the surgical margins of resected glioblastomas excised using photodynamic visualization with both 5-aminolevulinic acid and fluorescein sodium", *Journal of Neuro-Oncology*, vol. 133, p. 389–397, 2017.

[19] Y. Kitagawa, S. Tanaka, M. Kamiya, Y. Kuriki, K. Yamamoto, T. Shimizu, T. Nejo, T. Hana, R. Matsuura, T. Koike, E. Yamazawa, Y. Kushihara, S. Takahashi, M. Nomura, H. Takami, S. Takayanagi, A. Mukasa, Y. Urano, and N. Saito, "A Novel Topical Fluorescent Probe for Detection of Glioblastoma", *Clinical Cancer Research*, vol. 27, p. 3936–3947, 2021.

[20] E. Belykh, E. J. Miller, A. A. Patel, B. Bozkurt, K. Yağmurlu, T. R. Robinson, P. Nakaji, R. F. Spetzler, M. T. Lawton, L. Y. Nelson, E. J. Seibel, and M. C. Preul, "Optical Characterization of Neurosurgical Operating Microscopes: Quantitative Fluorescence and Assessment of PpIX Photobleaching", *Scientific Reports*, vol. 8, 2018.

[21] F. Le Guern, V. Mussard, A. Gaucher, M. Rottman, and D. Prim, "Fluorescein Derivatives as Fluorescent Probes for pH Monitoring along Recent Biological Applications", *International Journal of Molecular Sciences*, vol. 21, p. 1–23, 2020.

[22] M. K. Hamamcioğlu, M. O. Akçakaya, B. Göker, M. Ö. Kasimcan, and T. Kiris, "The use of the YELLOW 560 nm surgical microscope filter for sodium fluorescein-guided resection of brain tumors: Our preliminary results in a series of 28 patients", *Clinical Neurology and Neurosurgery*, vol. 143, p. 39–45, 2016.

[23] K. M. Schebesch, M. Proescholdt, J. Höhne, C. Hohenberger, E. Hansen, M. J. Riemenschneider, W. Ullrich, C. Doenitz, J. Schlaier, M. Lange, and A. Brawanski, "Sodium fluorescein–guided resection under the YELLOW 560 nm surgical microscope filter in malignant brain tumor surgery—a feasibility study", *Acta Neurochirurgica*, vol. 155, p. 693–699, 2013.

[24] D. W. Roberts, and J. Olson, "Fluorescein Guidance in Glioblastoma Resection", *The New England Journal of Medicine*, vol. 376, 2017.

[25] L. C. Wyatt, J. S. Lewis, O. A. Andreev, Y. K. Reshetnyak, and D. M.Engelman, "Applications of pHLIP Technology for Cancer Imaging and Therapy", *Trends in Biotechnology*, vol. 35, p. 653–664, 2017.

[26] J. L. Daniels, T. M. Crawford, O. A. Andreev, and Y. K. Reshetnyak, "Synthesis and characterization of pHLIP® coated gold nanoparticles", *Biochemistry and Biophysics Reports*, vol. 10, p. 62–69, 2017.

[27] A. I. Hashim, X. Zhang, J. W. Wojtkowiakk, and R. J. Gillies, "Imaging pH and Metastasis", *NMR in Biomedicine*, vol. 24, p. 582–591, 2011.

[28] O. A. Andreev, D. M. Engelman, and Y. K. Reshetnyak, "Targeting diseased tissues by pHLIP insertion at low cell surface pH", *Frontiers in Physiology*, vol. 5, 2014.

[29] R. C. Adochite, A. Moshnikova, J. Golijanin, O. A. Andreev, N. V. Katenka, and Y. K. Reshetnyak, "Comparative Study of Tumor Targeting and Biodistribution of pH (Low) Insertion Peptides (pHLIP® Peptides) Conjugated with Different Fluorescent Dyes", *Molecular Imaging and Biology*, vol. 18, p. 686–696, 2016.

[30] A. Kyrychenko, "Nanogold decorated by pHLIP peptide: comparative force field study", *Physical Chemistry Chemical Physics*, vol. 17, p. 12648–12660, 2015.

[31] B. D. Rao, H. Chakraborty, A. Chaudhuri, and A. Chattopadhyay, "Differential sensitivity of pHLIP to ester and ether lipids", *Chemistry and Physics of Lipids*, vol. 226, 2020.

[32] O. A. Andreev, A. G. Karabadzhak, D. Weerakkody, G. O. Andreev, D. M. Engelman, and Y. K. Reshetnyak, "pH (low) insertion peptide (pHLIP) inserts across a lipid bilayer as a helix and exits by a different path", *Proceedings of the National Academy of Sciences of the United States of America*, vol. 107, 2010.

[33] O. A. Andreev, D. M. Engelman, and Y. K. Reshetnyak, "pH-sensitive membrane peptides (pHLIPs) as a novel class of delivery agents", *Molecular Membrane Biology*, vol. 27, p. 341–352, 2010.

[34] A. G. Karabadzhak, D. Weerakkody, D. Wijesinghe, M. S. Thakur, D. M. Engelman, O. A. Andreev, V. S. Markin, and Y. K. Reshetnyak, "Modulation of the pHLIP Transmembrane Helix Insertion Pathway", *Biophysical Journal*, vol. 102, p. 1846–1855, 2012.

[35] S. A. Otieno, S. Z. Hanz, B. Chakravorty, A. Zhang, L. M. Klees, M. An, and W. Qiang, "pH-dependent thermodynamic intermediates of pHLIP membrane insertion determined by solid-state NMR spectroscopy", *Proceedings of the National Academy of Sciences of the United States of America*, vol. 115, 2018.

[36] L. Yao, J. Daniels, A. Moshnikova, S. Kuznetsov, A. Ahmed, D. M. Engelman, Y. K. Reshetnyak, and O. A. Andreev, "pHLIP peptide targets nanogold particles to tumors", *Proceedings of the National Academy of Sciences of the United States of America*, vol. 110, p. 465–470, 2013.

[37] O. A. Andreev, D. M. Engelman, and Y. K. Reshetnyak, "Targeting acidic diseased tissue: New technology based on use of the pH (Low) Insertion Peptide (pHLIP)", *Chimica Oggi*, vol. 27, p. 34–37, 2009.

[38] Y. K. Reshetnyak, O. A. Andreev, U. Lehnert, and D. M. Engelman, "Translocation of molecules into cells by pH-dependent insertion of a

transmembrane helix", *Proceedings of the National Academy of Sciences of the United States of America*, vol. 103, p. 6460–6465, 2006.

[39] O. A. Andreev, A. D. Dupuy, M. Segala, S. Sandugu, D. A. Serra, C. O. Chichester, D. M. Engelman, and Y. K. Reshetnyak, "Mechanism and uses of a membrane peptide that targets tumors and other acidic tissues in vivo", *Proceedings of the National Academy of Sciences of the United States of America*, vol. 104, p. 7893–7898, 2007.

[40] Y. K. Reshetnyak, L. Yao, S. Zheng, S. Kuznetsov, D. M. Engelman, and O. A. Andreev, "Measuring Tumor Aggressiveness and Targeting Metastatic Lesions with Fluorescent pHLIP", *Molecular Imaging and Biology*, vol. 13, p. 1146–1156, 2011.

[41] Y. K. Reshetnyak, O. A. Andreev, M. Segala, V. S. Markin, and D. M. Engelman, "Energetics of peptide (pHLIP) binding to and folding across a lipid bilayer membrane", *Proceedings of the National Academy of Sciences of the United States of America*, vol. 105, p. 15340–15345, 2008.

[42] L. Yao, J. Daniels, D. Wijesinghe, O. A.Andreev, and Y. K. Reshetnyak, "pHLIP®-mediated delivery of PEGylated liposomes to cancer cells", *Journal of Controlled Release*, vol. 167, p. 228–237, 2013.

[43] Y. K. Reshetnyak, A. Moshnikova, O. A. Andreev, and D. M. Engelman, "Targeting Acidic Diseased Tissues by pH-Triggered Membrane-Associated Peptide Folding", *Frontiers in Bioengineering and Biotechnology*, vol. 8, 2020.

[44] M. N. Loja, Z. Luo, D. G. Farwell, Q. C. Luu, P. J. Donald, D. Amott, A. Q. Truong, R. F. Gandour-Edwards, and N. Nitin, "Optical Molecular Imaging Detects Changes in Extracellular pH with the Development of Head and Neck Cancer", *International Journal of Cancer*, vol. 132, p. 1613–1623, 2013.

[45] K. Pinker-Domenig, and M. Morrow, "A Study of Multiparametric MRI and pHLIP® ICG in Breast Cancer Imaging During Surgery", *U. S. National Library of Medicine*, ClinicalTrials.gov Identifier: NCT05130801, 2022.

[46] Zetasizer APS User Manual, Manual on- http://www.malvern.com [Online], December 2008.

[47] A. Akbarzadeh, R. Rezaei-Sadabady, S. Davaran, S. W. Joo, N. Zarghami, Y. Hanifehpour, M. Samiei, M. Kouhi, and K. Nejati-Koshkiand, "Liposome:

classification, preparation, and applications", *Nanoscale Research Letters*, vol. 8, 2013.

[48] A. Micsonai, E. Bulyáki, and J. Kardos, "BeStSel: From Secondary Structure Analysis to Protein Fold Prediction by Circular Dichroism Spectroscopy", *Structural Genomics: General Applications, Methods in Molecular Biology*, vol. 2199, 2021.

[49] V. Vasquez-Montes, J. Gerhart, K. E. King, D. Thévenin, and A. S. Ladokhin, "Comparison of lipid-dependent bilayer insertion of pHLIP and its P20G variant", *Biochimica et Biophysica Acta (BBA) - Biomembranes*, vol. 1860, p. 534–543, 2018.

[50] D. Migoń, T. Wasilewski, and D. Suchy, "Application of QCM in Peptide and Protein-Based Drug Product Development", *Molecules*, vol. 25, 2020.

[51] N. J. Cho, C. W. Frank, B. Kasemo, and F. Höök, "Quartz crystal microbalance with dissipation monitoring of supported lipid bilayers on various substrates", *Nature Protocols*, vol. 5, p. 1096–1106, 2010.

[52] L. C. Wyatt, A. Moshnikova, T. Crawford, D. M. Engelman, O. A. Andreev, and Y. K. Reshetnyak, "Peptides of pHLIP family for targeted intracellular and extracellular delivery of cargo molecules to tumors", *Proceedings of the National Academy of Sciences of the United States of America*, vol. 115, p. 2811–2818, 2018.

[53] R. Sjöback, J. Nygren, and M. Kubista, "Absorption and fluorescence properties of fluorescein", *Spectrochimica Acta Part A*, vol. 51, p. 7–21, 1995.

List of Figures

List of Tables

Acknowledgments

I would like to thank Professor Francesca Bombelli Baldelli for giving me the opportunity to work with her in the research group and for all the professional and personal suggestions. Thank you also for the great availability and understanding that you have demonstrated in guiding me along this path.

A special thanks goes to my tutor, Dr. Cristina Chirizzi, who patiently trained me in the laboratory with passion and enthusiasm during these months. I will surely treasure in the future all her teachings and the challenges that we have overcome together. Thanks also to all the members of the SupraBioNanoLab group, for the warm welcome received and for the genuine assistance they have offered me whenever I needed help.

I want to thank Dr. Alessandro Gori from National Research Council (CNR) not only for the synthesis of the peptides required for my thesis work but also for his kind indications. Thanks also to Dr. Serena Pellegatta from Carlo Besta Neurological Institute for her contribution to the *in vitro* cellular experiments. A proper recognition must be received by the Cividini family and the Brainy association for financing the project to which this study belongs.

Heartfelt thanks to my family, and in particular to my mother Maria, my father Roberto, my sister Claudia and my grandparents Pasqua and Saverio, for having always believed in me and for their inestimable affection that day by day gives me the strength to never give up. I thank also all my friends for their support and for all the cheering moments that we have shared together. An exceptional thank you goes to Chiara, who has grown with me during this experience in the lab and with whom I shared joys and worries until a real friendship was born.